ADVANCED MATERIALS
www.advmat.de

Active Materials for Functional Origami

*Sophie Leanza, Shuai Wu, Xiaohao Sun, H. Jerry Qi, and Ruike Renee Zhao**

In recent decades, origami has been explored to aid in the design of engineering structures. These structures span multiple scales and have been demonstrated to be used toward various areas such as aerospace, metamaterial, biomedical, robotics, and architectural applications. Conventionally, origami or deployable structures have been actuated by hands, motors, or pneumatic actuators, which can result in heavy or bulky structures. On the other hand, active materials, which reconfigure in response to external stimulus, eliminate the need for external mechanical loads and bulky actuation systems. Thus, in recent years, active materials incorporated with deployable structures have shown promise for remote actuation of light weight, programmable origami. In this review, active materials such as shape memory polymers (SMPs) and alloys (SMAs), hydrogels, liquid crystal elastomers (LCEs), magnetic soft materials (MSMs), and covalent adaptable network (CAN) polymers, their actuation mechanisms, as well as how they have been utilized for active origami and where these structures are applicable is discussed. Additionally, the state-of-the-art fabrication methods to construct active origami are highlighted. The existing structural modeling strategies for origami, the constitutive models used to describe active materials, and the largest challenges and future directions for active origami research are summarized.

1. Introduction

The art of paper folding transforms 2D sheets into 3D architectures, with the earliest paper folding being traced to 1st century China when the papermaking process was invented. Origami, the Japanese paper folding art, began from the 6th century and gradually developed into more meticulous designs, such as the well-known paper crane (**Figure 1**a). Origami has remained popular over the years as a form of art, while it has also become a prominent scientific topic, also referred to as engineering origami (Figure 1b), with great relevance to the fields of mathematics and mechanics. Its capability of transforming a 2D sheet into a complicated 3D shape or reshaping a deployed structure into a compact folded state attracts significant attention and development in different engineering fields and research areas, including aerospace structures,[1,2] metamaterials,[3–7] robotics,[8,9,10,11] biomedical devices,[12,13] reconfigurable electronics,[14–16] and architecture,[5,17] encompassing a wide range of length scales, at which prestresses or actuators are built into the origami system to facilitate the folding. As mechanical properties of origami are tunable by the geometrical parameters of the origami pattern, structures with versatile mechanical properties such as metamaterials can be designed (Figure 1b, left).[5] Properties of origami such as the auxetic nature of Miura–ori or variable stiffness during folding have been utilized for metamaterial applications.[3,5] In aerospace applications, a significant change in size from the deployed to folded configurations is necessary for efficient storage and/or transportation of structures such as solar arrays (Figure 1b, middle),[1,18,19] space habitats,[20] and bellows.[21] Through folding, origami-based aerospace structures can exhibit such immense changes in size, and origami patterns such as the flasher, Miura–ori, and Yoshimura have been commonly demonstrated for this purpose. In addition, origami has been used for biomedical applications where tools or devices capable of folding and reconfiguration can aid in or improve certain procedures, such as deployable origami stents (Figure 1b, right),[12] origami forceps,[22] and origami-inspired surgical robots.[23]

While the foldability and shape reconfigurability of origami offers significant reconfiguration of structures, the conventional methods to actuate the shape change has largely relied on mechanical loads provided by hands, motors,[24–26] or pneumatic pumps.[4,11,27–29] However, the use of manual loading for engineering applications is often impractical, while motors and pneumatically driven systems are often bulky and require complicated control, especially for high degrees-of-freedom (DOF) actuation. On the other hand, active materials reconfigure in response to external stimuli, eliminating the need for external mechanical loads and bulky actuation systems.

In recent decades, active materials, also referred to as stimuli-responsive or smart materials, provide alternative strategies for

S. Leanza, S. Wu, R. R. Zhao
Department of Mechanical Engineering
Stanford University
Stanford, CA 94305, USA
E-mail: rrzhao@stanford.edu
X. Sun, H. J. Qi
The George W. Woodruff School of Mechanical Engineering
Georgia Institute of Technology
Atlanta, GA 30332, USA

The ORCID identification number(s) for the author(s) of this article can be found under https://doi.org/10.1002/adma.202302066

DOI: 10.1002/adma.202302066

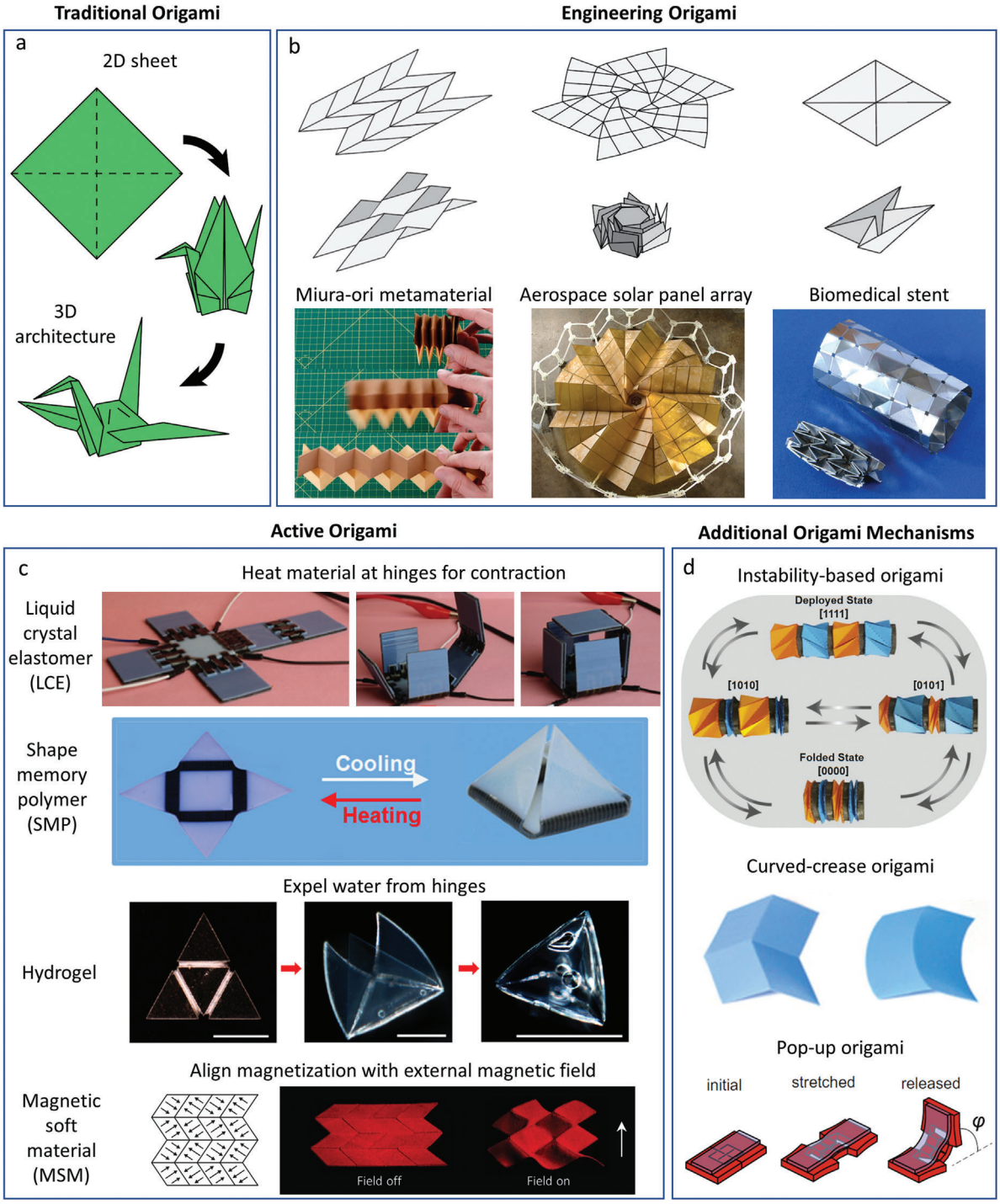

Figure 1. Introduction to traditional, engineering, and active origami. a) Schematic of traditional origami crane folding process. b) Different types of common engineering origami such as the Miura–ori pattern and associated metamaterials (Adapted with permission.[5] Copyright 2015, National Academy of Sciences); flasher origami pattern and deployable solar array (Reproduced with permission from the authors).[18] waterbomb base origami pattern and waterbomb tube biomedical stent (Reproduced with permission from the authors).[12] c) Representation of common actuation strategies for active origami, including heating of LCE hinges (Adapted with permission.[33] Copyright 2017, The Royal Society of Chemistry); heating of SMP hinges (Adapted with permission.[35] Copyright 2014, IOP Publishing); heating of hydrogel to expel water at hinges (Adapted with permission.[30] Copyright 2014, IOP Publishing); applied external magnetic field to actuate a magnetized MSM (Adapted with permission.[37] Copyright 2018, Springer Nature). d) Additional common origami mechanisms, including instability-based origami such as the Kresling pattern (Reproduced with permission.[73] Copyright 2020, National Academy of Sciences); curved-crease origami (as compared to straight-crease origami) (Adapted with permission.[98] Copyright 2020, the Authors, some rights reserved; exclusive licensee AAAS); pop-up origami initiated by a stretched kirigami substrate and maintained by an elastic layer of material (Adapted with permission.[101] Copyright 2019, Elsevier).

the actuation of reconfigurable systems. These materials and their composites with functional groups/fillers show response to external stimuli including light, heat, electric or magnetic fields, and pH. Utilizing active materials, for instance, shape memory polymers (SMPs) and alloys (SMAs), hydrogels, liquid crystal elastomers (LCEs), magnetic soft materials (MSMs), and covalent adaptable network (CAN) polymers, conventional origami has been advanced to active origami.[1,30–36] These origami systems actuated by stimuli-responsive materials have the advantages of being less bulky, as they do not require motors or other external actuators, light weight, programmable (and oftentimes re-programmable), remotely controllable or tetherless in many cases, as well as capable of selective or distributed actuation. These merits can enable applications in remote or biological spaces where conventionally actuated systems are less viable. To illustrate how these materials generally operate, several examples of active origami are shown in Figure 1c, in which a box with LCE at its hinges can be folded when heat is applied, causing the LCE to contract.[33] Similarly, a pyramid structure is actuated by its SMP hinges upon heating,[35] a hydrogel-based pyramid can fold when water is expelled from its hinges,[30] and a Miura–ori patterned MSM with embedded magnetic particles and precisely programmed magnetization aligns its magnetization with an external magnetic field and thus folds.[37]

Given many excellent recent reviews on stimuli-responsive materials and their applications,[38–44] origami-inspired functional designs,[7,45–48] and origami modeling,[49] this review will focus on summarizing the recent advances in origami systems that are enabled by active materials. We will qualitatively discuss the different origami mechanisms, material types and their actuation mechanisms, and advanced manufacturing of active origami systems and their applications. Section 1 briefly summarizes the common origami mechanisms and different hinge design strategies for the structural implementation of origami, followed by the actuation mechanisms of active materials and their applications in Section 2. In Section 3, manufacturing methods for active origami systems are introduced, including molding, additive manufacturing, and micro/nano-scale fabrication. Next, theoretical frameworks including both structural modeling and material constitutive laws that guide the design of active origami are briefly reviewed in Section 4. Lastly, in Section 5, we provide a discussion on the challenges and outlooks for the field of active origami.

1.1. Origami Mechanisms

In this section, different mechanisms which facilitate reconfiguration of origami structures are discussed, starting from classic origami patterns, and then moving on to discuss origami based on instability, curved-crease origami, and pop-up origami. It should be noted that certain types of origami fall under several of these categories. Additionally, "kirigami", or the art of paper folding where cuts are permitted, is inherently very closely tied to the art of origami. It is common for these two arts to be discussed in tandem,[7,45,46,50–53] especially when discussing real-world applications of origami which require more sophisticated structural designs and functional materials.

1.1.1. Classic Origami Patterns

Origami patterns transform between their folded and deployed states through rigid body rotation of panels, which are connected by hinges. Conventional origami patterns do not require bending, twisting, or stretching of panels, for example, Miura–ori,[54] waterbomb,[55,56] Tachi–Miura polyhedron,[57] stacked Miura–ori patterns,[5,58] square-twist,[59] Yoshimura,[60] and Ron Resch origami.[61,62] In real paper-based or polymer-based origami structures, however, deformation occurs most at the hinges while panel deformation can also occur. This enlarges the origami design space for patterns such as Kresling,[63–65] flasher,[1,18] and hypar origami,[66,67] and allows for higher DOF shape morphing.[68]

1.1.2. Origami based on Instability

Instabilities are commonly utilized in the folding and deployment of origami structures. Kresling origami,[69,70] for example, whose pattern is generated from the twist buckling of thin cylindrical shells, can be designed to be monostable or bistable. Bistability or multistability of other patterns such as the hypar[66] or square-twist[59,71] can be reached when allowing for panel bending. Another way that multi-stable origami structures have been achieved is via stacking of patterns. For example, the stacking of Miura–ori sheets yields a structure with multiple stable states.[72] In a similar way, stacked Kresling units have been demonstrated intensively as multistable structures (Figure 1d, top),[73,74] locomotive robots,[75] and metamaterials.[65] Multistable structures have the advantages of not requiring constant external force or stimulus for folding/deployment and can additionally allow for programmable stiffness of structures[73] or can be used for mechanical memory applications.[25,76]

Additional examples of reconfigurable structures based on instability can be found in slender structures. Examples include buckling of thin strips or patterned sheets to generate 3D architectures,[77–79] snap buckling of twisted rods to looped configurations,[80] and twisting of composite structures with prestressed flanges.[81] A related topic is ring origami,[82–85] or slender ring structures capable of folding via buckling instability when loads are applied. Those studied recently have been generalized to multiple different ring geometries, follow a self-guided snap-folding mechanism, and have been demonstrated for foldable trusses and devices.[86–90]

1.1.3. Curved-Crease Origami

Curved-crease origami was first documented in the 1930s[91] and then expanded to various patterns by artists, for example, concentric circles[92] and pleated hyperbolic paraboloid,[66,93] in which introduced curved creases distinguish them from the straight creases seen with conventional origami patterns (see Figure 1d, middle).[98] Elastic deformations in both the hinges and panels during the folding of curved-crease origami are essential and can lead to complex energy landscapes which are worth exploring for engineering design. While studies on curved-crease origami have largely been related to the mathematics of

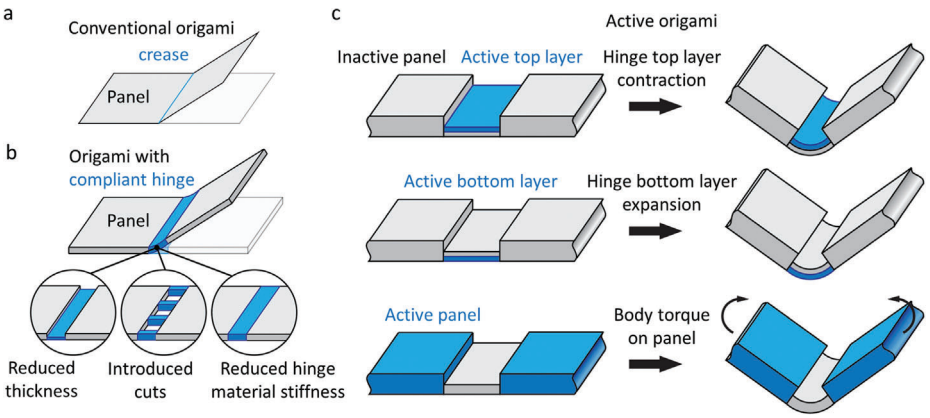

Figure 2. Hinge design and considerations for origami structures. a) Hinges for conventional paper-based origami that are introduced by creasing a sheet. b) Several methods to generate compliant hinges for origami with finite thickness including reduced thickness at the hinge, cuts introduced at the hinge, or reduced material stiffness at the hinge. c) Mechanisms for actuation when active materials are introduced to the structure.

describing different curved-crease patterns,[52] recent studies encompass engineering applications as well, with topics including metamaterials,[94] membranes for aerospace structures,[95] adaptive shading systems,[96] high-strength performance foldcores,[97] and robotic grippers with programmable stiffness and snapping behaviors.[98]

1.1.4. Pop-Up Origami

An additional type of origami, pop-up origami, is characterized by 2D sheets that can "pop up"/assemble to 3D configurations. Pop-up origami is most often achieved through the release of prestressed substrates to trigger out-of-plane deformation of thin sheets to a variety of different 3D states.[77,99,100] Other pop-up origami, however, can be triggered by multistability or plasticity of kirigami patterns paired with elastic materials (Figure 1d, bottom),[101] external mechanical loading of kirigami,[102] lamination of layered sheets,[103] or ion beam irradiation of thin metal films.[104] While pop-up origami is applicable to many size scales, it has shown especial promise for the fabrication of small-scale electronics,[105] biomedical devices,[23,106] and reconfigurable robots[107–109] with complex geometries.

1.2. Structural Implementation of Origami

For conventional paper-based origami, creases are introduced by plastically deforming the sheet (**Figure 2**a). The creases, whose stiffness is lower than the undeformed panels, serve as the hinges about which the panels rotate so that different configurations of the origami can be realized. While paper-based origami has been widely used for artistic purposes and for some additional small-scale electronic or sensing applications,[110–112] many other practical applications of origami, however, involve materials with more appreciable thickness. Because of this, there have been many works to address the structural design of origami that accounts for the panel and hinge thickness.[113,114,18] Thus, to enable folding of these more broadly encompassed origami structures, tactics are needed to generate compliant hinges. As depicted in Figure 2b, reduction in thickness at the hinge, introduction of cuts at the hinge, or introduction of a lower-stiffness material at the hinge are all methods that make folding possible for these origami structures (see Section 4.1 for details on structural modeling of origami). Starting from a structure with the compliant hinge design, there are several hinge actuation mechanisms enabled by the incorporation of active materials that result in the desired folding of an active origami structure (Figure 2c). By either introducing a bilayer hinge with a contractible material on top, a bilayer hinge with an expandable material on the bottom, or an inactive hinge attached to active panels capable of generating torques (most common with MSMs), the same general upward folding of the panels can be achieved once the active material is actuated. From here, it can be seen that there is a considerable design space for structural implementations of active origami.

2. Active Materials for Origami Actuation

Table 1 summarizes the main active materials that will be discussed in this review, along with the stimulus that leads to the actuation, the mechanism by which these materials operate, a broad summary of performance details such as actuation speed and stiffness of the materials, and the applications that these active origami systems have been designed for. The details of these different active origami will be discussed in their respective sections.

2.1. Shape Memory Polymers (SMPs)

SMPs can be programmed into temporary shapes and recover their permanent shape upon external stimuli, such as heat, light, or magnetic field. The shape of SMPs can be changed and easily recovered, enabling a wide variety of uses in deployable aerospace structures,[193] biomedical applications,[194] and flexible electronics.[195] SMPs have the ability to be programmed into arbitrary shapes and to maintain this temporary shape at ambient conditions. In addition, for amorphous polymer-based SMPs,

Table 1. Summary of active materials, actuation mechanisms, performance details, and applications.

Material	Actuation stimulus	Actuation Mechanism	Performance Details	Applications
Shape memory polymers (SMPs)	Heat[1,35,115–136] Light[137–143] Humidity[144,145] Chemical[141]	Release of pre-stress at hinges[1,35,115–136,138–145]	Moderate actuation time (s–min) Higher stiffness and actuation stress (MPa–GPa) Oftentimes only have one-way actuation	Biomedical[131,132] Aerospace structures[1,126,128] Energy harvesting[130] Shock absorption[127,129]
Hydrogels	Water[59,146,147] Heat[59,147–152] Light[148,153,154] pH[152,155–157] Ionic strength[156,157]	Swelling at bilayer hinge[59,146–149,151,152,154–157] Swelling with porosity gradient[153] Swelling with crosslinking gradient[155]	Slow actuation (min–hrs) Lower stiffness and actuation stress (kPa) Reversible deformation Operate in aqueous environments	Metamaterials[158,159] Drug delivery robots[160] Cell encapsulation or excision robots[161–164]
Liquid crystal elastomers (LCEs)	Heat[33,165–173] Humidity[174,175] Light[176,177]	Bilayer hinges[33,177] Fiber actuation at hinges[33,178–180] Twisted nematic or splayed hinges[171,173]	Fast actuation (ms–s) Moderate stiffness and actuation stress (kPa–MPa) Reversible deformation	Biomimetic actuators[165,168] Locomotive robots[168,172,181]
Magnetic soft materials (MSMs)	Magnetic field[31,37,182–189]	Body torque of panels[37,182–186,188–192]	Fast actuation (ms–s) Material properties depend on matrix material Reversible deformation Tetherless actuation	Drug delivery[75] Biomimetic robots[75,183] Robots for object transportation[31,183,186] Metamaterials[187,189]

their elastic modulus can shift by nearly three to four orders of magnitude before and after their glass transition.[196] This high modulus (oftentimes on the scale of a few GPa) at low temperatures can offer the advantage of load-carrying capabilities. In addition, the actuation of SMPs typically takes several seconds to several minutes.[193,197,198]

2.1.1. Shape Memory Mechanism

From a mechanistic point of view, SMPs are network polymers composed of switching segments (molecular chains) and netpoints (chemical or physical crosslinks),[198] as indicated by the blue lines and black dots, respectively, in **Figure 3**a. These polymers have a transition temperature (T_{trans}) such as a glass transition (T_g) or melting (T_m) temperature, above which the material will be programmable. A typical shape memory cycle involves two steps. In the first step (or the programming step), the SMP is heated to above T_{trans}. It becomes rubbery, exhibits an increase in chain mobility, and can be easily deformed into a programmed shape. As the deformation is maintained and the temperature is lowered to below T_{trans}, the segments become frozen and maintain their deformed chain configurations as well as the deformed shape of the SMP. This state is commonly referred to as the temporary shape. During the second step (or the recovery step), the SMP is heated above its T_{trans} again, during which the polymer chains regain mobility and entropy drives the polymer back to its permanent shape. An example of the process is shown in Figure 3b,[115] where an SMP box programmed to be temporarily open (Figure 3b-i) gradually returns to its permanent folded shape (Figure 3b-ii) upon heating. It should be noted that, for most SMPs, this is a one-way shape memory process: the SMP cannot shift between two shapes as it is heated and cooled, and it must be mechanically programmed again to exhibit another cycle of the shape memory effect. Two-way shape memory, a reversible process in which the material can switch back and forth between two shapes by heating above and cooling below T_{trans} is also achievable, but typically requires special design of polymer composites or macromolecular structures.[199–201] It should also be mentioned that multi-shape-SMPs[202,203] are those which can switch between more than two shapes and can be obtained by using multiple transition temperatures and programming steps.

2.1.2. SMP Origami

Depending on the T_{trans} of the material, SMP-based active origami has the advantage of maintaining its temporary shape at ambient conditions. One way that SMPs have been used to achieve active origami is to utilize pre-stretched sheets.[116,125,133,138–140,143] Since these sheets begin as pre-stretched, they are initially in their "temporary" shapes and, upon heating, they relax and thus contract. Origami constructed of these sheets was first demonstrated by Liu et al.,[139] where black ink (serving as hinges) was printed on either side of a polystyrene (an SMP) sheet. Under IR light, the black ink absorbed light and transferred heat to the SMP underneath, causing a temperature gradient through the thickness of the film to result in bending toward the ink-patterned side. Thus, by patterning ink on either side of the film, unidirectional or bidirectional folding (Figure 3c) was achieved under the stimulus of unfocused light. Folding structures such as a box, pyramid, and bidirectional folding strips were demonstrated with this approach, and similar approaches were used later on.[138,140,143] Tolley et al.[116] developed

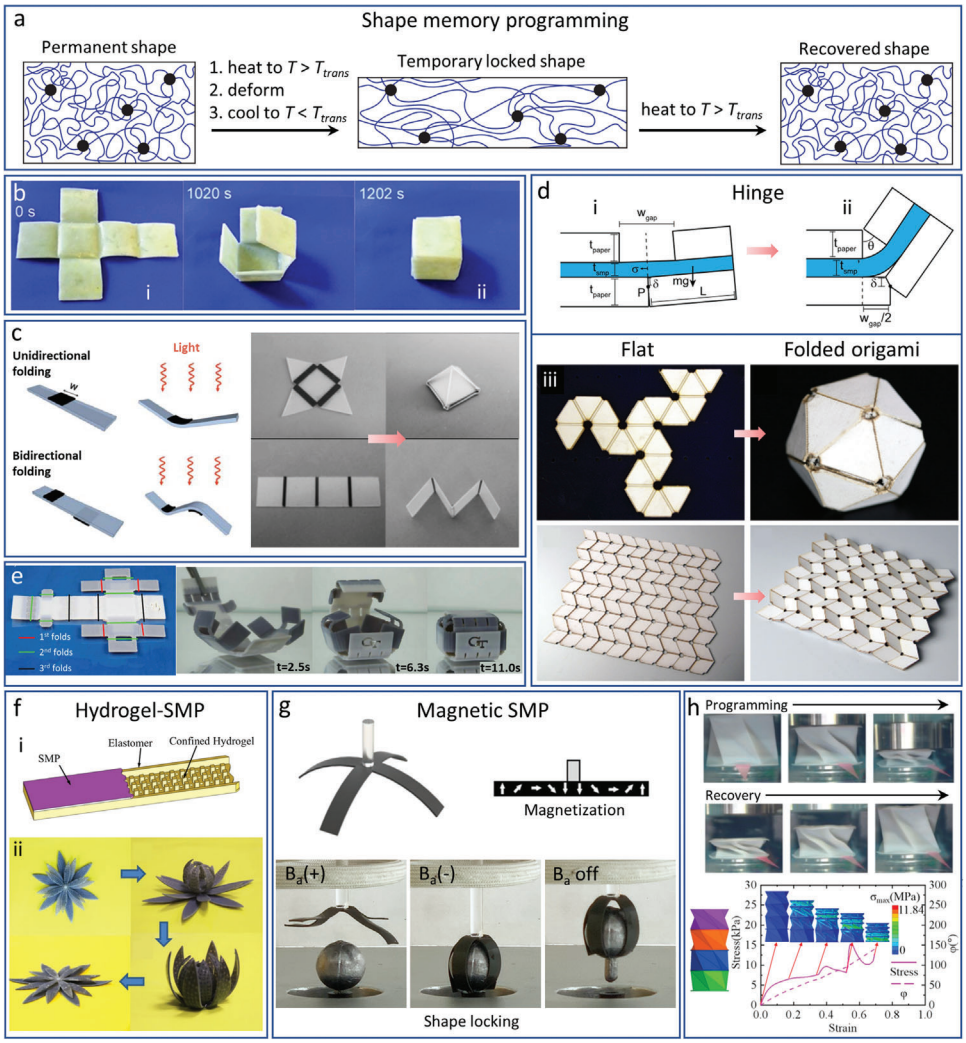

Figure 3. SMP mechanism, origami, and applications. a) Shape memory effect of an amorphous SMP. b) One-way shape memory process of an SMP box upon heating (Adapted with permission.[115] Copyright 2010, Wiley). c) Self-folding of pre-stretched sheets by local light absorption (Adapted with permission.[139] Copyright 2012, The Royal Society of Chemistry). d) Self-folding of layered structures with prescribed folding angle under uniform heating (Adapted with permission.[116] Copyright 2014, IOP Publishing). e) Sequentially folded and locked box by hinges of different T_{trans} under uniform heating (Adapted with permission.[117] Copyright 2015, Springer Nature). f) Hydrogel-SMP composite structures with reversible actuation (Adapted with permission.[204] Copyright 2016, Springer Nature). g) Magnetic SMP gripper with locking capabilities (Adapted with permission.[207] Copyright 2020, Wiley). h) SMP Kresling-based metamaterial with tunable mechanical properties (Adapted with permission.[127] Copyright 2020, Elsevier).

one-way SMP origami structures with predictable folding angles by placing the SMP sheet between two stiff paper layers, with the hinges located at the gaps between paper layers (Figure 3d-i). When heated, the sheet contracted, causing bending at the hinges, which ceased when the panels were in contact with one another, resulting in a controlled bending angle (Figure 3d-ii). With this approach, they demonstrated the folding of a polyhedron, Miura–ori (Figure 3d-iii), and various other origami structures.

While the hinges discussed above exhibit the same general response to a homogeneous stimulus, hinges can also be designed to fold sequentially and enable complex folding routines. Mao et al.[117] used SMPs with different glass transition temperatures to design hinges and achieved sequentially self-folding and self-locking structures. They demonstrated a folding box (Figure 3e), which requires sequential actuation of hinges to avoid interference or collision of panels during the folding process. Guided by finite element analysis (FEA) simulations and a reduced order model to predict collision of panels during folding, SMP hinges of three different T_{trans} were chosen, in which fast-folding hinges had low T_{trans} and slow-folding hinges had high T_{trans}, to enable the sequential folding of a self-locking box (Figure 3e). This work emphasized the importance of the planning of folding sequence in complex active origami structures. Other approaches have also been taken to achieve sequential folding. For example, by using the same material as that in their initial[139] work, Liu et al.[140] later achieved sequential folding by using hinges of different colored inks that absorbed IR light with different efficiency, allowing for sequential folding of a variety of structures.

As discussed previously, most SMPs cannot achieve reversible actuation. Therefore, active origami that solely uses SMPs cannot typically have desirable reversible folding and unfolding. One way to realize reversibly foldable active origami is through SMP composites, in which another active material drives (or programs) the shape change while the SMP locks it. Mao et al.[204] demonstrated this concept with structures composed of a hydrogel, an elastomer, and an SMP. As seen in Figure 3f-i, a structure was designed with an SMP top layer, elastomer side and bottom layers, and hydrogels confined by columns between the top and bottom layers. Upon swelling in water and heating to soften the SMP layer, the structure bent toward the elastomer layer. The structure was then cooled to stiffen the SMP and thus lock the temporary shape. After drying of the hydrogel, the locked shape was still maintained. The original shape of the structure could be recovered by heating it again, allowing the SMP to return to its equilibrium shape. This process could be repeated, enabling reversibly foldable and un-foldable SMP composite structures (Figure 3f-ii). Recently, this approach was further developed by simply using an SMP/hydrogel bilayer to enable reversible shape change by Yuan et al.[205]

Magnetic particles have also been used to establish similar functionality in SMPs. This type of material capable of reversible shape transformation has been termed as magnetic SMP (M-SMP). Photothermally heated M-SMP and inductively heated M-SMP have been developed by Liu et al.[206] and Ze et al.,[207] respectively. In the work by Ze et al.,[207] an M-SMP with two different types of magnetic particles (NdFeB and Fe_3O_4) was created. The Fe_3O_4 particles enabled inductive heating of the SMP under a high frequency alternating current (AC) magnetic field (heating magnetic field), while magnetized NdFeB particles drove shape change of the SMP by aligning the polymer's magnetization direction to an actuation magnetic field. When the heating magnetic field was turned on, the M-SMP became soft and could easily be deformed into a desirable shape by the actuation magnetic field. Further, by keeping the actuation magnetic field on but ceasing the heating magnetic field, the M-SMP cooled down until it stiffened. After the actuation magnetic field was turned off, the temporary shape was fixed, and this method was demonstrated for the use of a soft gripper (Figure 3g). The incorporation of SMP with other active materials such as LCEs has also been demonstrated recently,[208] and it can be seen that SMP composites allow for various interesting deformations and functionalities.

SMPs enable a wide variety of applications, across many different fields of research. One application of SMPs has been active metamaterials,[119,125,129,209] which can exhibit special mechanical properties. For example, Tao et al.[127] designed SMP Kresling-based metamaterials in which temperature could be used to control the load bearing and energy absorption capabilities of the structures. As shown in Figure 3h, structures could be designed to fold in sequential ways due to the geometry of the Kresling origami used, which could be utilized for impact mitigation or soft robotic applications. Recently, biocompatible shape memory materials such as keratin[210] have also been explored for active origami, potentially for use as smart textiles. Chen et al.[1] demonstrated the use of SMPs in facilitating the deployment of flasher origami solar arrays for potential aerospace applications. Additionally, SMPs have been used for other exciting applications such as robotic joints with tunable stiffness,[211,212] deployable origami sandwich structures,[126] origami reflector antennas,[128] carbon nanotube (CNT)-SMP-based foldable solar evaporators,[130] and origami biomedical devices.[131,132]

2.2. Hydrogels

Hydrogels are network polymers that can absorb large amounts of water. Some hydrogels can exhibit macroscopic deformation by absorbing (swelling) or expelling (de-swelling) water in response to changes in stimulus such as heat, pH change, ionic strength, and light. The stiffness and actuation stress of hydrogels typically lie between a few kPa to several hundred kPa.[213,214] Hydrogel actuation is slow, as it is driven by a diffusion process. This results in hydrogel actuation occurring anywhere from tens of minutes to several hours. Storage of elastic potential energy,[215] utilization of instabilities,[216] incorporation of particles for hydrogel composites,[148,153] or confined swelling environment for retention of high osmotic pressures[217] have all been taken advantage of for increasing either the actuation speed, force, or mechanical strength of hydrogels. Due to their low elastic modulus comparable to biological materials and tissue,[218] hydrogels are often designed by using biocompatible polymers, making them widely used for biomedical applications, such as patches[219] and drug delivery.[160] Hydrogels are also used in soft robotics including biomimicking systems,[220] locomotive robots,[221–223] as well as active origami.[147,148,156]

2.2.1. Hydrogel Mechanism

In general, hydrogel swelling or de-swelling is due to the interaction between the polymer chains and the surrounding solvent molecules. In a good solvent, in which the interaction between the polymer chains and the solvent is preferred, polymer chains are arranged as hydrophilic "coils" and the hydrogel can absorb solvent (such as water). On the other hand, in a poor solvent, in which the interaction between polymer chains with one another is preferred, polymer chains become hydrophobic "globules" and the solvent will be expelled. Under different conditions such as varied temperatures or pH, a solvent can be good or poor with respect to the polymer chains, leading to a volume phase transition of the hydrogel.[224,225] For example, some hydrogels, such as poly(N-isopropylacrylamide) (pNIPAM), will repel water once heated above the hydrogel's lower critical solution temperature (LCST) and the hydrophilic coils will become hydrophobic globules (**Figure 4**a). It is important to note that swelling of neat hydrogels is isotropic, so to achieve more complex deformation necessary for origami, tactics such as varied crosslinking densities,[150,226] porosity gradients,[153] or structures such as bilayers of materials with different swelling capabilities,[147,161,227] are often used. Among these tactics, bilayers are the overwhelmingly popular method for the creation of hydrogel hinges for origami.

2.2.2. Hydrogel Origami

Bilayer-based hinge design typically consists of a layer of active material and a layer of inactive material, or two active

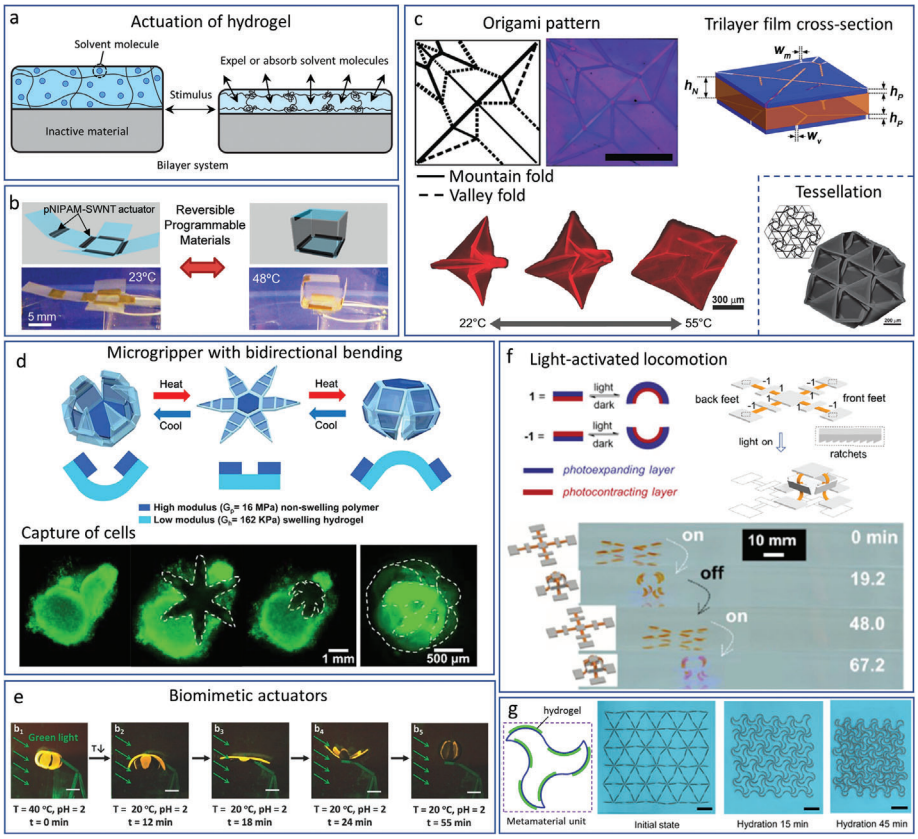

Figure 4. Hydrogel actuation mechanism, origami, and applications. a) Hydrogel actuation mechanism: swelling, de-swelling. b) Reversible folding and un-folding of a box with hydrogel at the hinges (Reproduced with permission.[148] Copyright 2011, American Chemical Society). c) Micro-scale trilayer origami with complex deformation (Adapted with permission.[147] Copyright 2015, Wiley). d) Hydrogel gripper capable of locomotion and cell capture/excision (Adapted with permission.[161] Copyright 2015, American Chemical Society). e) Hydrogel actuator with synergistic deformation and color change (Adapted with permission.[152] Copyright 2018, Wiley). f) Hydrogel robot with octopus-like locomotion (Adapted with permission.[237] Copyright 2021, Elsevier). g) Hydrogel metamaterials with negative swelling behavior (Adapted with permission.[159] Copyright 2018, the Authors, some rights reserved; exclusive licensee AAAS).

materials with different stimuli-responsiveness. For example, Zhang et al.[148] used a hinge consisting of a layer of pNIPAM hydrogel and a layer of low-density polyethylene (LDPE) for different origami structures (Figure 4b). To simplify the fabrication, hydrogel was only used in the patterned hinge regions. They further loaded CNTs in the hydrogel to tune the response time and to allow for near-IR irradiation-induced folding. Many other materials such as graphene oxide or reduced graphene oxide,[152,153,228–230] MoS_2,[154] and clay[151,157,228] have also been incorporated with hydrogels to enhance the response time and/or mechanical properties. It should be noted that other various demonstrations of bilayer hydrogel origami have been conducted by Ionov and coworkers, who have studied self-rolling bilayer films[227] which can fold to 3D structures[149,216] such as pyramids.

While the abovementioned bilayer origami is relatively simple, multi-layered designs have also been used to enable more complex hydrogel origami.[59,147] Na et al.[147] demonstrated micro-scale origami with controlled mountain and valley folds with a three-layer design: a thermoresponsive hydrogel layer between two rigid polymer layers patterned with crease lines for either mountain folds or valley folds. Upon immersion in water below the LCST, the origami self-folded to its complex micro-scale shape (Figure 4c), while it nearly reversibly returned to its original configuration when heated above the LCST. They also demonstrated the folding of a tessellation with 198 patterned creases (Figure 4c). Although the origami shown is very impressive, it is important to note that such complex self-folding origami can suffer from mis-folding,[116,231] resulting in final configurations that are different from the desired ones. To address this issue, the same group used hydrogels with two different LCSTs, patterned in a way such that the vertices of a complex origami design could be pre-biased[232] toward certain directions, allowing for more reliable sequential folding of the origami creases to the desired final 3D shape.

As mentioned previously, hydrogels have been widely used for biomedical applications. Self-rolled tubes for vascularization[233] as well as numerous grippers[30,161,162,234] for drug delivery or cell removal (biopsy) in surgical applications have been demonstrated with hydrogels. Notably, Gracias and coworkers[161,162] have created origami microgrippers by incorporating stiff polymer panels with a thermoresponsive hydrogel substrate, where the stiffness of the panels granted additional functionality to the gripper, such as the possibility of cell excision. Grippers were able to locomote[161] via the incorporation of magnetic particles into the hydrogel layer, allowing remote control by a magnetic

probe. Cell excision was accomplished by placing the grippers in a warm environment with cell tissue. Starting in a closed configuration, upon heating, the gripper opened up and folded in the opposite direction, grasping a portion of tissue (Figure 4d) and excising the cells from the tissue upon full closure of the gripper. Additionally, drug delivery[162] from the grippers was demonstrated by the incorporation of drugs into the layers of the gripper. Other origami-like approaches to drug delivery[160] and cell/particle encapsulation[163,164] using hydrogels have been explored as well.

Aside from biomedical applications, hydrogels are also pertinent to biomimetic applications, with some hydrogels exhibiting synergistic fluorescent color and shape change.[152,235] Ma et al.[152] designed a bilayer gripper (Figure 4e) with the bottom side as a thermoresponsive hydrogel. At high temperatures, the bottom layer expelled water and this led to downward bending, exhibiting a fluorescent top layer under the green light. Upon a decrease in temperature, however, the actuator would bend upward and the color would change as a result. Another exciting and recent example of biomimetic origami was the utilization of hydrogel on a polydimethylsiloxane (PDMS) substrate with microfluidic channels.[220] The device could respond to temperature, light, and humidity for an environmentally responsive actuator with plant-like movements and photosynthesis capabilities. Lastly, light-actuated hydrogel origami[230,236,237] has enabled soft robots capable of crawler and octopus-like[237] motions. By utilizing bilayers composed of spiropyran functionalized with photocontracting and photo-expanding hydrogel, Li et al.[237] achieved large bending deformation. By integrating the bilayers with ratcheted feet for anisotropic friction with a substrate, they achieved biomimetic, octopus-like motions (Figure 4f) upon repeated relaxing and contraction of the bilayers.

Additional hydrogel origami applications entail metamaterials with negative swelling enabled by positive-swelling hydrogel.[159,238] Zhang et al.[159] utilized hydrogel to achieve metamaterials with negative swelling (Figure 4g) by adjusting the initial geometry of the metamaterial units. In changing the unit geometries, metamaterials with expansion in one direction and contraction in the orthogonal direction were achieved, demonstrating interesting mechanical properties. Also, hydrogel for the assembly of 3D, origami-like structures used for acoustic metamaterials has been demonstrated by Deng et al.[158]

2.3. Liquid Crystal Elastomers (LCEs)

LCEs are a class of active materials that exhibit large, reversible[239] deformation upon exposure to stimuli such as heat,[240,241] light,[242,243] solvents,[244] electric,[245,246] or magnetic[247] fields. LCEs are elastomers which have elongated, anisotropic mesogens (typically composed of rigid aromatic or cyclohexyl rings[248,249]) fixed to the polymer main chain or sidechains by covalent bonds and crosslinks.[248] The flexible nature of the elastomer allows for changes in the ordering of the mesogens upon stimuli, along with reversible actuation.[250,251] Mesogens in LCEs are programmed to have long-range orientational order described by a director, which means that it has a high level of molecular order similar to that of a crystalline solid, while maintaining fluidity similar to a viscous liquid.[252] LCEs can exhibit mechanical, optical, electrical, and magnetic anisotropic properties[248,253] in their ordered, or most commonly "nematic", state and isotropic behaviors in their disordered, or "isotropic", state.[248] Due to their ease of reversible deformation and large actuation strain, LCEs are used for a number of applications, including artificial muscles[239,241,254] and smart textiles.[255] Additionally, because the actuation of LCEs is a phase transition process not governed by diffusion, LCEs can actuate in several seconds, or even in a fraction of a second.[181,256] The stiffness of LCE and the actuation stress, on the other hand, usually range from hundreds of kPa to several MPa.[241,256,257]

2.3.1. LCE Mechanism

The actuation of LCEs is due to the transition from a liquid crystalline phase, such as nematic or smectic, to an isotropic phase in response to a stimulus (typically temperature) that disrupts mesogen alignment (**Figure 5**a). For most LCEs, there exists a phase transition temperature referred to as the nematic to isotropic phase transition temperature (T_{NI}). Application of an appropriate stimulus leads to a contraction parallel to the director of the LCE.[239,258] Upon heating, polymer chains gain entropy and become more coiled, causing mesogens to lose their alignment and become randomly oriented, resulting in a macroscopic shrinkage of the LCE.[249,250,259] Thus, the alignment and orientation of mesogens in LCEs are of critical consideration in LCE applications. Previously, mesogens were commonly aligned via surface rubbing[260] or electric fields,[261] which are relatively tedious methods. More recently, a two-step reaction method developed by Yakacki et al.[262] is often used, which first involves a thiol-Michael addition "click" reaction to form the polydomain LCE (or LCE without long-range order), followed by alignment of mesogens by stretching, and final locking of the alignment via photopolymerization reaction. Planar nematic, twisted nematic, and splay are common liquid crystal orientations for LCEs. Twisted and splay orientations (Figure 5b)[263] involve variations in the director through the thickness of the material, allowing for more complex deformation. In twisted and splay orientations, there exists a 90-degree rotation of the director through the material thickness. Twisted orientation involves an in-plane rotation of the director while splayed is out-of-plane. When an appropriate stimulus is applied, mismatches in the expansion of the surfaces leads to bending/folding behaviors.[244,264] Because of this, different mesogen orientations can be exploited for origami-like deformations of materials.

2.3.2. LCE Origami

Thermo- and light- responsive LCEs comprise the majority of LCE origami works, although it should be noted that humidity and water-stimulated folding of LCE-based structures is also achievable, often via bilayers,[265] alkaline,[174] or acidic[175] surface treatment to enable asymmetric humidity response. White, Ware, and collaborators have done a series of works related to the folding of LCE. In a seminal work, they enabled the programming of complex director orientations into thin LCE via surface

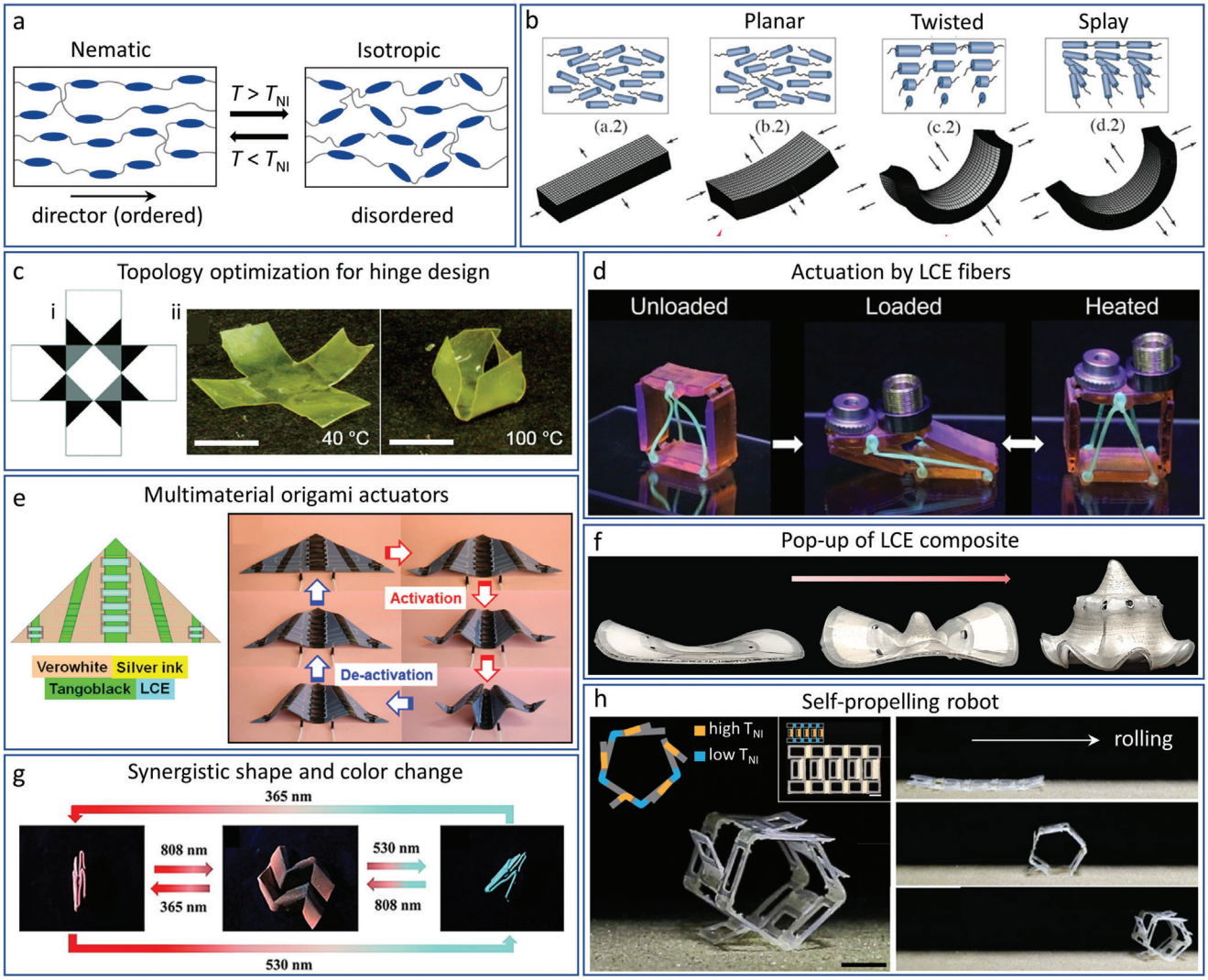

Figure 5. LCE actuation mechanism and origami. a) Nematic (ordered) to isotropic (disordered) transition of LCEs. b) Macroscopic deformation of LCE according to common mesogen alignments (Adapted with permission.[263] Copyright 2020, AIP Publishing). c) Optimal hinge design for LCE box and folding of LCE upon heating (Adapted with permission.[171] Copyright 2015, The Royal Society of Chemistry). d) Deployment of reconfigurable structure by actuation of LCE fibers (Reproduced with permission.[179] Copyright 2022, Wiley). e) Multimaterial origami airplane structure with LCE actuators triggered by Joule heating (Adapted with permission.[033] Copyright 2017, The Royal Society of Chemistry). f) Pop-up of a liquid metal (LM)-LCE composite triggered by induction heating (Adapted with permission from the authors).[181] g) LCE origami with synergistic shape and color change (Reproduced with permission.[168] Copyright 2021, Wiley). h) Self-propelled LCE rolling robot (Adapted with permission.[172] Copyright 2019, AAAS).

alignment, in which local twisted nematic alignments were effectively defined as the origami hinges.[173] Upon heating, the flat sheet would fold into Miura–ori. However, a downside was the lack of control over folding upon heating. They later used the same surface alignment technique and developed a topology optimization[171] method to generate more reliable hinge designs, with an aim to avoid anti-clastic, saddle-like curvature seen in the actuation of twisted nematic LCEs.[264,266,267] Their optimal hinge involved programmed triangular regions near the substrate's corners (Figure 5c-i) with approximately twisted nematic order patterned through the thickness for nearly complete closure of the box upon heating (Figure 5c-ii). They further used LCE-CNT composites[176] as the hinges to enable a light-activated LCE folding box that took advantage of CNT photothermal effects. Lastly, Donovan et al.[268] demonstrated a long-lasting folded LCE box by incorporating o-fluorinated azobenzene into the polymer network. The trans-to-cis isomerization of the o-fluorinated chromophores resulted in directional strains on the LCE and allowed for the macroscopic deformation, which could last for multiple days. This type of prolonged deformation of LCE can be beneficial, as a constant stimulus would typically be needed for LCE to maintain its deformation, which may unnecessarily consume energy. This topic will be discussed further in Section 2.5.

Other origami-like folding of flat sheets to 3D shapes has been achieved by introducing complex LCE director distributions realized by photoaligned substrates or molds with micrometer-scale channels.[269–272] Another more simplified approach was to

program the folding of bilayer origami LCE sheets by spraying LCE onto thermoplastic sheets, as demonstrated by Verpaalen et al.[177] Upon thermally shaping and fixing the sheets, sharp, origami-like folds could be introduced. These thin bilayer strips were actuated by UV and blue light and simple deformation from accordion to flower-like shape was demonstrated.

Instead of designing LCE origami based on entire sheets of LCE, axially aligned LCE fibers, or strips of LCE that contract along their length when actuated, can also be selectively placed among origami structures to generate folding.[178–180,33] As seen in Figure 5d, Peng et al.[179] printed LCE fibers onto a square-shaped reconfigurable structure. When the structure was loaded, it fell to a parallelogram-like shape that could be deployed back to the initial state upon heating the fibers. In their work, they also demonstrated deployment of a printed tensegrity structure and reconfiguration of an LCE lattice pyramid. An additional advantage of the use of LCE fibers/strips compared to LCE sheets is that they can be selectively actuated by methods such as Joule heating, which can enable more complicated folding routines. By using LCE fibers as the actuators, Yuan et al.[33] demonstrated a variety of multimaterial origami structures composed of an elastomeric material (Tangoblack by Stratasys (Rehovot, Israel)), a rigid polymer (Verowhite by Stratasys), and a conductive ink. They obtained an inactive substrate by inkjet printing and then printed conductive ink onto this substrate via direct ink writing (DIW), after which they incorporated the LCE strips into the predetermined positions atop the ink. Under an applied current, the conductive ink was Joule heated, leading to the actuation of the origami. Once the current was ceased, the LCE cooled down and the actuator gradually returned to its original flat state. An airplane actuator, as seen in Figure 5e, utilized LCE fibers on the top and bottom sides to serve as actuators for upward and downward bending, respectively. Miura–ori, as well as a sequential folding box were also demonstrated with this method.

While sequential or selective actuation (and thus folding) of LCE origami can be obtained from Joule heating, a limitation of this is that wires are often needed to supply current, which complicates the structure. In a recent work, Maurin et al.[181] developed liquid metal (LM)-LCE composites that could be remotely heated by induction under alternating magnetic fields. The heating of LCE was concentrated in regions where the LM was located, and the LM could be patterned arbitrarily due to the LM-spraying method that was used. By varying the quantity of LM and the LM pattern, as well as the alignment of LCE and the magnitude of the applied magnetic field, the actuated shape of the LCE could be programmed. As shown in Figure 5f, an LCE sample with circumferential alignment (which buckles out of plane when actuated[173]) and LM throughout the composite sequentially "pops up" under an increasing magnetic field, where the centermost LCE buckles first, followed by the outermost LCE. In their work, the LM-LCE composite was also used to design sea-turtle-inspired actuator "fins" for a biomimetic turtle robot.

Efforts have also been taken to realize color change during the actuation of LCE origami.[165,168] Huang et al.[168] recently presented luminescent LCE origami by incorporating fluorescent and color-changing agents into the LCE matrix, including a blue-green fluorescent moiety tetraphenylethene, a photochromic moiety spiropyran, and an NIR photothermal dye YHD796. NIR light was used as a heat source to facilitate the deformation of the LCE, while UV and visible light were used for reversible color change between green-blue and red at folded states and dull red at deployed states (Figure 5g). Both Miura–ori and Yoshimura origami were demonstrated by introducing folds mechanically, creating a gradient of mechanical stress that allowed for reversible folding and unfolding. By controlling the applied light, synergistic shape and color change of the origami was achieved, enabling biomimetic behaviors such as camouflaging.

LCE-based active origami has also been used to generate locomotion for robotics applications. Kotikian et al.[172] assembled multiple different examples of LCE origami, taking advantage of thermoresponsive LCEs with different nematic to isotropic transition temperatures. They utilized rigid acrylate panels with LCE bilayer hinges. The hinges involved two LCE layers printed orthogonal to one another to enable large bending curvatu res (up to 180 degrees). To achieve sequential folding, they strategically used hinges with LCEs of either high T_{NI} or low T_{NI} throughout their designs, and demonstrated sequentially foldable structures, as well as a self-propelling, rolling robot, as shown in Figure 5h. This robot utilizes low T_{NI} (blue) hinges to gradually fold the body into a pentagonal prism and high T_{NI} (orange) hinges to propel the robot forward, allowing for continual rolling motion. Upon activation by a hot plate, the hinges provide torques which sustain the forward motion of the robot, even after undergoing a full revolution. Other works have demonstrated locomotion via LCE actuation for crawling[273] origami robots. Additional exciting LCE origami applications include thermoresponsive LCE kirigami metasurfaces[274] and LCE metamaterials demonstrated as shrinkable patches for skin regeneration.[275]

2.4. Magnetic Soft Materials (MSMs)

MSMs are a class of active materials that permit fast, reversible, and untethered deformation under an applied external magnetic field. MSMs for active origami are obtainable by various strategies, including embedding magnetic particles into a polymeric matrix or coating structures with magnetically responsive metal particles.[182] The magnetic fillers or coatings are the essential components of MSMs for generating mechanical load (body torque) or heat under the external magnetic field, realizing the shape morphing of active origami. Various types of magnetic fillers, with ferromagnetic (soft-magnetic, hard-magnetic), or superparamagnetic properties, behave differently under a magnetic field and require specific control strategies. Magnetic fillers can be integrated with inactive soft polymers or functional active matrices of SMP, LCE, hydrogel, dynamic polymer, etc. Due to the wide range of materials that MSMs can be based on, the stiffness and actuation stress of these materials varies accordingly. In addition, MSMs can actuate rapidly, from tens of microseconds to seconds.[37,38,276] This section focuses on how magnetic fillers and magnetic control facilitate reconfiguration and locomotion of active origami systems. Active origami that incorporates magnetic fillers with specialized polymeric matrices, for example, inductive heating of SMP by embedding superparamagnetic particles, is discussed in the corresponding material section.

2.4.1. Magnetic Actuation Mechanism

The certain magnetic fillers and coatings used in MSMs decide their actuation mechanisms. Soft-magnetic materials (iron, nickel, iron–nickel alloys) cannot retain strong remanent magnetization and can be easily de-magnetized and re-magnetized by an applied magnetic field. Because of this, these materials rely on a gradient magnetic field to generate force. Therefore, structures and materials embedded/coated with soft-magnetic materials require a gradient magnetic field in order to be actuated. A gradient magnetic field can simply be obtained by a permanent magnet.[277] A moving magnet can be used for locomotion and navigation of MSM active origami systems due to the attraction force toward the magnet. However, the magnetic field gradient is typically nonuniform around a magnet, making the programmability and accurate control of soft-MSMs relatively limited. On the other hand, hard-magnetic materials such as chromium dioxide (CrO_2), neodymium–iron–boron (NdFeB), and hard ferrite can retain strong remanent magnetization after being magnetized under a strong magnetic field (1.5 to 2 T). When a uniform magnetic field is applied, a torque can be generated to rotate the magnetic materials so that their magnetization is aligned with the applied magnetic field. Since a uniform magnetic field can be generated by a pair of Helmholtz coils, the use of hard-magnetic particles as fillers is thus promising, as more accurate programmability and control can be obtained. Therefore, this section mainly discusses MSMs using hard-magnetic materials (referred to as hard-MSMs). It should be noted that hard-MSMs can be re-magnetized by either heating them to above their Curie temperature followed by applying a strong magnetic field (1.5–2 T) or by directly applying a strong magnetic field. As illustrated by a beam with the programmed magnetization along its axial direction (**Figure 6**a), micro-torques are exerted on the hard-magnetic particles when their magnetization is not aligned with the applied magnetic field B. These micro-torques are transmitted to the soft matrix and lead to a bending deformation under an upward magnetic field.[278] Another prominent feature of hard-MSMs is the flexibility to pattern magnetization distributions on demand, permitting complex shape reconfiguration of active origami. Kim et al.[37] developed a DIW printing method of hard-MSMs, which programs the magnetization along the filament printing direction (more details discussed in Section 3.2.1). This enabled the fabrication of magnetically responsive origami, for example, the Miura–ori pattern in Figure 1c as well as the hexapedal structure with various magnetizations shown in Figure 6b, which realized wirelessly controlled, fast and reversible contraction under an applied magnetic field.

2.4.2. MSM Origami

Magnetic actuation has been demonstrated for effective folding of origami structures on a variety of scales, based on different structural fabrication and magnetization strategies. The patterned magnetization, the external magnetic field, and the structural design (panels and hinges) determine the origami folding. Cui et al.[184] encoded magnetization of microscale origami structures by fabricating nanomagnet arrays on submicron panels with electron beam lithography. As illustrated by the crane microrobot in Figure 6c, the panels were assigned with distributed magnetizations and the flat sheet reconfigured to a "flapping configuration" under the applied magnetic field. Note that the designed nanomagnet array possessed anisotropic properties, enabling reprogrammable magnetization by a specially designed sequence of magnetic fields for a "hovering" mode. The re-programmability of magnetic materials allows for adaptable shape changing and tunable properties even after material fabrication and thus enhances the functionality of active origami for applications such as soft robotics, metamaterials, and reconfigurable structures. Alapan et al.[189] developed a reprogrammable metamaterial (Figure 6d) using a soft composite embedded with CrO_2 particles, which have a relatively low Curie temperature of 118°C. Specific panels were selectively heated > 150°C (using a laser) while a moderate 15 mT encoding magnetic field was applied, which reprogrammed the magnetization pattern and maintained 90% of the initial magnetization magnitude. Alternatively, Song et al.[279] demonstrated reprogrammable origami sheets by first integrating NdFeB particles and phase change material (oligomeric polyethylene glycol) into microspheres, and then embedding the magnetic microspheres into the elastomeric matrix as shown in Figure 6e. Upon heating, the phase change material in the microspheres melted and the magnetized magnetic particles rotated based on the applied magnetic field direction. After cooling down, the phase change material solidified, locking the alignment of magnetic particles and the corresponding magnetization. Through this strategy, an origami sheet was demonstrated with various transformations into desired shapes under magnetic actuation (Figure 6e). Other reprogrammable MSMs with further integrated functions are also available based on covalent adaptable networks due to the nature of the polymeric matrix, which will be discussed in the next section.

Apart from shape morphing structures and metamaterials, MSM origami systems are also widely used for soft robotics. Gracias and collaborators[186] have done extensive work on untethered origami microgrippers (Figure 6f). The microgrippers with magnetic coating allowed for wirelessly controlled navigation in complex environments such as the stomach and intestines. In addition, the reversible opening and closing abilities of the microgrippers under different stimuli including pH change,[30] temperature,[161,280] chemicals,[186] etc., have been demonstrated for functions of object grasping, cargo transportation, and biopsy. Inspired by jellyfish, Ren et al.[183] demonstrated a hard-MSM swimming robot with an engineered hinge as shown in Figure 6g. By manipulating the applied magnetic field profiles, the swimming robot had different swimming motion modes for multiple functionalities such as the mixing of chemicals and transporting of objects. Recently, Wu et al.[185] demonstrated a magnetic origami robotic arm that integrated multimodal deformations of stretching, folding, omnidirectional bending, and multi-axis twisting into one system as illustrated in Figure 6h. By integrating the distributed magnetizations and precise magnetic control into serially arranged Kresling origami, the robotic arm illustrated sophisticated motions that mimic an octopus arm. In addition, a small-scale origami crawler was also realized by Ze at al.[75] via simultaneous contraction of four Kresling units (Figure 6i). Here, the magnetic actuation separated the power source and control system out of the robot, enabling the miniaturization of the origami structure. The crawler was

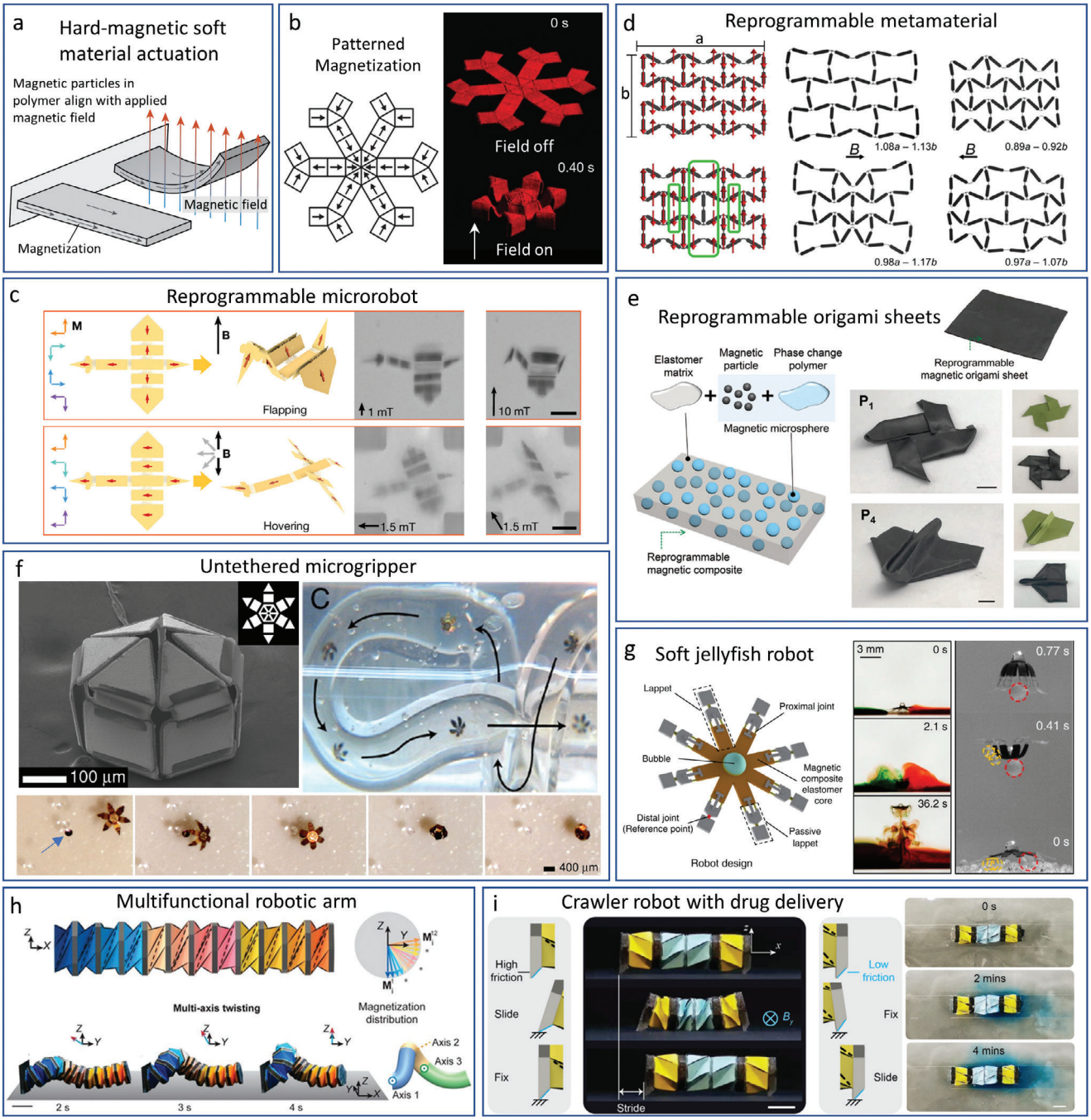

Figure 6. MSM actuation mechanisms, origami, and applications. a) Actuation mechanism of hard-MSMs. b) Patterned magnetization of hard-MSMs for complex shape morphing (Adapted with permission.[37] Copyright 2018, Springer Nature). c) Microrobot with reprogrammable shape morphing (Adapted with permission.[184] Copyright 2019, Springer Nature). d) Reprogrammable metamaterial through coupled magnetic and thermal loadings (Adapted with permission.[189] Copyright 2020, the Authors, some rights reserved; exclusive licensee AAAS). e) Reprogrammable origami sheets by integrating phase change materials with magnetic particles in a soft matrix (Adapted with permission.[279] Copyright 2020, American Chemical Society). f) Untethered microgripper capable of navigation in complex environments and grasping of objects (Adapted with permission.[186] Copyright 2009, National Academy of Sciences). g) Soft jellyfish robot with multiple functionalities such as chemical mixing and object transportation (Adapted with permission.[183] Copyright 2019, Springer Nature). h) Robotic arm with integrated multimodal deformations of stretching, folding, omnidirectional bending, and multi-axis twisting (Adapted with permission.[185] Copyright 2021, National Academy of Sciences). i) Soft robotic origami crawler with drug delivery capability (Adapted with permission.[75] Copyright 2022, the Authors, some rights reserved; exclusive licensee AAAS).

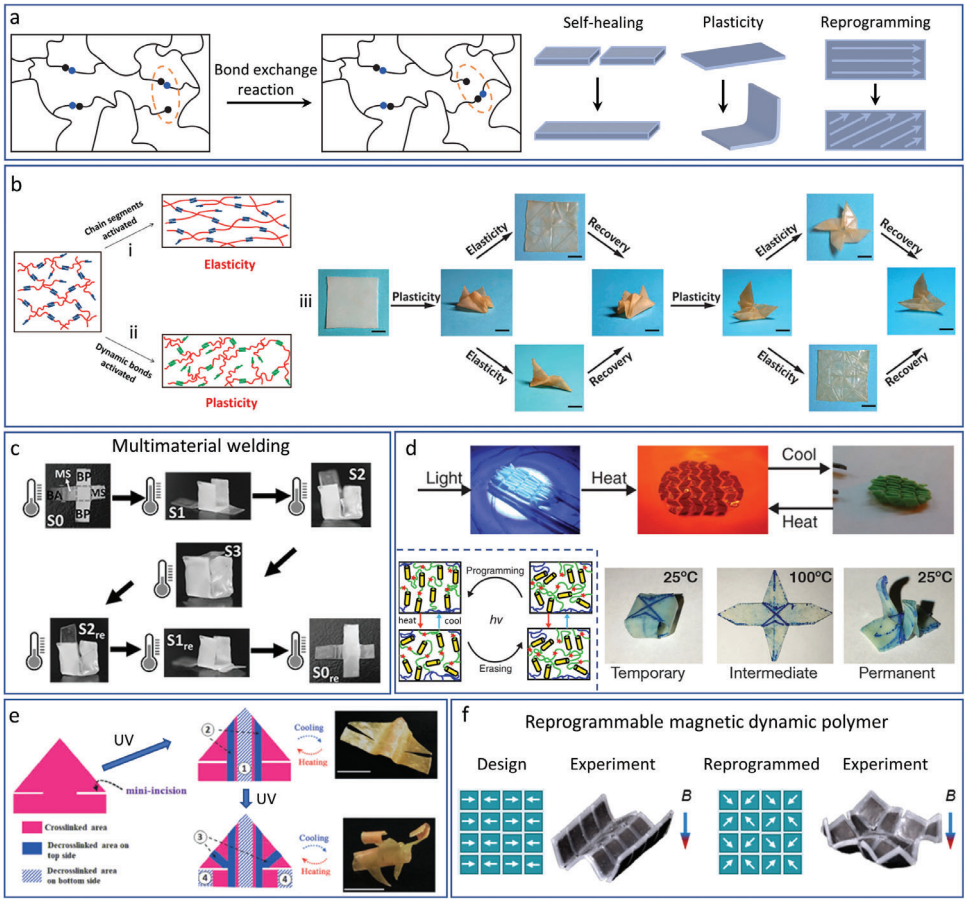

Figure 7. CAN mechanism and origami. a) Bond exchange reaction schematic and typical CAN properties of self-healing, plasticity, and reprogramming. b) Elasticity and plasticity of an SMP with dynamic covalent bonds and reprogrammable permanent shapes. Adapted with permission.[292] Copyright 2016, AAAS). c) Shape memory and welding of materials for sequentially foldable structures (Adapted with permission.[298] Copyright 2016, Wiley). d) LCE with multi-shape memory capabilities controlled by light-activated bond exchange and heat for shape deformation (Adapted with permission.[169] Copyright 2018, the Authors, some rights reserved; exclusive licensee AAAS). e) LCE with photo-patterned, de-crosslinked regions as hinges (Adapted with permission.[170] Copyright 2019, Wiley). f) Magnetic dynamic polymers with reprogrammable magnetization (Adapted with permission.[307] Copyright 2021, Wiley).

explored for multiple functionalities such as movement in a confined space, drug storage, and drug release. An additional notable work based on Kresling origami was a soft amphibious robot with swimming, jumping, and cargo transportation functionalities.[31]

2.5. Covalent Adaptable Network (CAN) Polymers

Covalent adaptable network (CAN) polymers[281] are crosslinked polymers with dynamic covalent bonds that can reversibly break and re-form while maintaining network integrity (**Figure 7**a). They are also often referred to as dynamic covalent polymer networks (DCPNs),[282] or vitrimers.[283] Under an applied stimulus, often heat,[283–285] light,[286] or solvent,[287] the so-called bond exchange reactions (BERs) become active in the network (see Figure 7a, left), which lead to interesting merits such as plasticity, recyclability, self-healing, and ease of reprogramming, equipping CANs with specialized functionalities as compared to the aforementioned materials (Figure 7a, right).[281,282] These have led to applications such as healable sensors[288] and healable triboelectric nanogenerators.[289] As we will discuss, dynamic covalent chemistry (DCC) can be incorporated with active materials to achieve active origami with outstanding properties.

2.5.1. CAN Mechanism

Typical CAN polymers involve BERs that enable the rearrangement of networks. Common chemistries that possess BERs include transesterification, disulfide exchange, imine exchange, Diels–Alder (D–A), etc. Generally, the reactions that allow for adaptability of bonds are dissociative or associative.[290] Dissociative (such as D–A) networks involve covalent bonds that are not necessarily re-formed upon breaking, allowing for significant decrease in the number of crosslinks in the network. For associative (such as the abovementioned exchange reactions except for D–A) networks, the overall number of crosslinks in the network remains the same.[281] Upon activation of BERs, topological rearrangement of the network occurs, where nearby bonds break and re-form, which can allow

for plastic deformation of the material[282] and shape reprogramming. In addition, when BERs cross the interface between two CAN polymers, welding, reprocessing and recycling are enabled. Figure 7b shows how BERs can be used together with shape memory effects to achieve diverse programmability and shape change. The shape memory effect allows the polymer sheet to be programmed into a temporary shape and to be elastically recovered to the permanent shape (Figure 7b-i) while the permanent shape can be plastically reprogrammed by BERs (Figure 7b-ii). Since the chemical reaction kinetics typically follow Arrhenius law,[291] thermoresponsive BERs only become fast enough (or active) to allow appreciable changes at high temperatures (T_{BER}). In addition, since BERs require macromolecular chains to have enough mobility for exchange reactions, the temperature for BERs to be active is typically higher than T_g. This permits the possibility to combine the merits of BERs with shape memory effects.

2.5.2. CAN Origami

Xie and coworkers have pioneered multiple notable works on CANs paired with SMPs to create active origami. In their initial works,[292,293] they achieved elasticity and plasticity within the same polymer network. Plasticity could be induced by transesterification BERs, allowing for reprogramming of complex 3D permanent shapes upon heating to T_{BER}. By deforming the sheet while above its T_{trans} (but below T_{BER}) followed by cooling, temporary origami shapes could be imparted (Figure 7b-iii). Upon heating, the original origami shape would be recovered. By raising the temperature close to or above T_{BER}, the permanent shape could be reprogrammed. In a later work, they again used plasticity and elasticity concepts, but to demonstrate the ability of 2D origami substrates to transform to 3D origami[294] via plasticity, while reversible elastic deformation could occur at this state, showing value for deployable structures that require subsequent localized actuation. Plasticity of SMP CAN origami has also been explored by other groups recently.[295,296]

Pei et al. incorporated reversible links into LCEs to achieve easy processing and alignment after the initial cross-linking, enabling reprogramming.[297] They later utilized this concept to demonstrate CAN active origami.[298–302] Via transesterification reaction, they showed that light-activated CNT-dispersed LCE could be aligned spatio-selectively, in which local parts of the material could be photothermally heated until transesterification was activated, after which those parts of the LCE actuator could be aligned via stretching.[299] They presented another approach that used CANs for jigsaw-like assembly of multimaterial origami substrates.[298] Three CANs with different T_{BER}s were used to weld the materials via hot press to flat crosses of varying material arrangement. Upon programming a box shape and subsequent heating, un-folding of multimaterial boxes (Figure 7c) could occur in different sequential orders due to the order in which the material phase transitions occurred. They additionally demonstrated LCE CANs activated by solvent,[301,302] allowing for actuation of LCE origami, such as Miura–ori, 3D kirigami structures, and flower-like actuators at relatively moderate temperatures.

Bowman and coworkers have made significant advancements in the understanding of covalent adaptable networks[281] and developed the first known light-triggered bond exchange reaction.[286] Unlike photothermal effects, they used light to directly trigger bond exchange reaction (or reversible addition-fragmentation chain transfer (RAFT)).[286] The light-triggered BER was later used to demonstrate photo-origami[34] and has demonstrated active origami with exciting properties.[169,303] Depicted in Figure 7d, they developed LCEs which have light-activated BERs that allowed for separate control of the LCE deformation and alignment.[169] Here, the RAFT functionality was incorporated into the polymer backbone and enabled bond exchange of allyl sulfides within the network. The light-induced BER allowed for stabilized alignment of LCEs in a strained state, resulting in stable, permanent origami shapes upon removal of strain. When heated, these structures deformed to flat sheets and returned to the 3D shape upon cooling. In this way, reversible folding of Miura–ori was achieved. Additionally, they demonstrated transformation between three distinct shapes, as shown in Figure 7d, in which the 3D crane was the permanent shape programmed via BER, the flat crane was the isotropic state, and a third temporary state was able to be temporarily programmed via thermal quenching. Li et al. also demonstrated triple shape memory of LCE boxes,[304,305] taking advantage of both the glass and isotropic phase transition temperatures of the LCE.

Active CAN LCE origami has also been demonstrated by Zhao and coworkers,[170,306] who utilized anthracene moieties with liquid crystals, achieving light-controlled cleavage (de-crosslinking) and dimerization (crosslinking) under two UV lights of different wavelengths.[170] In this way, de-crosslinked, inactive domains could be introduced through the thickness of an LCE sheet, which effectively created a bilayer of the original LCE and the newly de-crosslinked LCE. The de-crosslinked regions acted as flexible hinges and caused curvature of the sheet at ambient temperatures, with the extent of bending controllable by the extent of decrosslinking that was programmed through the thickness. Regions with thicker inactive domains resulted in smaller bending angles toward the de-crosslinked side. Upon heating the sheet, contraction of the crosslinked regions led to an overall flattening of the sheet and temporary loss of the origami shape. They used the same sheet and progressively patterned more inactive domains (See Figure 7e), to achieve origami shapes such as an airplane, bull, and frog.

CANs were also recently demonstrated with MSMs. Kuang et al.[307] introduced magnetic dynamic polymers by embedding hard magnetic NdFeB particles in a D–A polymer matrix. At elevated temperatures, cleavage of dynamic linkages was triggered, allowing for reprogramming of the magnetization under relatively low magnetic fields. They demonstrated this with a foldable array of magnetic dynamic polymer squares, initially with horizontal magnetizations opposite to those in neighboring columns (see Figure 7f, left). This type of magnetization resulted in a 3D "W" shape upon an applied downward magnetic field. With the use of a photomask and IR light for photothermal heating, the magnetizations of squares were selectively reprogrammed to four different diagonal magnetizations (Figure 7f, right). They also demonstrated the use of simultaneous applied magnetic field and bond exchange to obtain stress-free bistable and multistable kirigami structures that would otherwise be difficult to fabricate without BER.

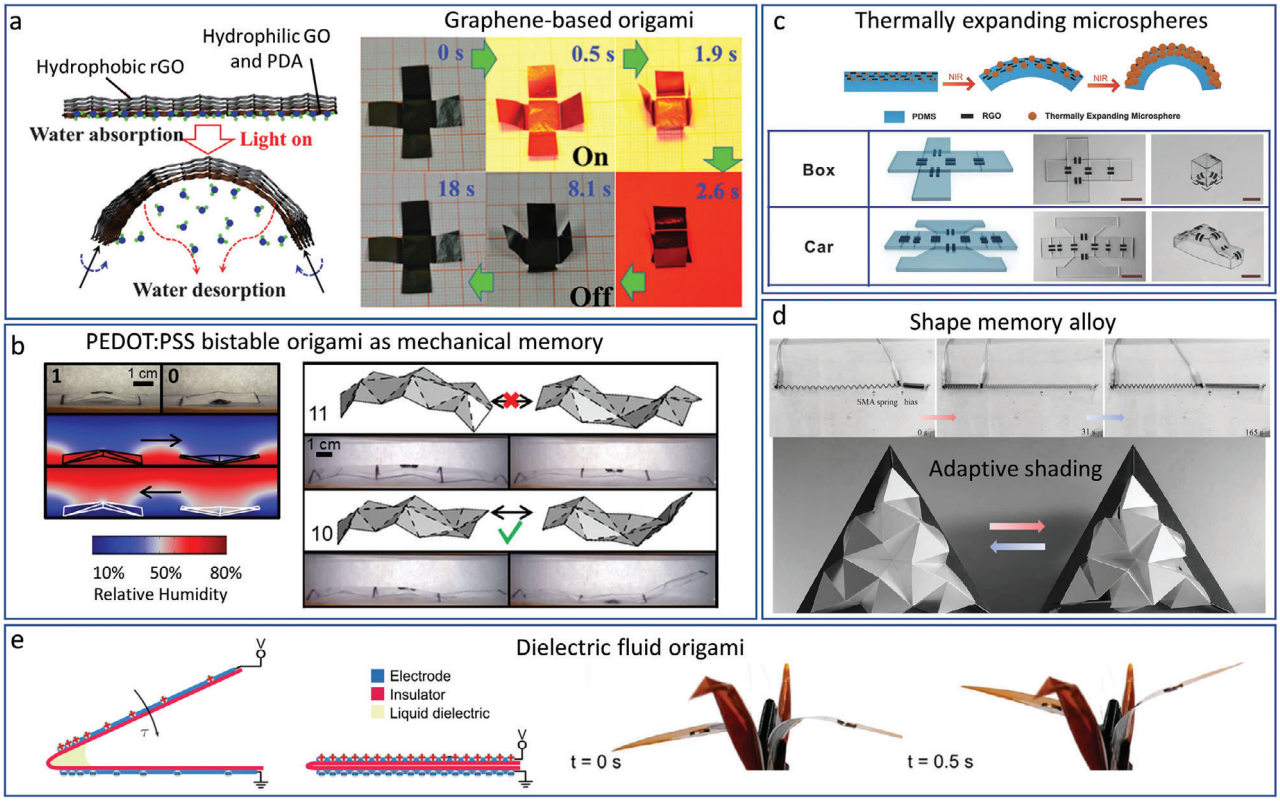

Figure 8. Additional materials for active origami. a) Hydrophilic and hydrophobic graphene-based origami, which absorbs and desorbs water molecules for actuation (Adapted with permission.[312] Copyright 2015, AAAS). b) PEDOT:PSS-based origami which uses origami multistability to store mechanical information (Adapted with permission.[076] Copyright 2018, National Academy of Sciences). c) Origami with thermally expanding microspheres which result in bending of structures upon heating (Adapted with permission.[322] Copyright 2018, Wiley). d) Actuation of SMA spring by heating and adaptive shading device which reduces its surface coverage when springs are heated (Adapted with permission.[017] Copyright 2018, ASCE). e) Active origami with dielectric fluid at hinges to actuate wings of a crane under an applied voltage (Adapted with permission.[336] Copyright 2018, AAAS).

Although not thoroughly covered in this section, DCC can impart shape memory capabilities on hydrogels as well. Chen et al. have recently developed fluorescent hydrogel origami, which utilizes dynamic covalent bonding to enable shape memory function of hydrogel and dual encryption applications. Messages patterned on the hydrogel could be decrypted upon shape recovery and UV light illumination.[308,309] Generally, CANs enable unique properties of active origami that are otherwise difficult to achieve in SMPs, hydrogels, LCEs, or MSMs without DCC.

2.6. Other Materials

While numerous active origami works have been done with SMPs, hydrogels, LCEs, and MSMs, there are additional stimuli-responsive materials used for active origami worth highlighting here. For simplicity, the materials discussed in this section are categorized into the general groups of hygroscopic, thermoresponsive, and electroactive materials.

Hygroscopic materials are those that can absorb or desorb water vapor and will thus change shape in response to variations in humidity. These materials are similar to hydrogels in mechanism, however, unlike hydrogels, they do not require an aqueous environment to operate. In an early study, Okuzaki et al.[310] found that, for accordion-like origami actuators with polypyrrole films, sorption and desorption of vapor drastically changed the elastic modulus of the polypyrrole material, resulting in reversible strains of nearly 150%. Other materials, such as GO (graphene oxide), are hydrophilic and can adsorb water molecules.[311] As seen in **Figure 8**a, Mu et al.[312] developed a graphene-based "paper" that was composed of a hydrophobic rGO (reduced graphene oxide) layer and a hydrophilic GO-polydopamine (GO-PDA) layer. They fabricated a flat cross substrate with patterned GO-PDA hinges. Upon the photoinduced heat of NIR light irradiation, the GO-PDA regions released water by desorption, causing a contraction of the layer and leading to upward bending of the rGO outer panels, which was quickly recovered back to a flat state by water adsorption upon removal of the light. PDA along with PNIPAM have also been functionalized as hinges on graphene origami substrates.[313] Cai et al.[314] have demonstrated the humidity response of MXene cellulose composites for actuation of bilayer origami structures with polycarbonate membranes. Other membranes such as the porous cationic poly(ionic liquid) demonstrated by Zhao et al.[315] exhibited rapid folding and un-folding in response to humidity changes in the presence of organic solvents such as acetone. Another common material used for hygroscopic response is poly(3,4-ethylenedioxythiophene) polystyrene sulfonate

(PEDOT:PSS), a conductive polymer used for a myriad of electronic devices.[316] It has been used to create active origami structures.[76,317] For example, Treml et al.[76] used PEDOT:PSS as the active material for origami logic structures, in which PEDOT:PSS was used with polypropylene to create humidity-responsive waterbomb origami films with bistability or multistability (Figure 8b).

While thermal expansion mismatch in bilayer or multilayer systems is often used to drive the shape change of active origami, heat has been used in other ways to actuate origami. For example, as temperature increases, polymers tend to soften, which has been taken advantage of for origami structures, such as the heating of polymer at pre-stressed metallic hinges of microgrippers,[186,318] polymer sheets with reduced-thickness patterned hinges and stretched rubber bands which actuate structures upon hinge softening,[319] as well as the folding of graphene polyhedrons as a result of melting its polymer hinges.[320] Instances of the incorporation of graphene with bilayers in active origami have been demonstrated.[321,322] For example, Tang et al.[322] embedded thermally expanding microspheres (TEM) into rGO/PDMS bilayers (Figure 8c). The microspheres, which were heated via photothermal effect by the rGO upon exposure to light, were liquid hydrocarbons encapsulated by thermoplastic shells. When heated, the shell softened and the hydrocarbon transitioned to a gas, enabling an expansion of the spheres which remained after the outer shell hardened upon cooling. This expansion of the rGO/TEM portion of the bilayer caused irreversible bending toward the PDMS.

Shape memory alloys (SMAs) are an additional type of thermoresponsive materials that have been used often in active origami applications.[323,324] As the name indicates, SMAs exhibit a shape memory effect similar to that of SMPs (but note that SMAs had been used and developed prior to SMPs). In short, these alloys can undergo a reversible phase transformation between martensite and austenite phases during which the crystal structures change.[325] Due to their ability to recover their shape even when under appreciable loads, SMAs have relatively high actuation energy density as compared to other stimuli-responsive materials and can be advantageous in this way. Note that the allowable strain of SMAs varies by alloy, but is generally limited to < 8%.[325,326] Different SMA waterbomb-based designs with reduced-thickness hinges have been used to demonstrate biomedical stents capable of coupled radial and axial[12] or circumferential[327] deployment. SMAs have also been used for the deployment of waterbomb-based transformable wheels, where SMA wire contracts radially when heated, allowing for reconfiguration of the wheels.[328] Additional works have used SMA wires/springs as actuators for sunlight-adaptive Ron Resch (Figure 8d)[17] or waterbomb[329] origami-based shading devices. Additionally, SMA has been used toward robotics applications, for instance the use of SMA wires for actuation of a peristaltic origami crawler robot.[330] It should be noted that other impressive examples of metal-based origami[331–333] include the surface oxidation of platinum films[334] and metallic bilayers.[335]

Dielectric materials are also used to create active origami, or so-called electroactive origami. Common dielectric materials involve fluids, for example, dielectric liquid can be displaced upon an applied voltage and subsequently drive the movement of panels.[336,337] Figure 8e shows an example by Taghavi et al.,[336] in which dielectric liquid was applied at the hinge of two oppositely charged panels. Upon an applied voltage, the electrostatic attraction drew the panels closer to one another, resulting in folding. With this concept, they demonstrated an accordion-like artificial muscle and a flapping origami crane. Dielectric elastomers can reduce in thickness and increase in area when a voltage is applied to electrodes across the thickness direction[338] and can be used for simple motions such as bending,[339–342] as well as for more complex origami.[272,343–345] Recently, Sun et al.[346] utilized origami systems with elastomer between carbon grease electrodes. The initial 3D structures (via pre-stretching) were actuated by applying a voltage (enabling electrostatic force between electrodes), which caused the dielectric elastomer to expand, unfolding the structure. The applied voltage could selectively actuate the hinges individually, enabling boxes and pyramids as well as gripper functionality.

Lastly, ceramics are also suitable materials for active origami. Several works have utilized inactive ceramics, such as elastomer-derived ceramics[347,348] for origami demonstrations, while others use active materials such as piezoelectric ceramics. Under an applied electric field, piezoelectric ceramic materials such as PZT (lead zirconate titanate) can expand in one direction.[349] By placing PZT between electrodes, voltage-driven actuation of the ceramic can be achieved, which has been used for robotics[350–352] and active origami applications.[23,353] Specifically, Suzuki and Wood[23] have demonstrated the use of PZT as linear actuators for an origami-inspired surgical robot.

3. Fabrication of Active Origami

As active origami involves the shape evolution of materials, the fabrication and patterning of materials that facilitate complex deformations are of great importance. Here, we discuss the most common methods used to fabricate active origami, including molding and 3D/4D printing, as well as techniques used for micro and nano scale active origami. **Table 2** provides a brief summary of the common fabrication methods.

3.1. Molding

Molding is a common method for fabrication of soft materials in which precursor materials are poured into a mold and cured, resulting in structures that take on the inner cavity of the mold. Molding has been used in fabrication of SMPs, hydrogels, LCEs, MSMs, and CANs. For SMPs, molding can initially be used to obtain the "permanent" shape of the material, while additional molds or methods for shape fixation can be used to program temporary shapes. Fabrication of hydrogel structures also commonly utilizes molding,[148,154,354,355] where multi-step processes can be used to create bilayers or in which photomasks are used to introduce crosslinking densities. Molding of LCEs[168,169] has been used to introduce origami patterns into LCE sheets. Intricate molds with micro-scale features such as microchannels[269,271] have been used, which leads to alignment of the mesogens along the channels to produce films with complex director fields. For cured MSMs with hard-magnetic particles such as NdFeB, the material can be placed in fixtures which configure the material

Table 2. Summary of fabrication methods.

Method	Material properties	Active materials used	Pros	Cons
Molding	Photo or thermally curable	SMPs, Hydrogels, LCEs, MSMs	Inexpensive	Low structural complexity; requires mold for each new design
Direct ink writing (DIW)	Viscous ink, shear-thinning	SMPs, Hydrogels, LCEs, MSMs	Inexpensive; more material choices	Low resolution; slow
Fused filament fabrication (FFF)	Thermoplastic	SMPs, Hydrogels, MSMs	Inexpensive	Low resolution; slow
Digital light processing (DLP)	Photocurable, liquid resin	SMPs, Hydrogels, LCEs, MSMs	Fast (cures entire layer)	Multimaterial printing challenging
Two-photon polymerization (TPP)	Photocurable via two-photon absorption	Hydrogels, LCEs, MSMs	High resolution	Difficult to scale up
Inkjet	Photocurable liquid ink	SMPs, Hydrogels	Fast; high resolution; multimaterial capability	Expensive; limited material choice

to a desired actuation shape. The material can then be magnetized by applying a large magnetic field, imparting a magnetization distribution in the MSM[73,356,357] so that it would later configure to that shape under an appropriate magnetic field. It should be noted that CANs can be fabricated in a similar way to that of their matrix material, but with special considerations to the material's chemistry.

3.2. 3D/4D Printing

3D printing, or additive manufacturing (AM), has enabled the rapid manufacture of custom designed parts. These techniques have since been expanded to stimuli-responsive/shape-changing materials to bring forth 4D printing,[358,359] or the printing of structures whose shape, properties, or functions can evolve over time. 4D printing has been widely adopted for the fabrication of complex, shape-evolving structures and materials. Here, we will briefly discuss the 3D/4D printing methods commonly used to fabricate active origami, including extrusion-based printing such as direct ink writing and fused filament fabrication, the resin-vat based digital light processing, inkjet printing, as well as two-photon polymerization for high-resolution printing.

3.2.1. Extrusion-Based Printing

Extrusion-based printing includes direct ink writing (DIW) and fused filament fabrication (FFF; often called fused deposition modeling (FDM)). These two methods share many common features, such as they both use nozzles to write lines to form layers and eventually form 3D solids. Both methods have been popular in the fabrication of active origami.

DIW deposits viscous liquid inks in the form of a line onto a platform.[360] The rheological properties of the ink are of critical importance, as shear-thinning and rapid transition to dilatant behavior are needed for efficient extrusion and subsequent rapid shape-holding of the ink.[361] Because of this, rheological modifiers, such as nanoclays, are often added to active material inks, which can then be used to print origami structures or hinges. The resolution depends on nozzle inner diameter as well as the rheological properties of the ink. Since DIW utilizes liquid resin, the deposited ink needs to be cured, either directly after printing, or after the entire structure is printed. Naficy et al.[354] developed a DIW printing method for hydrogels that exhibit complex deformation by creating bilayer structures with two different hydrogels, thermoresponsive pNIPAM and thermally inactive poly(2-hydroxyethyl methacrylate) (pHEMA). Using pHEMA as the base, active pNIPAM hinges were patterned onto it, which were then surrounded by remaining inactive material (**Figure 9**a-i). The folding box shown in Figure 9a-ii experienced reversible folding and unfolding as the temperature changed below and above the pNIPAM's LCST, respectively. More complex deformation of hydrogel origami was demonstrated by Gladman et al.,[362] who achieved biomimetic, plant-like deformations of hydrogel bilayers upon immersion in water. The ink used was mainly an acrylamide matrix embedded with cellulose fibrils, which were aligned along the printing direction during extrusion (Figure 9b-i, enhanced swelling along the filament direction) and allowed for anisotropic swelling. After immersion in water and swelling of the bilayers, complex curvatures of flowers (Figure 9b-ii) were achieved, dictated by the angles between the filaments of the bilayers. Aside from cellulose, other materials such as nanomagnets have been used in DIW printing of hydrogel. An acrylamide ink with NdFeB magnets and nanoclay for shear-thinning was printed.[363] After the matrix resin was cured, the magnetic hydrogel could be deformed and held in desired shapes for magnetization, imparting a distributed magnetization within the material upon a large applied magnetic field. With this technique, origami folding such as Miura–ori, as well as box and flower-like folding structures were fabricated. Other works involving magnetic materials and elastomers such as PDMS have demonstrated origami-like structures, such as a flapping butterfly[364] under a gradient magnetic field and reprogrammable movements of 3D magnetic soft objects[365] via large impulse magnetic fields. First demonstrated by Kim et al.,[37] DIW to program the magnetization of MSM inks

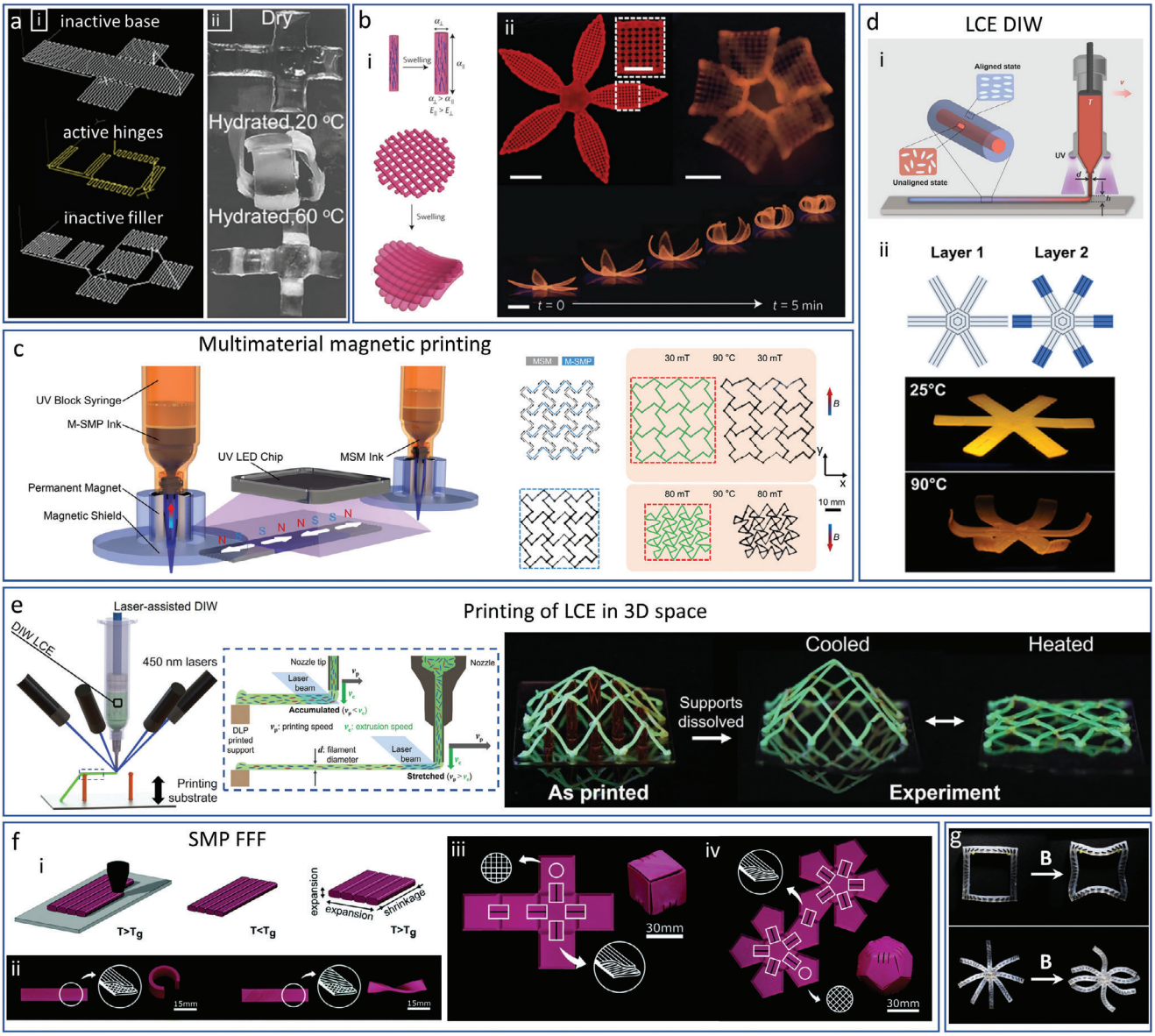

Figure 9. Extrusion-based DIW and FFF for active origami structures. a) DIW of a hydrogel cross with thermoresponsive hydrogel hinges (Adapted with permission.[354] Copyright 2016, Wiley). b) DIW of hydrogel with anisotropic cellulose ink for bilayer structures with complex bending (Adapted with permission.[362] Copyright 2016, Springer Nature). c) Multimaterial DIW printing of MSM and magnetic SMP (Adapted with permission.[366] Copyright 2021, American Chemical Society). d) DIW of LCE with tunable actuation strain (Adapted with permission.[373] Copyright 2020, the Authors, some rights reserved; exclusive licensee AAAS). e) Printing of LCE in 3D space onto supports which were then dissolved to result in a 3D LCE lattice (Adapted with permission.[179] Copyright 2022, Wiley). f) FFF of SMP with programmed stress during printing (Adapted with permission.[378] Copyright 2017, The Royal Society of Chemistry). g) FFF of cylindrical MSM embedded in a silicone matrix for biomimetic motions (Adapted with permission.[382] Copyright 2020, Elsevier).

along the print direction[37,366,367] allows for materials with precisely defined magnetization distributions (see also Figures 1c and 6b). Ma et al.[366] used this method in a multimaterial approach, such that MSMs and M-SMP were printed, enabling metamaterials with segments of either M-SMP or MSM. The obtained metamaterials had unique deformation modes, with the MSMs deforming under magnetic fields and the M-SMPs requiring heat for their deformation (Figure 9c). Other SMP origami via DIW has been achieved, such as the work by Rodriguez et al.,[368] which involved ink based on epoxidized soybean oil. With their printing method, origami with initially flat or 3D shapes could be achieved.

DIW is also well-suited for printing of LCEs.[167,369–372] Due to the shear forces experienced by the ink during extrusion through the nozzle, mesogens in LCE ink can be aligned along the print direction,[369,370] thus programming the material. Roach et al.[180] demonstrated the use of a room temperature printable LCE ink for its use in actuating the hinges of multimaterial structures.

Wang et al.[373] tuned printing parameters to show the variable actuation strain of LCE filaments in folding structures. By varying printing parameters such as the printing temperature, the nematic order of the inner filament could be tuned. For example, with high printing temperatures, the inner part of a filament largely remained in a polydomain state (Figure 9d-i), which resulted in reduced actuation strain of the material after curing. Using this approach, they demonstrated controllable actuated 3D states of a flower-like substrate (Figure 9d-ii). DIW LCE printed bilayers have also been demonstrated as hinges with controllable fold angles[172] for robotics applications, as highlighted previously in Figure 5h by Kotikian et al. Additionally, Peng et al.[179,374] have developed fabrication strategies that combine DIW of LCEs with other methods of 4D printing for multimaterial origami (as highlighted previously in Figure 5d). In a recent pioneering work, as opposed to printing LCE onto a plate, they successfully extruded LCE into 3D space, allowing for the creation of LCE-based structures that are not achievable by conventional DIW methods. As shown in Figure 9e, by first printing dissolvable (non-LCE) structural supports and then using the support as a starting point of an LCE fiber, LCE ink was extruded and then stretched to generate fibers in 3D space that maintained the ability of generating high actuation strains. By printing numerous lines and then dissolving the structural supports, complex 3D LCE structures such as the lattice pyramid in Figure 9e were achieved.

FFF (or FDM) involves the extrusion of melted thermoplastic filaments, which experience solidification after cooling. The main differences between DIW and FFF lie in material types: FFF predominately prints thermoplastics and DIW is mainly used for network polymers. SMPs (such as polyurethane or polyethylene) printed by FDM have been used for programming of temporary shapes.[137,375–377] In addition, tuning of printing parameters can be used to introduce the desired stress during the printing process, which later can be employed for shape change.[378–380] van Manen et al.[378] utilized the polymer chain alignment along the direction of extrusion enabled by the stretching of the melted thermoplastic materials through the nozzle. The stretched deformation was memorized into the material after the filaments cooled below T_{trans}. By stacking layers with different print directions (Figure 9f), deformations such as bending and twisting were achievable, due to strain mismatch between layers upon heating. Origami capable of water absorption has also been fabricated by FFF. Baker et al.[381] printed hydrophilic polyurethane sandwiched between two layers of hydrophobic polyurethane, with gaps to create bilayer hinges than would bend when placed in water. Lastly, FFF has also been used for magnetic material origami,[382,383] in which FFF-printed magnetic components[382] were oriented in a soft silicone matrix to program magnetization and enable biomimetic motions (Figure 9g) as well as direct printing of thermoplastic rubbers with incorporated soft magnetic particles.[383]

3.2.2. Digital Light Processing (DLP)

DLP is a vat-photopolymerization printing approach that involves light projected onto a vat of photocurable resin, which cures one layer of the resin at a time, after which the printing stage is moved, allowing for subsequent layers of the desired structure to be printed. DLP is relatively fast, as an entire layer of the resin can be cured at one time, with resolution possible at tens of microns.[384,385] As DLP involves a vat of resin, it is often challenging to achieve multimaterial printing, but Ge et al.[386] addressed this by using an automated material exchange system (**Figure 10**a), in which acrylate networks of different compositions could be used to create SMP structures, for example a flower with petals of different T_{trans}. Multimaterial DLP has also been achieved by use of multicomponent resins in which materials could be preferentially cured under different wavelengths of light, resulting in structures containing components of different stiffness and swelling behaviors.[387] While SMPs often need to be mechanically programmed after printing,[129] other methods have avoided this by introducing differential crosslinking along the thickness direction[388] to cause bending. Zhao et al.[389] did this by utilizing frontal photopolymerization to fabricate Miura–ori, a crane, and a variety of polyhedron. In a later work,[390] they used DLP to introduce out-of-plane crosslinking gradients into a flat film, which, upon immersion in water, resulted in desolvation of uncured chains from the film, inducing contraction toward the side of the film that was less cured. By creating films with fully cured panels and hinges that were differentially crosslinked, origami structures were made which exhibited bending at the hinges only (Figure 10b). The structures could be flattened again by immersing the substrate in acetone, during which the less cured region swelled. Another similar approach involving volatilization with an added post-curing step enabled origami with enhanced material stiffness and the ability to hold appreciable weight.[391]

Another method to introduce different material properties into the same network was achieved with the use of grayscale light, such that light intensity varies within the projected light pattern. With a two-stage curing approach, Kuang et al.[392] developed SMP structures with specific material properties imparted both within the layers and throughout the part, involving, for example, structures with materials of different moduli and T_{trans}. As shown in Figure 10c, a long strip with hinges of different T_{trans} allowed sequential folding of the SMP strip to a spiral shape upon gradual heating. The advantage of this approach is that it uses only one resin vat and retains DLP's merits of high speed and high resolution.

DLP has also been applied to LCEs with the assistance of post-processing. Jin et al.[393] used a solvent-assisted programming approach. In their work, liquid crystalline organogels were used, in which swollen and crosslinked 2D sheets or 3D LCE structures were deformed, followed by solvent evaporation in the deformed shape. The swelling of the organogels lead to flexibility of the LC alignment and, upon deformation and subsequent drying, a new alignment of the mesogens was obtained, with micropores formed during drying helping to memorize the programmed director. Upon heating, the structure returned to its printed shape (Figure 10d). Hydrogel origami fabrication has also benefitted from DLP,[394–396] with a notable example from Kim et al.,[394] in which biomimetic structures were achieved with hydrogel bilayers made from silk fibroin bio-ink. The bilayer consisted of a flat layer and a patterned layer, where differential swelling led to curling toward the patterned layer in water. Structures such as a folding flower and venus flytrap were demonstrated (Figure 10e). CANs have also been fabricated

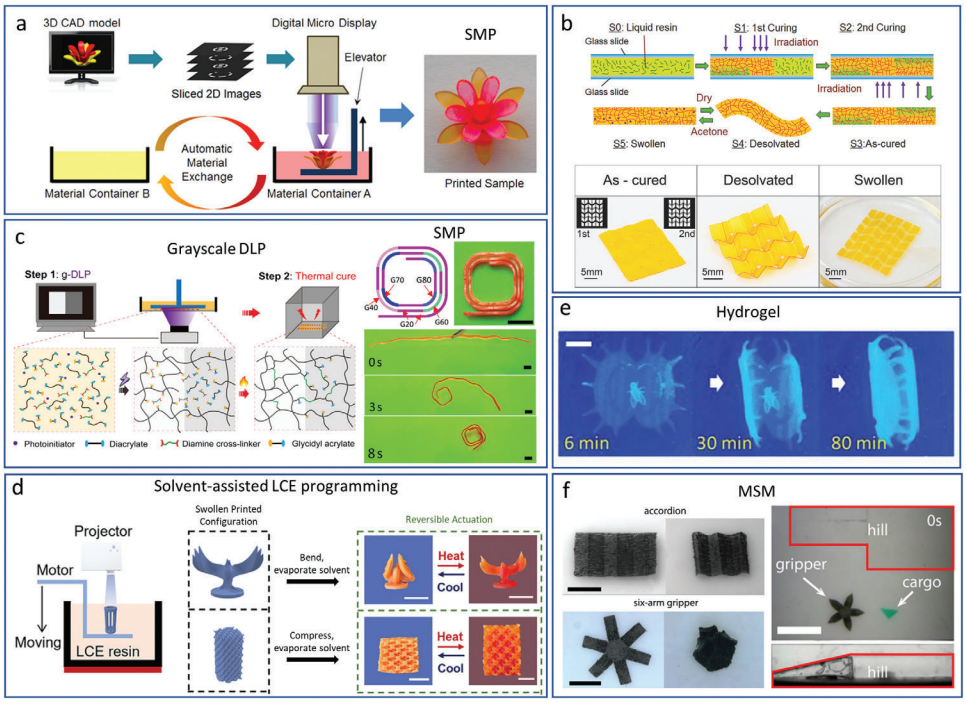

Figure 10. Digital light processing for fabrication of active origami. a) Multimaterial DLP of SMP origami structures (Reproduced with permissionf.[386] Copyright 2016, Springer Nature). b) Differentially crosslinked and desolvation-induced folding of a Miura–ori sheet (Adapted with permission.[390] Copyright 2017, Wiley). c) Grayscale DLP for SMP origami structures with tunable mechanical properties (Adapted with permission.[392] Copyright 2019, the Authors, some rights reserved; exclusive licensee AAAS). d) Solvent-assisted programming and reprogramming of LCE structures (Adapted with permission.[393] Copyright 2021, Wiley). e) Bioinspired silk hydrogel origami structures (Adapted with permission.[394] Copyright 2020, Elsevier). f) Variety of foldable and remotely controllable DLP MSMs (Adapted with permission.[192] Copyright 2019, AAAS).

with DLP,[32,397,398] specifically, shape memory networks with self-healing capability[398,399] and welding for modular assembly[32] of origami structures. Although the use of photopolymerization via DLP is typically not well-suited for the opacity of soft magnetic materials, Xu et al.[192] utilized DLP to construct magnetic soft robots with NdFeB particles that could be aligned to arbitrary 3D magnetizations. Foldable structures such as an accordion sheet and grippers (Figure 10f) were achieved, which could locomote with cargo.

3.2.3. Inkjet Printing

Inkjet printing, which utilizes commercial printers such as those from Stratasys, is a common method for the fabrication of multimaterial origami structures. Inkjet printers deposit droplets of ink onto the printer bed, which is then smoothed and photocured to produce layers of material (see **Figure 11**a). Inkjet printers often have multiple printing heads, which enable printing with multiple materials, however, the materials that can be used with inkjet printing are limited by those commercially available, which are mainly SMP and hydrogels,[358] along with the fact that these exact materials are not typically disclosed. Nevertheless, many origami works fabricated by inkjet printing have been demonstrated, such as self-locking (Figure 3e) or sequentially foldable (Figure 1c) boxes, Kresling-based metamaterials (Figure 3h), pyramids (Figure 1c), flowers (Figure 3f), and planes (Figure 5e) as shown in previous figures.[35,71,117,127,135,204,400,401] Another example is shown in Figure 11b, where elastomer and glassy polymers are printed

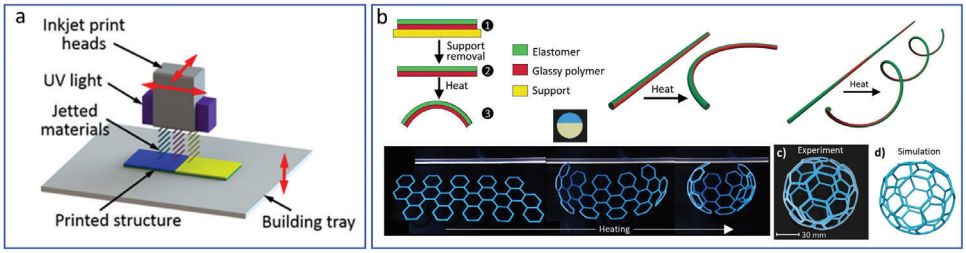

Figure 11. Inkjet printing for active origami fabrication. a) Schematic of an inkjet printing process with multiple materials (Adapted with permission.[403] Copyright 2017, AAAS). b) Rod-based multimaterial structure capable of folding from a flat lattice to 3D ball (Adapted with permission.[402] Copyright 2018, Elsevier).

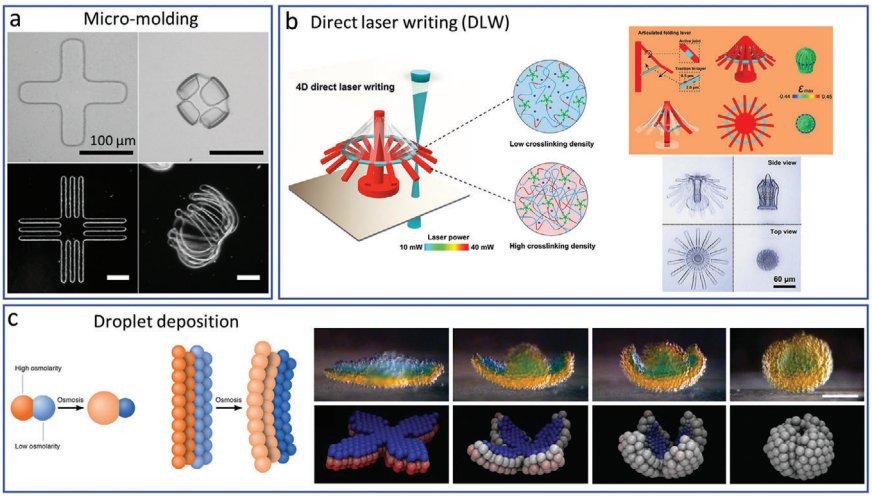

Figure 12. Micrometer and nanometer-scale fabrication techniques for active origami. a) Micrometer-scale molds used to fabricate different hydrogel bilayer actuators which fold in water (Adapted with permission.[355] Copyright 2005, American Chemical Society). b) Direct laser writing/two-photon polymerization to introduce voxels of different crosslinking densities into a hydrogel structure (Adapted with permission.[155] Copyright 2019, Elsevier). c) Printing of liquid droplets to create bilayers of different osmolarities (Adapted with permission.[413] Copyright 2013, AAAS).

within the same rods to produce patterns that generate different types of deformation upon heating.[402] Notably, inkjet printing has enabled the printing of "digital" materials,[117,358,400] which combine different ratios of base printing materials for origami structures with different material properties and folding capabilities.

3.3. Micro/Nano Scale Fabrication

As active origami shows great potential for applications in biomedical environments as well as foldable electronic devices such as microelectromechanical (MEMS) and nanoelectromechanical systems (NEMS),[53] methods that can be used to fabricate origami structures at the micrometer and nanometer scale are very important.[404] There have been numerous examples of micro and nano-scale origami largely composed of metal.[334,405–408] The demonstrated methods to fold these structures include surface tension of molten solder at hinges[405,406] and chemical reactions.[334,407] However, these methods are often not applicable to soft active materials. One approach taken by Guan et al.[355] to achieve microscale fabrication of soft materials was the use of molds with microwells to create bilayer hydrogel structures that bend in water (**Figure 12**a).

4D printing at the nanoscale is also possible through direct laser writing (DLW), which utilizes two-photon polymerization (TPP) to fabricate structures at a resolution of as high as 100 nm.[6] Via TPP, a laser initiates two-photon absorption and subsequent two-photon polymerization. The material near the pulse of the laser polymerizes while the rest does not, with the extent of polymerization depending on the power of the laser and duration of pulse. Thus, high-resolution heterogeneous structures can be obtained. TPP has been used for fabrication of foldable voxelated LCE,[409,410] swellable materials,[155,411] and magnetic materials.[412] As shown in Figure 12b, Jin et al.[155] utilized TPP for the tuned polymerization of voxels in a hydrogel structure. By scanning the laser in the hydrogel precursor and varying the laser power, voxels with different crosslinking density throughout the printed structure could be obtained. A pH-responsive hydrogel umbrella structure with interspersed bilayers was printed. Upon a change in pH, the hydrogel rim bilayer connected to the umbrella ribs would bend, causing rotation of the ribs in a lever-like folding process. Tissue-like materials can also be printed, as demonstrated by Villar et al.,[413] through utilization of printed layers of droplets with different osmolarities connected by lipid bilayers. When water flowed through the bilayer, it caused the droplets to either swell or shrink, resulting in bending of the microscale structures toward the layer of the initially more dilute droplets (Figure 12c). Aside from TPP, other methods used in fabrication of active origami at micrometer and nanometer scales include photolithography[186,407,414,415] and electron-beam lithography,[184,406] which use either light or electron beams to pattern small features in the surface of a material.

4. Origami Modeling

4.1. Modeling of Origami Structures

Structural modeling of origami enables the prediction of different mechanisms' deformations (single degree of freedom or multiple degrees of freedom) and mechanical behaviors (stiffness, foldability, and stability). Under the guidance of structural modeling, appropriately designed origami mechanisms permit preferred deformations and functions under mechanical loads or external stimuli. Various structural modeling approaches have been developed by using bar and hinge models, shell-element-based FEA models, and solid-element-based FEA models (**Figure 13**).

The bar and hinge model[416] is a simplified representation of an origami structure that substitutes the creases between panels with connected bars (green lines), and extra bars can

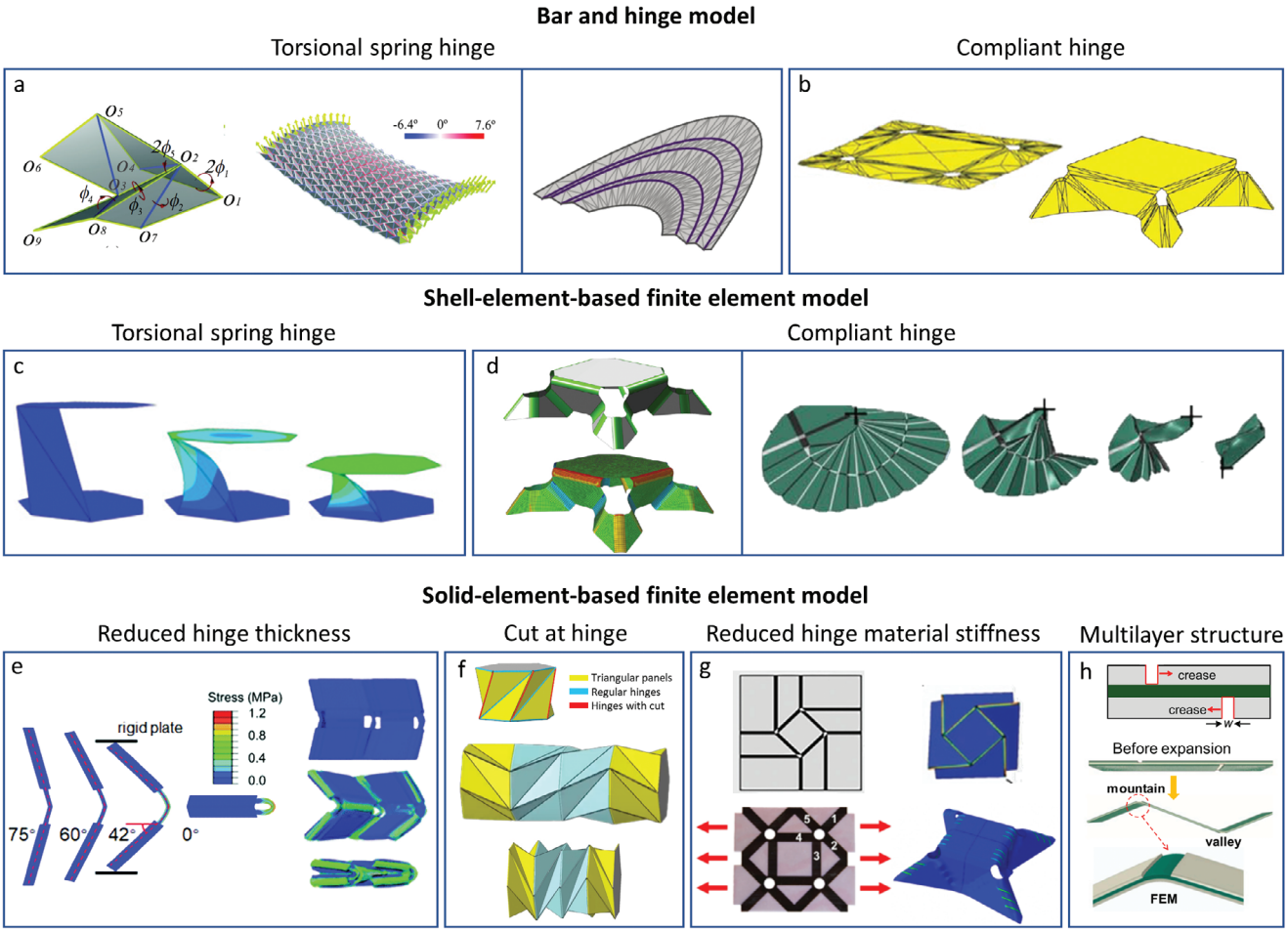

Figure 13. Strategies for structural modeling of origami. a) Bar and hinge models of both conventional origami patterns (left, adapted with permission.[417] Copyright 2013, American Physical Society) and curved-crease origami based on ideal torsional spring hinge without considering hinge width (right, adapted with permission.[420] Copyright 2020, Elsevier). b) Bar and hinge model of origami with compliant hinges (adapted with permission.[421] Copyright 2020, ASME). c) Shell-element-based finite element analysis (FEA) model with deformable panels connected by torsional spring hinges (adapted with permission.[064] Copyright 2018, Elsevier). d) Shell-element-based finite element (FE) models of origami with compliant hinges of an origami structure with smooth folds (adapted with permission.[426] Copyright 2016, Elsevier) and a bioinspired origami wing (adapted with permission.[427] Copyright 2018, AAAS). e–h) Solid-element based FE models of origami with specially designed hinges with e) reduced hinge thickness (adapted with permission.[428] Copyright 2018, The Royal Society of Chemistry.), f) introduced cuts at hinges (Adapted with permission.[075] Copyright 2022, the Authors, some rights reserved; exclusive licensee AAAS.), g) reduced material stiffness (Top: adapted with permission.[071] Copyright 2020, Wiley. Bottom: adapted with permission.[135] Copyright 2017, Springer Nature.) and h) multilayer structure (adapted with permission.[125] Copyright 2019, National Academy of Sciences).

be added across the origami panel (blue line) to accommodate for the in-plane stiffness (stretching and shearing), as illustrated in the left of Figure 13a.[417] Torsional hinge springs are placed along the bars between panels and along the bars across panels to model origami hinge folding and out-of-plane panel bending, respectively. Various types of bar and hinge models with one,[3,68,416,417] two,[418] or four[419] bars across the panel have been developed. These structural modeling methods were applied to predict both linear and nonlinear responses of traditional origami patterns (Figure 13a, left),[417] curved-creased origami (Figure 13a, right),[420] as well as origami structures accounting for compliant hinges with a finite width between the panels (Figure 13b)[421] and active hinges with stimuli-responsive actuations.[422] Based on the bar and hinge models, software such as Origami Simulator,[423] MERLIN2,[424] and Tessellatica[425] have been developed for origami structural modeling.

Although the bar and hinge models help reduce the cost of calculations, it leaves out valuable information such as stress and strain distributions in the origami structure during the folding process. FEA is a widely used simulation method based on physical modeling, providing a higher accuracy compared to the bar and hinge model. The shell-element-based FEA model is straightforward to adopt, as the thickness of origami panels is generally much smaller than the in-plane dimension.[61,64,98,127] The shell-element-based origami panels consider not only in-plane stretching and shearing, but out-of-plane bending as well. To account for the rotation of panels about the hinges, both ideal rotational spring hinges with zero width (Figure 13c)[64] and compliant hinges with finite width (Figure 13d, left[426] and right[427])

have been used, which are capable of capturing highly nonlinear mechanical responses such as snap-through deformations.[64,427]

FEA simulations of origami structures based on 3D solid elements consider the finite thickness of origami panels and hinges. Although this simulation technique is more computationally expensive than the others, the 3D modeling can take into account the complex geometry of origami, for example, layered origami structures composed of active and inactive materials, and thus provides the most information for the origami folding process. In addition, other physical information such as temperature gradient, swelling due to water absorption, etc. can be incorporated. Considering the actual hinge width and thickness in the 3D models, different methods have been adopted to ensure that the folding of panels happens at preferred positions, namely at the compliant hinges (Figure 13e–h).[71,75,125,135,428] Reduction in hinge thickness (Figure 13e)[428] or introduction of cuts at hinges (Figure 13f)[75] are generally used to generate compliant hinges in structures based on a single material.[307,429] When multimaterial fabrication is allowed, reduction in the material stiffness (Figure 13g, top[71] and bottom[135]) at hinges is an alternative option to reduce the effective hinge stiffness. As discussed before, layered structures combining active materials and inactive materials are commonly used for shape reconfiguration of active origami. Correspondingly, 3D FEA models with multilayer structures (Figure 13h)[125] are also widely seen in different works for the prediction of active origami actuation.[30,101,135,138,161,430] It should be noted that the dynamics of actuation become important to the folding behaviors of origami structures, especially for soft materials which can exhibit instabilities when actuated rapidly.

4.2. Modeling of Active Materials

Active origami modeling inevitably requires modeling of the mechanical deformation and stresses of constituent active materials in response to external stimuli. Depending on the material type, the mechanical behaviors are coupled with certain physical fields. Continuum mechanics-based constitutive models typically give the equations describing how state functions, such as internal energy, entropy, and stress, depend on state variables such as deformation gradient (or strain) and temperature, and sometimes on internal variables specific to each physical field. Incorporation of constitutive models with numerical simulation tools, such as FEA, enables the simulation of active response of materials and origami under mechanical and multiphysical stimuli.

Active materials used in origami are often based on polymeric materials, which exhibit large deformations. In this case, the multiphysics behaviors (or constitutive behaviors) are generally described by first specifying the Helmholtz free energy as a function of macroscopic deformation and internal variables associated with the coupled physical fields.[431] The stress–strain relationship can then be given by taking the derivative of the free energy with respect to the deformation. For instance, the Cauchy stress $\boldsymbol{\sigma}$ is given by:

$$\boldsymbol{\sigma} = J^{-1}\frac{\partial \mathrm{fi}}{\partial \mathbf{F}}\mathbf{F}^{\mathrm{T}} \tag{1}$$

where Ψ is the Helmholtz free energy density, $\mathbf{F}$ is the deformation gradient, the superscript "T" represents the transpose, and $J = \det(\mathbf{F})$ is the volume change. For a purely elastic network, the free energy, denoted by Ψ_{stretch}, recovers the strain energy, which depends on the configurational entropy due to network stretching only. Some specific forms of Ψ_{stretch} are available, such as neo-Hookean,[432] Arruda–Boyce,[433] Ogden,[434] etc. Note that, in addition to Equation 1, certain equations that constrain other state or internal variables may need to be satisfied due to the laws of thermodynamics. A summary of the modeling of different active materials is given in **Table 3**.

4.2.1. SMPs

A large number of models have been developed for SMPs, as summarized in the literature.[196,471] These models can be divided into two classes: thermoviscoelastic models[197,435,436,439,440,443] and phase evolution models.[437,438,441,442] The thermoviscoelastic model has been widely used for amorphous polymers, in which the shape memory effects are due to the change in chain mobility during glass transition. Based on this mechanism, the general idea is to adopt the temperature-dependent viscosity in the framework of viscoelasticity, thus leading to the term "thermoviscoelasticity". For example, assuming the relaxation time to follow the time-temperature superposition principle (TTSP) in simple viscoelastic models, the shape memory effects can be captured.[436,443] Multibranch viscoelastic models are often used to accommodate multiple relaxation modes in real polymers. Integration of TTSP with multibranch models showed improved capability in predicting the shape memory behaviors[197,435,440] or capturing multi-shape memory effects.[439]

The phase evolution model captures the physics in semi-crystalline polymers, although it is also used to model amorphous SMPs, in a so-called phenomenological manner. In the phase evolution model, the material is continuously crystallized in a loading process and the newly formed polymer crystals are assumed stress-free. Crystals formed at different instants can be seen as different phases, which undergo different deformation histories and thus carry different free energies. With this concept as the foundation, the Helmholtz free energy density function can be expressed as:[464]

$$\Psi = C_{OR}\Psi_{\mathrm{stretch}}\left(\mathbf{F}^{e}_{0\to t}\right) + \int_{0}^{t}\Delta\left(\tau, t\right)\Psi_{\mathrm{stretch}}\left(\mathbf{F}^{e}_{\tau\to t}\right)\mathrm{d}\tau \tag{2}$$

where C_{OR} and $\Delta(\tau, t)\mathrm{d}\tau$ are the fractions of the originally existed phases and the later formed phases, respectively, $\mathbf{F}^{e}$ is the mechanical deformation gradient for different phases with the subscript $t_1 \to t_2$ (or $0 \to t$) denoting the deformation from time t_1 to t_2 (or 0 to t), and Ψ_{stretch} is the free energy function due to network stretching. Note that C_{OR} and $\Delta(\tau, t)$ evolve based on certain kinetic laws[441] to capture the shape memory behaviors. All the evolving fractions in Equation 2 need to be tracked in numerical simulations, which is computationally expensive. The effective phase model has been developed to address this issue.[472] In addition, the concept of phase evolution has been used not only in the shape memory effects of semi-crystalline polymers but also in the shape memory or viscoelastic behavior of many active polymers, such as CANs. This will be discussed more in Section 4.2.5.

Table 3. Summary of modeling of active materials.

Material	Additional terms in free energy	State variables and internal variables
SMPs[197,435–443]		Deformations; phase fractions; temperature; light; moisture
Hydrogels[444–449]	Free energy due to substance mixing	Deformations; chemical species; temperature
LCEs[252,450–457]	Nematic free energy	Deformations; mesogen orientations;temperature; light
MSMs[356,458–463]	Magnetic potential	Deformations; magnetic field; magnetization density
CANs[464–470]		Deformations; phase fractions; temperature; light; moisture

4.2.2. Hydrogels

Hydrogels can exhibit reversible volumetric changes by absorbing or repelling water (or solvent). Thermodynamics and mechanics theories have been developed to capture the physical coupling between the stretching of the network, mixing of the solvent and the polymer, and network swelling.[444,446,447] In the pioneering work by Hong et al.,[444] the Helmholtz free energy density was expressed in two parts,

$$\Psi = \Psi_{\text{stretch}} + \Psi_{\text{mix}} \tag{3}$$

where Ψ_{stretch} and Ψ_{mix} represent the free energy due to the stretching and the mixing, respectively. A commonly used Ψ_{stretch} based on the Gaussian chain distribution is:[473]

$$\Psi_{\text{stretch}} = \frac{1}{2}NkT\left(\text{trace}\left(\mathbf{F}^{\text{T}}\mathbf{F}\right) - 3 - 2\ln J\right) \tag{4}$$

where N is the number of crosslinks per unit reference volume, k is Boltzmann constant, and T is the temperature. Note that Equation 4 is slightly different from the neo-Hookean form. Non-Gaussian statistics-based forms of Ψ_{stretch} have also been used to account for the limited extensibility of polymer chains.[447,448] The free energy Ψ_{mix} due to the mixing of polymer and the solvent is written based on the Flory–Huggins model:[474,475]

$$\Psi_{\text{mix}} = kTC\left(\ln\left(\frac{\nu C}{1+\nu C}\right) + \frac{\chi}{1+\nu C}\right) \tag{5}$$

where ν is the volume of a fluid molecule, C is the number of fluid molecules per unit reference volume, and χ is the Flory–Huggins interaction parameter characterizing the disaffinity between the polymer and the fluid.

With the above free energy form, Hong et al.[444] derived the constitutive relations for the stress, chemical potential and fluid flux under isothermal conditions. Later, Chester et al.[447,448] and Duda et al.[446] developed general, continuum-mechanics frameworks that could describe behaviors under complex thermo-chemo-mechanical loadings. The temperature-dependent $\chi(T)$ has also been used to model hydrogels with temperature-driven swelling/deswelling properties, such as pNIPAM.[448,449]

Implementation of the constitutive relations of hydrogels into FEA codes enables the direct simulation of hydrogels with complex geometry and under complex loadings.[448,476,477] For implementations in the FEA package ABAQUS (Dassault Systèmes, France), the user hyperelastic material (UHYPER)[476] or user element (UEL)[248,252,478] the mesogens may be reoriented and LCE may experience a phase transition between an ordered (nematic) and disordered (isotropic) state. To describe the intrinsic coupling between the deformation, reorientation of nematic order and other stimuli fields, many constitutive models have been developed.[252,450–453] Generally, the Helmholtz free energy density can be expressed as:[452]

$$\Psi = \Psi_{\text{stretch}} + \Psi_{\text{nematic}} \tag{6}$$

where Ψ_{stretch} is the free energy due to network stretching and Ψ_{nematic} is the nematic free energy.[248,452] The Ψ_{stretch} form first given by Bladon et al.[479] takes the energy form of neo-Hookean but is measured between the supposed isotropic phase and the current configuration, which has been widely used in literature.[450–454] The Ψ_{nematic} can be written as a function of the nematic order, and various forms have been used.[450,452,480] For polydomain LCEs, the free energy should take different forms in different nematic regions.[451,453] In general, the total free energy is a function of the network stretching, preferred orientation, and the nematic order. Recently, constitutive models have been developed for heat-[452] or light-responsive[455] LCEs, as well as LCEs with internal dissipations.[456,457] In addition, in many applications, the anisotropic thermal expansion of LCE with experimentally measured coefficients has been widely used in FEA to mimic the actuation of LCEs.[179,208,373]

4.2.3. MSMs

MSMs can be classified into soft-magnetic and hard-magnetic materials depending on the coercivity of the embedded magnetic particles. Many constitutive models on soft-magnetic elastomers have been developed.[481–483] However, here the hard-MSMs which are capable of complex active shape changes

will be focused on. Zhao et al.[458] developed the first general continuum framework for 3D finite deformation of hard-MSMs, in which the Helmholtz free energy density consists of two parts:

$$\Psi = \Psi_{\text{stretch}} + \Psi_{\text{magnetic}} \tag{7}$$

where Ψ_{stretch} represents the free energy due to the stretching of the soft matrix and the magnetic-related free energy Ψ_{magnetic} can be expressed as the magnetic potential of the embedded hard-magnetic particles, that is,

$$\Psi_{\text{magnetic}} = -\mathbf{FM} \cdot \mathbf{B}^{\text{applied}} \tag{8}$$

where $\mathbf{M}$ is the referential magnetization density and $\mathbf{B}^{\text{applied}}$ is the applied magnetic field. Note that with the above Helmholtz free energy, Zhao et al.[458] derived the constitutive relation for the stress of hard-MSMs, which has been implemented into ABAQUS through the user element (UEL) subroutine. Since the work of Zhao et al.,[458] many reduced-order models for hard-MSMs have also been developed to enable computationally low-cost simulations and designs.[460–462,484,485]

4.2.4. CANs

Modeling macroscopic behaviors of CANs generally requires incorporating the molecular-level kinetics of chemical reactions into the framework of continuum-level constitutive theory. According to how they are coupled, three main types of models which utilize different strategies have been developed. The first model is based on the concept of phase evolution. Long et al.[466] developed the first constitutive model for a light-activated associative CAN network based on this concept. Since then, the same concept has been applied to CAN systems with various types of stimuli and dynamic bonds.[464–466,472,486] Here, the phase is a more general representation of a small collection of polymer chains. Upon external stimuli, the polymer chains can continuously evolve due to the bond cleavage/re-formation. Using a similar concept for the crystallization, here the newly reformed chains are assumed stress-free. Therefore, the Helmholtz free energy density can be given by Equation 2.[464] Kinetic laws for the phase evolution are governed by the kinetics of chemical reactions and thus coupled to certain stimulus fields (e.g., temperature, light, and chemical species). The phase evolution model has been integrated with FEA, enabling predictive simulations of viscoelastic behaviors of CANs with complex 3D geometries.[487–490]

The second model was developed by Vernerey et al.,[468,469] who expressed the total free energy density in terms of a statistical distribution of the chain end-to-end vector $\mathbf{r}$, that is,

$$\Psi = \int_{\Omega} \phi\left(\mathbf{r}, t\right) \psi_C\left(\mathbf{r}\right) \mathrm{d}\Omega \tag{9}$$

where ϕ is the end-to-end vector distribution, ψ_C is the free energy density of the single chain, $\mathrm{d}\Omega = r^2 \sin\theta \mathrm{d}\theta \mathrm{d}\theta \mathrm{d}\omega$ is a small volume element of the conformation space Ω. Note that $\phi(\mathbf{r},t)$ describes the density of chains whose $\mathbf{r}$ is within the element $\mathrm{d}\Omega$. Upon deformation and chemical reactions, the distribution function is evolved following certain kinetic laws associated with the reaction kinetics, which can capture the macroscopic CAN behaviors.

The above two models physically incorporate the molecular-level reaction kinetics, as discussed in two recent reviews.[491,492] In addition, the third type of approach incorporates effects of dynamic reactions into phenomenological viscoelastic or viscoplastic frameworks.[470,493] The general idea is to use a rheological model with certain combinations of springs and dashpots to describe the CAN behavior. The viscous flow behavior of different dashpots can be chosen to depend on different stimuli following the reaction kinetics or the TTSP to capture complex multi-physics behaviors.

5. Conclusion

Active origami structures are appealing for many applications in reconfigurable devices, robotics, biomimetic actuators, metamaterials, aerospace, and biomedical environments and have seen rapid development in recent years. In this review, we have discussed common active materials and their actuation mechanisms, along with applications of active origami, common origami fabrication techniques, and a brief overview of the modeling of active materials and origami structures. Although we have highlighted here the many exciting advances in the field of active origami, such as structures with reprogrammable deformation, locomotive multifunctional origami robots, and state-of-the-art fabrication techniques to enable self-folding, we would like to point out the primary challenges currently faced, as well as the pertinent opportunities related to active origami.

While the low modulus of active polymers allows these materials to be applicable for several biomedical applications, soft polymer-based structures also suffer from low actuation force and poor mechanical strength, which is a significant limitation for many practical applications. Deeper exploration into special design of origami hinges[493] as well as further development of composite active materials[205,494–496] or methods to store elastic potential energy[215] may be able to help address these limitations.

Within the realm of fabrication, multimaterial structures, which can be used in multi-stimuli response applications and enable complex structures with distributed material rigidity, still face limitations such as the compatibility of materials, as well as printers capable of handling multiple different materials or even different printing methods within one setup.[179,374] Development of printers that could achieve this at a relatively low cost remains a challenge. Additionally, while rapid 4D printing methods such as DLP have been well developed for SMPs, further development of similar rapid 4D printing methods for materials such as hydrogels, LCEs, and MSMs would be beneficial. In addition to small-scale fabrication, the commercialization or wide-scale production of these materials becomes important. Hydrogels have been commercialized for use in several everyday items such as wound dressings and contact lenses[498] while CANs have been used for material recycling and reprocessing. Certain kinds of shape memory polymers are popular as heat shrink tubes or shrinkable plastic sheets while Nitinol, a type of shape memory

alloy, has been widely applied within biomedical, automotive, and aerospace industries. For a material with complicated fabrication such as LCE, however, industrialization may take considerably longer.

In addition, the design of accurate, controllable folding mechanisms is of great importance for practical applications of complex foldable structures. In terms of minimizing materials and weight of a structure, a simplified actuator arrangement is preferred that can still result in precise folding. The exploration of instabilities[499] and buckling mechanisms to enable precise folding and greater actuation force is suggested for deeper study, to address the limitations currently seen in the folding of soft materials.

Important to the future of active origami are systems which can effectively integrate sensing capabilities for data acquisition in a variety of applications. While the ability to change states in response to stimulus is inherent to the design of active origami systems, those which can adapt to environments and self-sense could result in nearly autonomous machines, especially for robotics and soft actuator applications. As active origami has enabled many biomimetic soft robotics applications, to further emulate these biological systems, more sophisticated interactions between the soft robot and its environment are required. There have been recent works which take advantage of active origami sensing,[73,220,500,501] however, the demonstrated sensing capabilities are still rather undeveloped and should be studied further. Ideally, these origami systems would be tetherless or have on-board control systems capable of intaking sensory information from the surrounding environment.

Overall, the field of active origami has seen many exciting advancements in the past few years, which can be used toward self-deployable and foldable structures on multiple size scales for many aerospace, metamaterial, robotic, and biomedical applications. With the further development and exploration of structural and material designs for active origami, unique solutions can be reached for many engineering challenges seen in the abovementioned areas.

Acknowledgements

R.R.Z., S.L., and S.W. acknowledge support from the NSF Award CPS-2201344 and the NSF Career Award CMMI-2145601. H.J.Q. and X.S. acknowledge the support of an AFOSR grant (FA9550-20-1-0306; Dr. B.-L. "Les" Lee, Program Manager).

Conflict of Interest

The authors declare no conflict of interest.

Keywords

active materials, folding, origami, origami modeling, stimuli-responsive materials

Received: March 4, 2023
Revised: April 13, 2023
Published online:

[1] T. Chen, O. R. Bilal, R. Lang, C. Daraio, K. Shea, *Phys. Rev. Appl.* **2019**, *11*, 064069.
[2] M. Schenk, A. D. Viquerat, K. A. Seffen, S. D. Guest, *J. Spacecr. Rockets* **2014**, *51*, 762.
[3] J. L. Silverberg, A. A. Evans, L. Mcleod, R. C. Hayward, T. Hull, C. D. Santangelo, I. Cohen, *Science* **2014**, *345*, 647.
[4] J. T. B. Overvelde, T. A. De Jong, Y. Shevchenko, S. A. Becerra, G. M. Whitesides, J. C. Weaver, C. Hoberman, K. Bertoldi, *Nat. Commun.* **2016**, *7*, 10929.
[5] E. T. Filipov, T. Tachi, G. H. Paulino, *Proc. Natl. Acad. Sci. USA* **2015**, *112*, 12321.
[6] Z. Lin, L. S. Novelino, H. Wei, N. A. Alderete, G. H. Paulino, H. D. Espinosa, S. Krishnaswamy, *Small* **2020**, *16*, 2002229.
[7] Z. Zhai, L. Wu, H. Jiang, *Appl. Phys. Rev.* **2021**, *8*, 041319.
[8] A. Pagano, T. Yan, B. Chien, A. Wissa, S. Tawfick, *Smart Mater. Struct.* **2017**, *26*, 094007.
[9] S.-J. Kim, D.-Y. Lee, G.-P. Jung, K.-J. Cho, *Sci. Rob.* **2018**, *3*, eaar2915.
[10] S. Felton, M. Tolley, E. Demaine, D. Rus, R. Wood, *Science* **2014**, *345*, 644.
[11] R. V. Martinez, C. R. Fish, X. Chen, G. M. Whitesides, *Adv. Funct. Mater.* **2012**, *22*, 1376.
[12] K. Kuribayashi, K. Tsuchiya, Z. You, D. Tomus, M. Umemoto, T. Ito, M. Sasaki, *Mater. Sci. Eng., A* **2006**, *419*, 131.
[13] S. Miyashita, S. Guitron, K. Yoshida, S. Li, D. D. Damian, D. Rus, in *2016 IEEE Int. Conf. on Robot. and Autom. (ICRA), Stockholm* **2016**.
[14] Q. Cheng, Z. Song, T. Ma, B. B. Smith, R. Tang, H. Yu, H. Jiang, C. K. Chan, *Nano Lett.* **2013**, *13*, 4969.
[15] S. A. Nauroze, L. S. Novelino, M. M. Tentzeris, G. H. Paulino, *Proc. Natl. Acad. Sci. USA* **2018**, *115*, 13210.
[16] Z. Song, T. Ma, R. Tang, Q. Cheng, Xu Wang, D. Krishnaraju, R. Panat, C. K. Chan, H. Yu, H. Jiang, *Nat. Commun.* **2014**, *5*, 3140.
[17] G. Masera, M. Pesenti, F. Fiorito, *J. Archit. Eng.* **2018**, *24*, 04018022.
[18] S. A. Zirbel, R. J. Lang, M. W. Thomson, D. A. Sigel, P. E. Walkemeyer, B. P. Trease, S. P. Magleby, L. L. Howell, *J. Mech. Des.* **2013**, *135*, 111005.
[19] S. A. Zirbel, B. P. Trease, M. W. Thomson, R. J. Lang, S. P. Magleby, L. H. Howell, *Micro- and Nanotechnology Sensors, Systems, and Applications VII*, **2015**, 94671C.
[20] J. Morgan, S. P. Magleby, L. L. Howell, *J. Mech. Des.* **2016**, *138*, 052301.
[21] J. Butler, J. Morgan, N. Pehrson, K. Tolman, T. Bateman, S. P. Magleby, L. L. Howell, in *Int. Des. Eng. Tech. Conf. and Comput. and Inform. in Eng. Conf.*, ASME, Charlotte, North Carolina, USA, **2016**.
[22] B. J. Edmondson, L. A. Bowen, C. L. Grames, S. P. Magleby, L. L. Howell, T. C. Bateman, in *ASME 2013 Conf. on Smart Mater., Adaptive Struct. and Intell. Syst.*, Snowbird, Utah, USA **2013**.
[23] H. Suzuki, R. J. Wood, *Nat. Mach. Intell.* **2020**, *2*, 437.
[24] P. Bhovad, J. Kaufmann, S. Li, *Extreme. Mech. Lett.* **2019**, *32*, 100552.
[25] H. Yasuda, T. Tachi, M. Lee, J. Yang, *Nat. Commun.* **2017**, *8*, 962.
[26] T. Liu, Y. Wang, K. Lee, *IEEE Robot Autom. Lett.* **2017**, *3*, 116.
[27] D. Melancon, B. Gorissen, C. J. García-Mora, C. Hoberman, K. Bertoldi, *Nature* **2021**, *592*, 545.
[28] S. Li, D. M. Vogt, D. Rus, R. J. Wood, *Proc. Natl. Acad. Sci. USA* **2017**, *114*, 13132.
[29] W. Kim, J. Byun, J.-K. Kim, W.-Y. Choi, K. Jakobsen, J. Jakobsen, D.-Y. Lee, K.-J. Cho, *Sci. Rob.* **2019**, *4*, eaay3493.
[30] C. Yoon, R. Xiao, J. Park, J. Cha, T. D. Nguyen, D. H. Gracias, *Smart Mater. Struct.* **2014**, *23*, 094008.
[31] Q. Ze, S. Wu, J. Dai, S. Leanza, G. Ikeda, P. C. Yang, G. Iaccarino, R. R. Zhao, *Nat. Commun.* **2022**, *13*, 3118.
[32] Z. Fang, H. Song, Y. Zhang, B. Jin, J. Wu, Q. Zhao, T. Xie, *Matter* **2020**, *2*, 1187.
[33] C. Yuan, D. J. Roach, C. K. Dunn, Q. Mu, X. Kuang, C. M. Yakacki, T. J. Wang, K. Yu, H. J. Qi, *Soft Matter* **2017**, *13*, 5558.

[34] J. Ryu, M. D'amato, X. Cui, K. N. Long, H. J. Qi, M. L. Dunn, *Appl. Phys. Lett.* **2012**, *100*, 161908.
[35] Q. Ge, C. K. Dunn, H. J. Qi, M. L. Dunn, *Smart Mater. Struct.* **2014**, *23*, 094007.
[36] E. A. Peraza-Hernandez, D. J. Hartl, R. J. Malak Jr, D. C. Lagoudas, *Smart Mater. Struct.* **2014**, *23*, 094001.
[37] Y. Kim, H. Yuk, R. Zhao, S. A. Chester, X. Zhao, *Nature* **2018**, *558*, 274.
[38] Y. Kim, X. Zhao, *Chem. Rev.* **2022**, *122*, 5317.
[39] Y. Park, T. S. Chung, G. Lee, J. A. Rogers, *Chem. Rev.* **2022**, *122*, 5277.
[40] J. M. Mccracken, B. R. Donovan, T. J. White, *Adv. Mater.* **2020**, *32*, 1906564.
[41] H. Yuk, J. Wu, X. Zhao, *Nat. Rev. Mater.* **2022**, *7*, 935.
[42] I. Apsite, S. Salehi, L. Ionov, *Chem. Rev.* **2022**, *122*, 1349.
[43] A. Kirillova, L. Ionov, *J. Mater. Chem. B* **2019**, *7*, 1597.
[44] S. Wu, W. Hu, Q. Ze, M. Sitti, R. Zhao, *Multifunct. Mater.* **2020**, *3*, 042003.
[45] X. Ning, X. Wang, Y. Zhang, X. Yu, D. Choi, N. Zheng, D. S. Kim, Y. Huang, Y. Zhang, J. A. Rogers, *Adv. Mater. Interfaces* **2018**, *5*, 1800284.
[46] D. Rus, M. T. Tolley, *Nat. Rev. Mater.* **2018**, *3*, 101.
[47] S. Li, H. Fang, S. Sadeghi, P. Bhovad, K.-W. Wang, *Adv. Mater.* **2019**, *31*, 1805282.
[48] V. A. Bolaños Quiñones, H. Zhu, A. A. Solovev, Y. Mei, D. H. Gracias, *Adv. Biosyst.* **2018**, *2*, 1800230.
[49] Y. Zhu, M. Schenk, E. T. Filipov, *Appl. Mech. Rev.* **2022**, *74*, 030801.
[50] J. J. Park, P. Won, S. H. Ko, *Int. J. Precis. Eng. Manuf. Green Technol.* **2019**, *6*.
[51] L. Xu, T. C. Shyu, N. A. Kotov, *ACS Nano* **2017**, *11*, 7587.
[52] S. J. P. Callens, A. A. Zadpoor, *Mater. Today* **2018**, *21*, 241.
[53] J. Rogers, Y. Huang, O. G. Schmidt, D. H. Gracias, *MRS Bull.* **2016**, *41*, 123.
[54] K. Miura, *The Institute of Space and Astronautical Sci. Rep.* **1985**, *618*, p. 1.
[55] D.-Y. Lee, J.-S. Kim, S.-R. Kim, J.-S. Koh, K.-J. Cho, in *Int. Des. Eng. Tech. Conf. and Comput. and Inform. in Eng. Conf.*, American Society of Mechanical Engineers, New York **2013**.
[56] S. Li, J. J. Stampfli, H. J. Xu, E. Malkin, E. V. Diaz, D. Rus, R. J. Wood, in *2019 Int. Conf. on Robot. and Autom. (ICRA)*, Montreal, QC, Canada **2019**.
[57] H. Yasuda, T. Yein, T. Tachi, K. Miura, M. Taya, *Proc. R. Soc. A* **2013**, *469*, 20130351.
[58] M. Schenk, S. D. Guest, *Proc. Natl. Acad. Sci. USA* **2013**, *110*, 3276.
[59] J. L. Silverberg, J.-H. Na, A. A. Evans, B. Liu, T. C. Hull, C. D. Santangelo, R. J. Lang, R. C. Hayward, I. Cohen, *Nat. Mater.* **2015**, *14*, 389.
[60] Y. Yoshimura, No. NACA-TM-1390., **1955**, 93R23165.
[61] C. Lv, D. Krishnaraju, G. Konjevod, H. Yu, H. Jiang, *Sci. Rep.* **2014**, *4*, 5979.
[62] T. Tachi, *J. Mech. Des.* **2013**, *135*, 111006.
[63] B. Kresling, in *Origami*^{3} (Ed: T. Hull), Taylor & Francis Group, California, **2002**, Part II, p. 197.
[64] N. Nayakanti, S. H. Tawfick, A. J. Hart, *Extreme Mech. Lett.* **2018**, *21*, 17.
[65] Z. Zhai, Y. Wang, H. Jiang, *Proc. Natl. Acad. Sci. USA* **2018**, *115*, 2032.
[66] K. Liu, T. Tachi, G. H. Paulino, *Nat. Commun.* **2019**, *10*, 4238.
[67] E. T. Filipov, M. Redoutey, *Extreme Mech. Lett.* **2018**, *25*, 16.
[68] L. H. Dudte, E. Vouga, T. Tachi, L. Mahadevan, *Nat. Mater.* **2016**, *15*, 583.
[69] J. Kaufmann, S. Li, *Soft Robot.* **2021, 9, 212**.
[70] Lu Lu, X. Dang, F. Feng, P. Lv, H. Duan, *Proc. R. Soc. A* **2022**, *478*, 20210712.
[71] L.-C. Wang, W.-L. Song, Y.-J. Zhang, M.-J. Qu, Z. Zhao, M. Chen, Y. Yang, H. Chen, D. Fang, *Adv. Funct. Mater.* **2020**, *30*, 1909087.
[72] S. Sengupta, S. Li, *J. Intell. Mater Syst. Struct.* **2018**, *29*, 2933.
[73] L. S. Novelino, Q. Ze, S. Wu, G. H. Paulino, R. Zhao, *Proc. Natl. Acad. Sci. USA* **2020**, *117*, 24096.
[74] Z. Li, N. Kidambi, L. Wang, K.-W. Wang, *Extreme Mech. Lett.* **2020**, *39*, 100795.
[75] Q. Ze, S. Wu, J. Nishikawa, J. Dai, Y. Sun, S. Leanza, C. Zemelka, L. S. Novelino, G. H. Paulino, R. R. Zhao, *Sci. Adv.* **2022**, *8*, eabm7834.
[76] B. Treml, A. Gillman, P. Buskohl, R. Vaia, *Proc. Natl. Acad. Sci. USA* **2018**, *115*, 6916.
[77] S. Xu, Z. Yan, K.-I. Jang, W. Huang, H. Fu, J. Kim, Z. Wei, M. Flavin, J. Mccracken, R. Wang, A. Badea, Y. Liu, D. Xiao, G. Zhou, J. Lee, H. U. Chung, H. Cheng, W. Ren, A. Banks, X. Li, U. Paik, R. G. Nuzzo, Y. Huang, Y. Zhang, J. A. Rogers, *Science* **2015**, *347*, 154.
[78] N. A. Alderete, L. Medina, L. Lamberti, C. Sciammarella, H. D. Espinosa, *Extreme Mech. Lett.* **2021**, *43*, 101146.
[79] X. Zhang, L. Medina, H. Cai, V. Aksyuk, H. D. Espinosa, D. Lopez, *Adv. Mater* **2021**, *33*, 2005275.
[80] V. G. A. Goss, G. H. M. Van Der Heijden, J. M. T. Thompson, S. Neukirch, *Exp. Mech.* **2005**, *45*, 101.
[81] X. Lachenal, P. M. Weaver, S. Daynes, *Proc. R. Soc. A* **2012**, *468*, 1230.
[82] Y. Goto, Y. Watanabe, T. Kasugai, M. Obata, *Int. J. Solids Struct.* **1992**, *29*, 893.
[83] P.-O. Mouthuy, M. Coulombier, T. Pardoen, J.-P. Raskin, A. M. Jonas, *Nat. Commun.* **2012**, *3*, 1290.
[84] P. F. Pai, A. N. Palazotto, *Int. J. Solids Struct.* **1996**, *33*, 1335.
[85] B. Audoly, K. A. Seffen, *J. Elast.* **2015**, *119*, 293.
[86] S. Wu, L. Yue, Y. Jin, X. Sun, C. Zemelka, H. J. Qi, R. Zhao, *Adv. Intell. Syst.* **2021**, *3*, 2100107.
[87] X. Sun, S. Wu, J. Dai, S. Leanza, L. Yue, L. Yu, Y. Jin, H. J. Qi, R. R. Zhao, *Int. J. Solids Struct.* **2022**, *248*, 111685.
[88] S. Leanza, S. Wu, J. Dai, R. R. Zhao, *J. Appl. Mech.* **2022**, *89*.
[89] L. Lu, S. Leanza, J. Dai, X. Sun, R. R. Zhao, *J. Mech. Phys. Solids* **2022**, *171*, 105142.
[90] S. Wu, J. Dai, S. Leanza, R. R. Zhao, *Extreme Mech. Lett.* **2022**, *53*, 101713.
[91] E. D. Demaine, M. L. Demaine, D. Koschitz, T. Tachi, *Symmetry: Cult. Sci.* **2015**, *26*, 145.
[92] M. A. Dias, L. H. Dudte, L. Mahadevan, C. D. Santangelo, *Phys. Rev. Lett.* **2012**, *109*, 114301.
[93] E. D. Demaine, M. L. Demaine, V. Hart, G. N. Price, T. Tachi, in *Graphs and Combinatorics*, Springer, Berlin **2011**.
[94] T.-U. Lee, Y. Chen, M. T. Heitzmann, J. M. Gattas, *Mater. Des.* **2021**, *207*, 109859.
[95] N. Lee, S. Pellegrino, in *Spacecraft Struct. Conf.*, AIAA, National Harbor, Maryland, USA, **2014**.
[96] A. Körner, L. Born, A. Mader, R. Sachse, S. Saffarian, A. S. Westermeier, S. Poppinga, M. Bischoff, G. T. Gresser, M. Milwich, T. Speck, J. Knippers, *Smart Mater. Struct.* **2018**, *27*, 017001.
[97] Y. Du, C. Song, J. Xiong, L. Wu, *Compos. Sci. Technol.* **2019**, *174*, 94.
[98] Z. Zhai, Y. Wang, K. Lin, L. Wu, H. Jiang, *Sci. Adv.* **2020**, *6*, eabe2000.
[99] Z. Yan, F. Zhang, J. Wang, F. Liu, X. Guo, K. Nan, Q. Lin, M. Gao, D. Xiao, Y. Shi, Y. Qiu, H. Luan, J. H. Kim, Y. Wang, H. Luo, M. Han, Y. Huang, Y. Zhang, J. A. Rogers, *Adv. Funct. Mater.* **2016**, *26*, 2629.
[100] Z. Yan, F. Zhang, F. Liu, M. Han, D. Ou, Y. Liu, Q. Lin, X. Guo, H. Fu, Z. Xie, M. Gao, Y. Huang, J. Kim, Y. Qiu, K. Nan, J. Kim, P. Gutruf, H. Luo, An Zhao, K.-C. Hwang, Y. Huang, Y. Zhang, J. A. Rogers, *Sci. Adv.* **2016**, *2*, e1601014.
[101] T. Van Manen, S. Janbaz, M. Ganjian, A. A. Zadpoor, *Mater. Today* **2020**, *32*, 59.
[102] M. Redoutey, A. Roy, E. T. Filipov, *Int. J. Solids Struct.* **2021**, *229*, 111140.
[103] J. P. Whitney, P. S. Sreetharan, K. Y. Ma, R. J. Wood, *J. Micromech. Microeng.* **2011**, *21*, 115021.

[104] Z. Liu, H. Du, J. Li, L. Lu, Z.-Y. Li, N. X. Fang, *Sci. Adv.* **2018**, *4*, eaat4436.
[105] H. Fu, K. Nan, W. Bai, W. Huang, K. Bai, L. Lu, C. Zhou, Y. Liu, F. Liu, J. Wang, M. Han, Z. Yan, H. Luan, Y. Zhang, Y. Zhang, J. Zhao, Xu Cheng, M. Li, J. W. Lee, Y. Liu, D. Fang, X. Li, Y. Huang, Y. Zhang, J. A. Rogers, *Nat. Mater.* **2018**, *17*, 268.
[106] F. Zhang, S. Li, Z. Shen, X. Cheng, Z. Xue, H. Zhang, H. Song, K. Bai, D. Yan, H. Wang, Y. Zhang, Y. Huang, *Proc. Natl. Acad. Sci. USA* **2021**, *118*, e2026414118.
[107] M. Han, X. Guo, X. Chen, C. Liang, H. Zhao, Q. Zhang, W. Bai, F. Zhang, H. Wei, C. Wu, Q. Cui, S. Yao, B. Sun, Y. Yang, Q. Yang, Y. Ma, Z. Xue, J. W. Kwak, T. Jin, Q. Tu, E. Song, Z. Tian, Y. Mei, D. Fang, H. Zhang, Y. Huang, Y. Zhang, J. A. Rogers, *Sci. Rob.* **2022**, *7*, eabn0602.
[108] B. H. Kim, K. Li, J.-T. Kim, Y. Park, H. Jang, X. Wang, Z. Xie, S. M. Won, H.-J. Yoon, G. Lee, W. J. Jang, K. H. Lee, T. S. Chung, Y. H. Jung, S. Y. Heo, Y. Lee, J. Kim, T. Cai, Y. Kim, P. Prasopsukh, Y. Yu, X. Yu, R. Avila, H. Luan, H. Song, F. Zhu, Y. Zhao, L. Chen, S. H. Han, J. Kim, et al., *Nature* **2021**, *597*, 503.
[109] K. Liu, F. Hacker, C. Daraio, *Sci. Rob.* **2021**, *6*, eabf5116.
[110] X. Zang, C. Shen, Y. Chu, B. Li, M. Wei, J. Zhong, M. Sanghadasa, L. Lin, *Adv. Mater.* **2018**, *30*, 1800062.
[111] J. Ding, B. Li, L. Chen, W. Qin, *Angew. Chem., Int. Ed.* **2016**, *55*, 13033.
[112] X. Chen, Y. Li, X. Wang, H. Yu, *ACS Appl. Mater. Interfaces* **2022**, *14*, 36227.
[113] Y. Chen, R. Peng, Z. You, *Science* **2015**, *349*, 396.
[114] T. Tachi, in *Origami5* (Eds: P. Wang-Iverson, R. J. Lang, M. Yim), Taylor & Francis Group, New York **2011**, Ch. 20.
[115] M. Behl, M. Y. Razzaq, A. Lendlein, *Adv. Mater.* **2010**, *22*, 3388.
[116] M. T. Tolley, S. M. Felton, S. Miyashita, D. Aukes, D. Rus, R. J. Wood, *Smart Mater. Struct.* **2014**, *23*, 094006.
[117] Y. Mao, K. Yu, M. S. Isakov, J. Wu, M. L. Dunn, H. J. Qi, *Sci. Rep.* **2015**, *5*, 13616.
[118] S. Janbaz, R. Hedayati, A. A. Zadpoor, *Mater. Horiz.* **2016**, *3*, 536.
[119] M. Wagner, T. Chen, K. Shea, *3D Print. Addit. Manuf.* **2017**, *4*, 133.
[120] A. Oyefusi, J. Chen, *Angew. Chem., Int. Ed.* **2017**, *56*, 8250.
[121] J. Cui, J. G. M. Adams, Y. Zhu, *Smart Mater. Struct.* **2017**, *26*, 125011.
[122] J. Cui, F. R. Poblete, Y. Zhu, *Adv. Funct. Mater.* **2018**, *28*, 1802768.
[123] G. Li, S. Wang, Z. Liu, Z. Liu, H. Xia, C. Zhang, X. Lu, J. Jiang, Y. Zhao, *ACS Appl. Mater. Interfaces* **2018**, *10*, 40189.
[124] D. H. Wang, L.-S. Tan, *ACS Macro Lett.* **2019**, *8*, 546.
[125] Y. Tang, Y. Li, Y. Hong, S. Yang, J. Yin, *Proc. Natl. Acad. Sci. USA* **2019**, *116*, 26407.
[126] X. Xin, L. Liu, Y. Liu, J. Leng, *Smart Mater. Struct.* **2020**, *29*, 065015.
[127] R. Tao, L. Ji, Y. Li, Z. Wan, W. Hu, W. Wu, B. Liao, L. Ma, D. Fang, *Composites, Part B* **2020**, *201*, 108344.
[128] S. Jape, M. Garza, J. Ruff, F. Espinal, D. Sessions, G. Huff, D. C. Lagoudas, E. A. Peraza Hernandez, D. J. Hartl, *Smart Mater. Struct.* **2020**, *29*, 115011.
[129] C. Yang, M. Boorugu, A. Dopp, J. Ren, R. Martin, D. Han, W. Choi, H. Lee, *Mater. Horiz.* **2019**, *6*, 1244.
[130] L. Zhao, L. Wang, J. Shi, X. Hou, Qi Wang, Y. Zhang, Y. Wang, N. Bai, J. Yang, J. Zhang, B. Yu, C. F. Guo, *ACS Nano* **2021**, *15*, 5752.
[131] T. Langford, A. Mohammed, K. Essa, A. Elshaer, H. Hassanin, *Appl. Sci.* **2021**, *11*, 332.
[132] W. Zhao, N. Li, L. Liu, J. Leng, Y. Liu, *Compos. Struct.* **2022**, *293*, 115669.
[133] S. Miyashita, L. Meeker, M. T. Tolley, R. J. Wood, D. Rus, *Smart Mater. Struct.* **2014**, *23*, 094005.
[134] J. Zhou, S. A. Turner, S. M. Brosnan, Q. Li, J.-M. Y. Carrillo, D. Nykypanchuk, O. Gang, V. S. Ashby, A. V. Dobrynin, S. S. Sheiko, *Macromolecules* **2014**, *47*, 1768.
[135] C. Yuan, T. Wang, M. L. Dunn, H. J. Qi, *Int. J. Precis. Eng. Manuf.-Green Technol.* **2017**, *4*, 281.
[136] J.-E. Suh, Y. Miyazawa, J. Yang, J.-H. Han, *Adv. Eng. Mater.* **2022**, *24*, 2101202.
[137] H. Yang, W. R. Leow, T. Wang, J. Wang, J. Yu, K. He, D. Qi, C. Wan, X. Chen, *Adv. Mater.* **2017**, *29*, 1701627.
[138] Q. Zhang, J. Wommer, C. O'rourke, J. Teitelman, Y. Tang, J. Robison, G. Lin, J. Yin, *Extreme Mech. Lett.* **2017**, *11*, 111.
[139] Y. Liu, J. K. Boyles, J. Genzer, M. D. Dickey, *Soft Matter* **2012**, *8*, 1764.
[140] Y. Liu, B. Shaw, M. D. Dickey, J. Genzer, *Sci. Adv.* **2017**, *3*, e1602417.
[141] J. R. Kumpfer, S. J. Rowan, *J. Am. Chem. Soc.* **2011**, *133*, 12866.
[142] Z. Li, X. Zhang, S. Wang, Y. Yang, B. Qin, K. Wang, T. Xie, Y. Wei, Y. Ji, *Chem. Sci.* **2016**, *7*, 4741.
[143] Y. Lee, H. Lee, T. Hwang, J.-G. Lee, M. Cho, *Sci. Rep.* **2015**, *5*, 16544.
[144] J. Xue, Y. Ge, Z. Liu, Z. Liu, J. Jiang, G. Li, *ACS Appl. Mater. Interfaces* **2022**, *14*, 10836.
[145] Y. Ge, H. Wang, J. Xue, J. Jiang, Z. Liu, Z. Liu, G. Li, Y. Zhao, *ACS Appl. Mater. Interfaces* **2021**, *13*, 38773.
[146] M. Jamal, S. S. Kadam, R. Xiao, F. Jivan, T.-M. Onn, R. Fernandes, T. D. Nguyen, D. H. Gracias, *Adv. Healthcare Mater.* **2013**, *2*, 1142.
[147] J.-H. Na, A. A. Evans, J. Bae, M. C. Chiappelli, C. D. Santangelo, R. J. Lang, T. C. Hull, R. C. Hayward, *Adv. Mater.* **2015**, *27*, 79.
[148] X. Zhang, C. L. Pint, M. H. Lee, B. E. Schubert, A. Jamshidi, K. Takei, H. Ko, A. Gillies, R. Bardhan, J. J. Urban, M. Wu, R. Fearing, A. Javey, *Nano Lett.* **2011**, *11*, 3239.
[149] G. Stoychev, S. Turcaud, J. W. C. Dunlop, L. Ionov, *Adv. Funct. Mater.* **2013**, *23*, 2295.
[150] J. Kim, J. A. Hanna, R. C. Hayward, C. D. Santangelo, *Soft Matter* **2012**, *8*, 2375.
[151] C. Yao, Z. Liu, C. Yang, W. Wang, X.-J. Ju, R. Xie, L.-Y. Chu, *Adv. Funct. Mater.* **2015**, *25*, 2980.
[152] C. Ma, W. Lu, X. Yang, J. He, X. Le, L. Wang, J. Zhang, M. J. Serpe, Y. Huang, T. Chen, *Adv. Funct. Mater.* **2018**, *28*, 1704568.
[153] E. Wang, M. S. Desai, S.-W. Lee, *Nano Lett.* **2013**, *13*, 2826.
[154] Z. Lei, W. Zhu, S. Sun, P. Wu, *Nanoscale* **2016**, *8*, 18800.
[155] D. Jin, Q. Chen, T.-Y. Huang, J. Huang, L. Zhang, H. Duan, *Mater. Today* **2020**, *32*, 19.
[156] N. Bassik, B. T. Abebe, K. E. Laflin, D. H. Gracias, *Polymer* **2010**, *51*, 6093.
[157] L. Zhao, J. Huang, Y. Zhang, T. Wang, W. Sun, Z. Tong, *ACS Appl. Mater. Interfaces* **2017**, *9*, 11866.
[158] H. Deng, X. Xu, C. Zhang, J.-W. Su, G. Huang, J. Lin, *ACS Appl. Mater. Interfaces* **2020**, *12*, 13378.
[159] H. Zhang, X. Guo, J. Wu, D. Fang, Y. Zhang, *Sci. Adv.* **2018**, *4*, eaar8535.
[160] H. He, J. Guan, J. L. Lee, *J. Controlled Release* **2006**, *110*, 339.
[161] J. C. Breger, C. K. Yoon, R. Xiao, H. R. Kwag, M. O. Wang, J. P. Fisher, T. D. Nguyen, D. H. Gracias, *ACS Appl. Mater. Interfaces* **2015**, *7*, 3398.
[162] K. Malachowski, J. Breger, H. R. Kwag, M. O. Wang, J. P. Fisher, F. M. Selaru, D. H. Gracias, *Angew. Chem., Int. Ed.* **2014**, *53*, 8045.
[163] T. S. Shim, S.-H. Kim, C.-J. Heo, H. C. Jeon, S.-M. Yang, *Angew. Chem., Int. Ed.* **2012**, *51*, 1420.
[164] G. Stoychev, N. Puretskiy, L. Ionov, *Soft Matter* **2011**, *7*, 3277.
[165] Y. Li, Y. Teixeira, G. Parlato, J. Grace, F. Wang, B. D. Huey, X. Wang, *Soft Matter* **2022**, 6857.
[166] G. Chen, B. Jin, Y. Shi, Q. Zhao, Y. Shen, T. Xie, *Adv. Mater. 34*, 2201679.
[167] L. Ren, B. Li, Y. He, Z. Song, X. Zhou, Q. Liu, Q. Liu, L. Ren, *ACS Appl. Mater. Interfaces* **2020**, *12*, 15562.
[168] Y. Huang, H. K. Bisoyi, S. Huang, M. Wang, X.-M. Chen, Z. Liu, H. Yang, Q. Li, *Angew. Chem., Int. Ed.* **2021**, *60*, 11247.
[169] M. K. Mcbride, A. M. Martinez, L. Cox, M. Alim, K. Childress, M. Beiswinger, M. Podgorski, B. T. Worrell, J. Killgore, C. N. Bowman, *Sci. Adv.* **2018**, *4*, eaat4634.

[170] Z.-C. Jiang, Y.-Y. Xiao, X. Tong, Y. Zhao, *Angew. Chem., Int. Ed.* **2019**, *58*, 5332.
[171] K. Fuchi, T. H. Ware, P. R. Buskohl, G. W. Reich, R. A. Vaia, T. J. White, J. J. Joo, *Soft Matter* **2015**, *11*, 7288.
[172] A. Kotikian, C. Mcmahan, E. C. Davidson, J. M. Muhammad, R. D. Weeks, C. Daraio, J. A. Lewis, *Sci. Rob.* **2019**, *4*, eaax7044.
[173] T. H. Ware, M. E. Mcconney, J. J. Wie, V. P. Tondiglia, T. J. White, *Science* **2015**, *347*, 982.
[174] L. T. De Haan, J. M. N. Verjans, D. J. Broer, C. W. M. Bastiaansen, A. P. H. J. Schenning, *J. Am. Chem. Soc.* **2014**, *136*, 10585.
[175] K. Kim, Y. Guo, J. Bae, S. Choi, H. Y. Song, S. Park, K. Hyun, S.-K. Ahn, *Small* **2021**, *17*, 2100910.
[176] H. Kim, J. A. Lee, C. P. Ambulo, H. B. Lee, S. H. Kim, V. V. Naik, C. S. Haines, A. E. Aliev, R. Ovalle-Robles, R. H. Baughman, T. H. Ware, *Adv. Funct. Mater.* **2019**, *29*, 1905063.
[177] R. C. P. Verpaalen, M. Pilz Da Cunha, T. A. P. Engels, M. G. Debije, A. P. H. J. Schenning, *Angew. Chem., Int. Ed.* **2020**, *59*, 4532.
[178] X. Pang, L. Qin, B. Xu, Q. Liu, Y. Yu, *Adv. Funct. Mater.* **2020**, *30*, 2002451.
[179] X. Peng, S. Wu, X. Sun, L. Yue, S. M. Montgomery, F. Demoly, K. Zhou, R. R. Zhao, H. J. Qi, *Adv. Mater.* **2022**, *34*, 2204890.
[180] D. J. Roach, X. Kuang, C. Yuan, K. Chen, H. J. Qi, *Smart Mater. Struct.* **2018**, *27*, 125011.
[181] V. Maurin, Y. Chang, Q. Ze, S. Leanza, R. R. Zhao, (Preprint) arXiv:2302. 13583, submitted: Feb **2023**.
[182] S. Yi, L. Wang, Z. Chen, J. Wang, X. Song, P. Liu, Y. Zhang, Q. Luo, L. Peng, Z. Wu, C. F. Guo, L. Jiang, *Nat. Commun.* **2022**, *13*, 4177.
[183] Z. Ren, W. Hu, X. Dong, M. Sitti, *Nat. Commun.* **2019**, *10*, 2703.
[184] J. Cui, T.-Y. Huang, Z. Luo, P. Testa, H. Gu, X.-Z. Chen, B. J. Nelson, L. J. Heyderman, *Nature* **2019**, *575*, 164.
[185] S. Wu, Q. Ze, J. Dai, N. Udipi, G. H. Paulino, R. Zhao, *Proc. Natl. Acad. Sci. USA* **2021**, *118*, e2110023118.
[186] T. G. Leong, C. L. Randall, B. R. Benson, N. Bassik, G. M. Stern, D. H. Gracias, *Proc. Natl. Acad. Sci. USA* **2009**, *106*, 703.
[187] L. Li, H. Yao, S. Mi, *ACS Appl. Mater. Interfaces* **2023**, *15*, 3486.
[188] D. Tang, C. Zhang, H. Sun, H. Dai, J. Xie, J. Fu, P. Zhao, *Nano Energy* **2021**, *89*, 106424.
[189] Y. Alapan, A. C. Karacakol, S. N. Guzelhan, I. Isik, M. Sitti, *Sci. Adv.* **2020**, *6*, eabc6414.
[190] H. Deng, K. Sattari, Y. Xie, P. Liao, Z. Yan, J. Lin, *Nat. Commun.* **2020**, *11*, 6325.
[191] B. S. Yeow, H. Yang, M. S. Kalairaj, H. Gao, C. J. Cai, S. Xu, P.-Y. Chen, H. Ren, *Adv. Mater. Technol.* **2022**, *7*, 2101140.
[192] T. Xu, J. Zhang, M. Salehizadeh, O. Onaizah, E. Diller, *Sci. Rob.* **2019**, *4*, eaav4494.
[193] Y. Liu, H. Du, L. Liu, J. Leng, *Smart Mater. Struct.* **2014**, *23*, 023001.
[194] W. Zhao, L. Liu, F. Zhang, J. Leng, Y. Liu, *Mater. Sci. Eng., C* **2019**, *97*, 864.
[195] H. Gao, J. Li, F. Zhang, Y. Liu, J. Leng, *Mater. Horiz.* **2019**, *6*, 931.
[196] Q. Zhao, H. J. Qi, T. Xie, *Prog. Polym. Sci.* **2015**, *49*, 79.
[197] K. Yu, Q. Ge, H. J. Qi, *Nat. Commun.* **2014**, *5*, 3066.
[198] A. Lendlein, S. Kelch, *Angew. Chem., Int. Ed.* **2002**, *41*, 2034.
[199] M. Behl, K. Kratz, J. Zotzmann, U. Nöchel, A. Lendlein, *Adv. Mater.* **2013**, *25*, 4466.
[200] T. Chung, A. Romo-Uribe, P. T. Mather, *Macromolecules* **2008**, *41*, 184.
[201] K. K. Westbrook, P. T. Mather, V. Parakh, M. L. Dunn, Q. Ge, B. M. Lee, H. J. Qi, *Smart Mater. Struct.* **2011**, *20*, 065010.
[202] I. Bellin, S. Kelch, R. Langer, A. Lendlein, *Proc. Natl. Acad. Sci. USA* **2006**, *103*, 18043.
[203] T. Xie, *Nature* **2010**, *464*, 267.
[204] Y. Mao, Z. Ding, C. Yuan, S. Ai, M. Isakov, J. Wu, T. Wang, M. L. Dunn, H. J. Qi, *Sci. Rep.* **2016**, *6*, 24761.
[205] C. Yuan, F. Wang, Q. Ge, *Extreme Mech. Lett.* **2021**, *42*, 101122.
[206] J. A.-C. Liu, J. H. Gillen, S. R. Mishra, B. A. Evans, J. B. Tracy, *Sci. Adv.* **2019**, *5*, eaaw2897.
[207] Q. Ze, X. Kuang, S. Wu, J. Wong, S. M. Montgomery, R. Zhang, J. M. Kovitz, F. Yang, H. J. Qi, R. Zhao, *Adv. Mater. 32*, 1906657.
[208] D. J. Roach, X. Sun, X. Peng, F. Demoly, K. Zhou, H. J. Qi, *Adv. Funct. Mater.* **2022**, *32*, 2203236.
[209] S. Wu, J. Eichenberger, J. Dai, Y. Chang, N. Ghalichechian, R. R. Zhao, *Adv. Intell. Syst.* **2022**, *4*, 2200106.
[210] L. Cera, G. M. Gonzalez, Q. Liu, S. Choi, C. O. Chantre, J. Lee, R. Gabardi, M. C. Choi, K. Shin, K. K. Parker, *Nat. Mater. 20*, 242.
[211] A. Firouzeh, M. Salerno, J. Paik, *IEEE Trans. Robot.* **2017**, *33*, 765.
[212] A. Firouzeh, J. Paik, *IEEE ASME Trans. Mechatron.* **2017**, *22*, 2165.
[213] X. Liu, J. Liu, S. Lin, X. Zhao, *Mater. Today* **2020**, *36*, 102.
[214] P. Calvert, *Adv. Mater.* **2009**, *21*, 743.
[215] Y. Ma, M. Hua, S. Wu, Y. Du, X. Pei, X. Zhu, F. Zhou, X. He, *Sci. Adv.* **2020**, *6*, eabd2520.
[216] G. Stoychev, L. Guiducci, S. Turcaud, J. W. C. Dunlop, L. Ionov, *Adv. Funct. Mater.* **2016**, *26*, 7733.
[217] H. Na, Y.-W. Kang, C. S. Park, S. Jung, H.-Y. Kim, J.-Y. Sun, *Science* **2022**, *376*, 301.
[218] V. R. Feig, H. Tran, M. Lee, Z. Bao, *Nat. Commun.* **2018**, *9*, 2740.
[219] S. J. Wu, H. Yuk, J. Wu, C. S. Nabzdyk, X. Zhao, *Adv. Mater. 33*, 2007667.
[220] Y. Pan, Z. Yang, C. Li, S. U. Hassan, H. C. Shum, *Sci. Adv.* **2022**, *8*, eabo1719.
[221] D. Morales, E. Palleau, M. D. Dickey, O. D. Velev, *Soft Matter* **2014**, *10*, 1337.
[222] C. Yang, W. Wang, C. Yao, R. Xie, X.-J. Ju, Z. Liu, L.-Y. Chu, *Sci. Rep.* **2015**, *5*, 13622.
[223] R. Luo, J. Wu, N.-D. Dinh, C.-H. Chen, *Adv. Funct. Mater.* **2015**, *25*, 7272.
[224] K. Otake, H. Inomata, M. Konno, S. Saito, *Macromolecules* **1990**, *23*, 283.
[225] T. Tanaka, *Phys. Rev. Lett.* **1978**, *40*, 820.
[226] J. Kim, J. A. Hanna, M. Byun, C. D. Santangelo, R. C. Hayward, *Science* **2012**, *335*, 1201.
[227] G. Stoychev, S. Zakharchenko, S. Turcaud, J. W. C. Dunlop, L. Ionov, *ACS Nano* **2012**, *6*, 3925.
[228] J. Wang, J. Wang, Z. Chen, S. Fang, Y. Zhu, R. H. Baughman, L. Jiang, *Chem. Mater.* **2017**, *29*, 9793.
[229] X. Peng, C. Jiao, Y. Zhao, N. Chen, Y. Wu, T. Liu, H. Wang, *ACS Appl. Nano Mater.* **2018**, *1*, 1522.
[230] Q. Zhao, Y. Liang, L. Ren, Z. Yu, Z. Zhang, L. Ren, *Nano Energy* **2018**, *51*, 621.
[231] M. E. Lee-Trimble, J.-H. Kang, R. C. Hayward, C. D. Santangelo, *Soft Matter* **2022**, *18*, 6384.
[232] J.-H Kang, H. Kim, C. D. Santangelo, R. C. Hayward, *Adv. Mater.* **2019**, *31*, 0193006.
[233] M. Trujillo-Miranda, I. Apsite, J. A. R. Agudo, G. Constante, L. Ionov, *Macromol. Biosci.* **2023**, *23*, 2200320.
[234] G. Go, V. D. Nguyen, Z. Jin, J.-O. Park, S. Park, *Int. J. Control Autom. Syst.* **2018**, *16*, 1341.
[235] Z. Li, P. Liu, X. Ji, J. Gong, Y. Hu, W. Wu, X. Wang, H.-Q. Peng, R. T. K. Kwok, J. W. Y. Lam, J. Lu, B. Z. Tang, *Adv. Mater. 32*, 1906493.
[236] A. Aggarwal, C. Li, S. I. Stupp, M. Olvera De La Cruz, *Soft Matter* **2022**, *18*, 2193.
[237] C. Li, Y. Xue, M. Han, L. C. Palmer, J. A. Rogers, Y. Huang, S. I. Stupp, *Matter* **2021**, *4*, 1377.
[238] Z. Chen, Y. Li, Q. M. Li, *Mater. Des.* **2021**, *207*, 109819.
[239] H. Wermter, H. Finkelmann, *e-Polymers* **2001**, *1*, 013.
[240] J. Küpfer, H. Finkelmann, *Makromol. Chem., Rapid Commun.* **1991**, *12*, 717.
[241] D. L. Thomsen, P. Keller, J. Naciri, R. Pink, H. Jeon, D. Shenoy, B. R. Ratna, *Macromolecules* **2001**, *34*, 5868.

[242] Y. Yu, M. Nakano, T. Ikeda, *Nature* **2003**, *425*, 145.
[243] M. Camacho-Lopez, H. Finkelmann, P. Palffy-Muhoray, M. Shelley, *Nat. Mater.* **2004**, *3*, 307.
[244] K. D. Harris, C. W. M. Bastiaansen, J. Lub, D. J. Broer, *Nano Lett.* **2005**, *5*, 1857.
[245] M. Brehmer, R. Zentel, G. Wagenblast, K. Siemensmeyer, *Macromol. Chem. Phys.* **1994**, *195*, 1891.
[246] C. M. Spillmann, B. R. Ratna, J. Naciri, *Appl. Phys. Lett.* **2007**, *90*, 021911.
[247] A. Kaiser, M. Winkler, S. Krause, H. Finkelmann, A. M. Schmidt, *J. Mater. Chem.* **2009**, *19*, 538.
[248] P. G. de Gennes, J. Prost, in *The Physics of Liquid Crystals*, Clarendon Press, Oxford **1993**.
[249] K. M. Herbert, H. E. Fowler, J. M. Mccracken, K. R. Schlafmann, J. A. Koch, T. J. White, *Nat. Rev. Mater.* **2022**, *7*, 23.
[250] M. Behl, A. Lendlein, *Soft Matter* **2007**, *3*, 58.
[251] H. Finkelmann, H.-J. Kock, G. Rehage, *Makromol. Chem., Rapid Commun.* **1981**, *2*, 317.
[252] M. Warner, E. M. Terentjev, in *Liquid Crystal Elastomers*, Vol. *120*, Oxford University Press, Oxford **2003**.
[253] S. W. Ula, N. A. Traugutt, R. H. Volpe, R. R. Patel, K. Yu, C. M. Yakacki, *Liq. Cryst. Rev.* **2018**, *6*, 78.
[254] P.-G. De Gennes, M. Hébert, R. Kant, *Macromol. Symp.* **1997**, *113*, 39.
[255] D. J. Roach, C. Yuan, X. Kuang, V. C.-F. Li, P. Blake, M. L. Romero, I. Hammel, K. Yu, H. J. Qi, *ACS Appl. Mater. Interfaces* **2019**, *11*, 19514.
[256] C. L. Van Oosten, K. D. Harris, C. W. M. Bastiaansen, D. J. Broer, *Eur. Phys. J. Spec. Top.* **2007**, *23*, 329.
[257] X. Lu, S. Guo, X. Tong, H. Xia, Y. Zhao, *Adv. Mater.* **2017**, *29*, 1606467.
[258] R. A. M. Hikmet, D. J. Broer, *Polymer* **1991**, *32*, 1627.
[259] C. Ohm, M. Brehmer, R. Zentel, *Adv. Mater.* **2010**, *22*, 3366.
[260] K.-W. Lee, S.-H. Paek, A. Lien, C. Durning, H. Fukuro, *Macromolecules* **1996**, *29*, 8894.
[261] S. Krause, R. Dersch, J. H. Wendorff, H. Finkelmann, *Macromol. Rapid Commun.* **2007**, *28*, 2062.
[262] C. M. Yakacki, M. Saed, D. P. Nair, T. Gong, S. M. Reed, C. N. Bowman, *RSC Adv.* **2015**, *5*, 18997.
[263] K. Mehta, A. R. Peeketi, L. Liu, D. Broer, P. Onck, R. K. Annabattula, *Appl. Phys. Rev.* **2020**, *7*, 041306.
[264] G. N. Mol, K. D. Harris, C. W. M. Bastiaansen, D. J. Broer, *Adv. Funct. Mater.* **2005**, *15*, 1155.
[265] J. M. Boothby, T. H. Ware, *Soft Matter* **2017**, *13*, 4349.
[266] M. Warner, C. D. Modes, D. Corbett, *Proc. R. Soc. A* **2010**, *466*, 2975.
[267] L. T. De Haan, A. P. H. J. Schenning, D. J. Broer, *Polymer* **2014**, *55*, 5885.
[268] B. R. Donovan, V. M. Matavulj, S.-K. Ahn, T. Guin, T. J. White, *Adv. Mater.* **2019**, *31*, 1805750.
[269] Yu Xia, G. Cedillo-Servin, R. D. Kamien, S. Yang, *Adv. Mater.* **2016**, *28*, 9637.
[270] S.-K. Ahn, T. H. Ware, K. M. Lee, V. P. Tondiglia, T. J. White, *Adv. Funct. Mater.* **2016**, *26*, 5819.
[271] H. Aharoni, Y. Xia, X. Zhang, R. D. Kamien, S. Yang, *Proc. Natl. Acad. Sci. USA* **2018**, *115*, 7206.
[272] Z. S. Davidson, H. Shahsavan, A. Aghakhani, Y. Guo, L. Hines, Y. Xia, S. Yang, M. Sitti, *Sci. Adv.* **2019**, *5*, eaay0855.
[273] A. F. Minori, Q. He, P. E. Glick, I. Adibnazari, A. Stopol, S. Cai, M. T. Tolley, *Smart Mater. Struct.* **2020**, *29*, 105003.
[274] M. Zhang, H. Shahsavan, Y. Guo, A. Pena-Francesch, Y. Zhang, M. Sitti, *Adv. Mater.* **2021**, *33*, 2008605.
[275] J. Wu, S. Yao, H. Zhang, W. Man, Z. Bai, F. Zhang, X. Wang, D. Fang, Y. Zhang, *Adv. Mater.* **2021**, *33*, 2106175.
[276] W. Hu, G. Z. Lum, M. Mastrangeli, M. Sitti, *Nature* **2018**, *554*, 81.
[277] W. Xi, A. A. Solovev, A. N. Ananth, D. H. Gracias, S. Sanchez, O. G. Schmidt, *Nanoscale* **2013**, *5*, 1294.
[278] R. Zhang, S. Wu, Q. Ze, R. Zhao, *J. Appl. Mech.* **2020**, *87*, 091008.
[279] H. Song, H. Lee, J. Lee, J. K. Choe, S. Lee, J. Y. Yi, S. Park, J.-W. Yoo, M. S. Kwon, J. Kim, *Nano Lett.* **2020**, *20*, 5185.
[280] A. Ghosh, L. Li, L. Xu, R. P. Dash, N. Gupta, J. Lam, Q. Jin, V. Akshintala, G. Pahapale, W. Liu, A. Sarkar, R. Rais, D. H. Gracias, F. M. Selaru, *Sci. Adv.* **2020**, *6*, eabb4133.
[281] C. J. Kloxin, T. F. Scott, B. J. Adzima, C. N. Bowman, *Macromolecules* **2010**, *43*, 2643.
[282] N. Zheng, Y. Xu, Q. Zhao, T. Xie, *Chem. Rev.* **2021**, *121*, 1716.
[283] D. Montarnal, M. Capelot, F. Tournilhac, L. Leibler, *Science* **2011**, *334*, 965.
[284] P. Zheng, T. J. Mccarthy, *J. Am. Chem. Soc.* **2012**, *134*, 2024.
[285] X. Chen, M. A. Dam, K. Ono, A. Mal, H. Shen, S. R. Nutt, K. Sheran, F. Wudl, *Science* **2002**, *295*, 1698.
[286] T. F. Scott, A. D. Schneider, W. D. Cook, C. N. Bowman, *Science* **2005**, *308*, 1615.
[287] A. M. Peterson, R. E. Jensen, G. R. Palmese, *ACS Appl. Mater. Interfaces* **2010**, *2*, 1141.
[288] X. He, Y. Lin, Y. Ding, A. M. Abdullah, Z. Lei, Y. Han, X. Shi, W. Zhang, K. Yu, *Int. J. Extreme Manuf.* **2021**, *4*, 015301.
[289] J. Deng, X. Kuang, R. Liu, W. Ding, A. C. Wang, Y.-C. Lai, K. Dong, Z. Wen, Y. Wang, L. Wang, H. J. Qi, T. Zhang, Z. L. Wang, *Adv. Mater.* **2018**, *30*, 1705918.
[290] W. Denissen, J. M. Winne, F. E. Du Prez, *Chem. Sci.* **2016**, *7*, 30.
[291] B. R. Elling, W. R. Dichtel, *ACS Cent. Sci.* **2020**, *6*, 1488.
[292] Q. Zhao, W. Zou, Y. Luo, T. Xie, *Sci. Adv.* **2016**, *2*, e1501297.
[293] G. Zhang, Q. Zhao, L. Yang, W. Zou, X. Xi, T. Xie, *ACS Macro Lett.* **2016**, *5*, 805.
[294] B. Jin, H. Song, R. Jiang, J. Song, Q. Zhao, T. Xie, *Sci. Adv.* **2018**, *4*, eaao3865.
[295] Z. Ding, Li Yuan, G. Liang, A. Gu, *J. Mater. Chem. A* **2019**, *7*, 9736.
[296] J. Zhou, H. Yue, M. Huang, C. Hao, S. He, H. Liu, W. Liu, C. Zhu, X. Dong, D. Wang, *ACS Appl. Mater. Interfaces* **2021**, *13*, 43426.
[297] Z. Pei, Y. Yang, Q. Chen, E. M. Terentjev, Y. Wei, Y. Ji, *Nat. Mater.* **2014**, *13*, 36.
[298] Z. Pei, Y. Yang, Q. Chen, Y. Wei, Y. Ji, *Adv. Mater.* **2016**, *28*, 156.
[299] Y. Yang, Z. Pei, Z. Li, Y. Wei, Y. Ji, *J. Am. Chem. Soc.* **2016**, *138*, 2118.
[300] Z. Li, Y. Yang, Z. Wang, X. Zhang, Q. Chen, X. Qian, N. Liu, Y. Wei, Y. Ji, *J. Mater. Chem. A* **2017**, *5*, 6740.
[301] Y. Yang, E. M. Terentjev, Y. Wei, Y. Ji, *Nat. Commun.* **2018**, *9*, 1906.
[302] Y. Wu, Y. Yang, X. Qian, Q. Chen, Y. Wei, Y. Ji, *Angew. Chem., Int. Ed.* **2020**, *59*, 4778.
[303] M. K. McBride, M. Podgorski, S. Chatani, B. T. Worrell, C. N. Bowman, *ACS Appl. Mater. Interfaces* **2018**, *10*, 22739.
[304] Y. Li, O. Rios, J. K. Keum, J. Chen, M. R. Kessler, *ACS Appl. Mater. Interfaces* **2016**, *8*, 15750.
[305] Y. Li, Y. Zhang, O. Rios, J. K. Keum, M. R. Kessler, *RSC Adv.* **2017**, *7*, 37248.
[306] X. Lu, H. Zhang, G. Fei, B. Yu, X. Tong, H. Xia, Y. Zhao, *Adv. Mater.* **2018**, *30*, 1706597.
[307] X. Kuang, S. Wu, Q. Ze, L. Yue, Yi Jin, S. M. Montgomery, F. Yang, H. J. Qi, R. Zhao, *Adv. Mater.* **2021**, *33*, 2102113.
[308] H. Qiu, S. Wei, H. Liu, B. Zhan, H. Yan, W. Lu, J. Zhang, S. Wu, T. Chen, *Adv. Intell. Syst.* **2021**, *3*, 2000239.
[309] Y. Zhang, X. Le, Y. Jian, W. Lu, J. Zhang, T. Chen, *Adv. Funct. Mater.* **2019**, *29*, 1905514.
[310] H. Okuzaki, T. Saido, H. Suzuki, Y. Hara, H. Yan, *J. Phys.: Conf. Ser.* **2007**, *127*, 012001.
[311] D.-D. Han, Y.-L. Zhang, H.-B. Jiang, H. Xia, J. Feng, Q.-D. Chen, H.-L. Xu, H.-B. Sun, *Adv. Mater.* **2015**, *27*, 332.
[312] J. Mu, C. Hou, H. Wang, Y. Li, Q. Zhang, M. Zhu, *Sci. Adv.* **2015**, *1*, e1500533.
[313] W. Xu, Z. Qin, C.-T. Chen, H. R. Kwag, Q. Ma, A. Sarkar, M. J. Buehler, D. H. Gracias, *Sci. Adv.* **2017**, *3*, e1701084.

[314] G. Cai, J.-H. Ciou, Y. Liu, Y. Jiang, P. S. Lee, *Sci. Adv.* **2019**, *5*, eaaw7956.
[315] Q. Zhao, J. W. C. Dunlop, X. Qiu, F. Huang, Z. Zhang, J. Heyda, J. Dzubiella, M. Antonietti, J. Yuan, *Nat. Commun.* **2014**, *5*, 4293.
[316] Xi Fan, W. Nie, H. Tsai, N. Wang, H. Huang, Y. Cheng, R. Wen, L. Ma, F. Yan, Y. Xia, *Adv. Sci.* **2019**, *6*, 1900813.
[317] S. Taccola, F. Greco, E. Sinibaldi, A. Mondini, B. Mazzolai, V. Mattoli, *Adv. Mater.* **2015**, *27*, 1668.
[318] K. E. Laflin, C. J. Morris, T. Muqeem, D. H. Gracias, *Appl. Phys. Lett.* **2012**, *101*, 131901.
[319] D. Davis, R. Mailen, E. Luong, A. Russell, M. D. Dickey, J. Genzer, *ACS Appl. Eng. Mater.* **2023**, *1*, 193.
[320] D. Joung, A. Nemilentsau, K. Agarwal, C. Dai, C. Liu, Q. Su, J. Li, T. Low, S. J. Koester, J.-H. Cho, *Nano Lett.* **2017**, *17*, 1987.
[321] B. Han, Y.-L. Zhang, L. Zhu, Y. Li, Z.-C. Ma, Y.-Q. Liu, X.-L. Zhang, X.-W. Cao, Q.-D. Chen, C.-W. Qiu, H.-B. Sun, *Adv. Mater.* **2019**, *31*, 1970029.
[322] Z. Tang, Z. Gao, S. Jia, F. Wang, Y. Wang, *Adv. Sci.* **2017**, *4*, 1600437.
[323] E. Hawkes, B. An, N. M. Benbernou, H. Tanaka, S. Kim, E. D. Demaine, D. Rus, R. J. Wood, *Proc. Natl. Acad. Sci. USA* **2010**, *107*, 12441.
[324] M. Boyvat, J.-S. Koh, R. J. Wood, *Sci. Rob.* **2017**, *2*, eaan1544.
[325] P. K. Kumar, D. C. Lagoudas, in *Shape Memory Alloys: Modeling and Engineering Applications*, Springer, Boston, MA **2008** p. 1.
[326] A. Rao, A. Srinivasa, J. Reddy, *Design of Shape Memory Alloy (SMA) Actuators*, Springer Cham, **2015**.
[327] P. Velvaluri, A. Soor, P. Plucinsky, R. L. De Miranda, R. D. James, E. Quandt, *Sci. Rep.* **2021**, *11*, 10988.
[328] L. M. Fonseca, G. V. Rodrigues, M. A. Savi, A. Paiva, *Chaos, Solitons & Fractals* **2019**, *122*, 245.
[329] H. Yi, D. Kim, Y. Kim, D. Kim, J.-S. Koh, M.-J. Kim, *Autom. Constr.* **2020**, *114*, 103151.
[330] C. D. Onal, R. J. Wood, D. Rus, in *2011 IEEE Int. Conf. on Robot. and Autom.*, Shanghai, China **2011**.
[331] N. Lazarus, G. L. Smith, M. D. Dickey, *Adv. Intell. Syst.* **2019**, *1*, 1900059.
[332] A. L. Bachmann, B. Hanrahan, M. D. Dickey, N. Lazarus, *ACS Appl. Mater. Interfaces* **2022**, *14*, 14774.
[333] Y. Shi, F. Zhang, K. Nan, X. Wang, J. Wang, Y. Zhang, Y. Zhang, H. Luan, K.-C. Hwang, Y. Huang, J. A. Rogers, Y. Zhang, *Extreme Mech. Lett.* **2017**, *11*, 105.
[334] Q. Liu, W. Wang, M. F. Reynolds, M. C. Cao, M. Z. Miskin, T. A. Arias, D. A. Muller, P. L. Mceuen, I. Cohen, *Sci. Rob.* **2021**, *6*, eabe6663.
[335] J. S. Randhawa, M. D. Keung, P. Tyagi, D. H. Gracias, *Adv. Mater.* **2010**, *22*, 407.
[336] M. Taghavi, T. Helps, J. Rossiter, *Sci. Rob.* **2018**, *3*, eaau9795.
[337] E. Acome, C. Keplinger, M. D. Gross, C. Bruns, D. Leithinger, in *Extended Abstracts of the 2021 CHI Conference on Human Factors in Computing Systems*, Association for Computing Machinery, Purnendu, Yokohama, Japan **2021**, Article 377.
[338] R. Pelrine, R. Kornbluh, Q. Pei, J. Joseph, *Science* **2000**, *287*, 836.
[339] S. Shian, K. Bertoldi, D. R. Clarke, *Adv. Mater.* **2015**, *27*, 6814.
[340] G. Kofod, W. Wirges, M. Paajanen, S. Bauer, *Appl. Phys. Lett.* **2007**, *90*, 081916.
[341] J. Shintake, S. Rosset, B. Schubert, D. Floreano, H. Shea, *Adv. Mater.* **2016**, *28*, 231.
[342] M. Duduta, R. J. Wood, D. R. Clarke, *Adv. Mater.* **2016**, *28*, 8058.
[343] J. Wang, S. Li, D. Gao, J. Xiong, P. S. Lee, *NPG Asia Mater.* **2019**, *11*, 71.
[344] W. Pang, X. Cheng, H. Zhao, X. Guo, Z. Ji, G. Li, Y. Liang, Z. Xue, H. Song, F. Zhang, Z. Xu, L. Sang, W. Huang, T. Li, Y. Zhang, *Natl. Sci. Rev.* **2019**, *7*, 342.
[345] J. Li, H. Godaba, Z. Q. Zhang, C. C. Foo, J. Zhu, *Extreme Mech. Lett.* **2018**, *24*, 30.
[346] Y. Sun, D. Li, M. Wu, Y. Yang, J. Su, T. Wong, K. Xu, Y. Li, L. Li, X. Yu, J. Yu, *Microsyst. Nanoeng.* **2022**, *8*, 37.
[347] G. Liu, Y. Zhao, G. Wu, J. Lu, *Sci. Adv.* **2018**, *4*, eaat0641.
[348] K. Huang, H. Elsayed, G. Franchin, P. Colombo, *Addit. Manuf.* **2020**, *33*, 101144.
[349] H. Jaffe, *J. Am. Ceram. Soc.* **1958**, *41*, 494.
[350] K. Y. Ma, P. Chirarattananon, S. B. Fuller, R. J. Wood, *Science* **2013**, *340*, 603.
[351] Q. Zhao, S. Liu, J. Chen, G. He, J. Di, L. Zhao, T. Su, M. Zhang, Z. Hou, *Robot. Auton. Syst.* **2021**, *140*, 103733.
[352] J. S. Pulskamp, R. G. Polcawich, R. Q. Rudy, S. S. Bedair, R. M. Proie, T. Ivanov, G. L. Smith, *MRS Bull.* **2012**, *37*, 1062.
[353] H. Mcclintock, F. Z. Temel, N. Doshi, J.-S. Koh, R. J. Wood, *Sci. Rob.* **2018**, *3*, eaar3018.
[354] S. Naficy, R. Gately, R. Gorkin, H. Xin, G. M. Spinks, *Macromol. Mater. Eng.* **2017**, *302*, 1600212.
[355] J. Guan, H. He, D. J. Hansford, L. J. Lee, *J. Phys. Chem. B* **2005**, *109*, 23134.
[356] G. Z. Lum, Z. Ye, X. Dong, H. Marvi, O. Erin, W. Hu, M. Sitti, *Proc. Natl. Acad. Sci. USA* **2016**, *113*, E6007.
[357] S. Wu, Q. Ze, R. Zhang, N. Hu, Y. Cheng, F. Yang, R. Zhao, *ACS Appl. Mater. Interfaces* **2019**, *11*, 41649.
[358] D. Raviv, W. Zhao, C. Mcknelly, A. Papadopoulou, A. Kadambi, B. Shi, S. Hirsch, D. Dikovsky, M. Zyracki, C. Olguin, R. Raskar, S. Tibbits, *Sci. Rep.* **2014**, *4*, 7422.
[359] Q. Ge, H. J. Qi, M. L. Dunn, *Appl. Phys. Lett.* **2013**, *103*, 131901.
[360] J. A. Lewis, G. M. Gratson, *Mater. Today* **2004**, *7*, 32.
[361] J. E. Smay, J. Cesarano, J. A. Lewis, *Langmuir* **2002**, *18*, 5429.
[362] A. Sydney Gladman, E. A. Matsumoto, R. G. Nuzzo, L. Mahadevan, J. A. Lewis, *Nat. Mater.* **2016**, *15*, 413.
[363] J. Tang, B. Sun, Q. Yin, M. Yang, J. Hu, T. Wang, *J. Mater. Chem. B* **2021**, *9*, 9183.
[364] P. Zhu, W. Yang, R. Wang, S. Gao, B. Li, Q. Li, *ACS Appl. Mater. Interfaces* **2018**, *10*, 36435.
[365] Y. Zhang, Q. Wang, S. Yi, Z. Lin, C. Wang, Z. Chen, L. Jiang, *ACS Appl. Mater. Interfaces* **2021**, *13*, 4174.
[366] C. Ma, S. Wu, Q. Ze, X. Kuang, R. Zhang, H. J. Qi, R. Zhao, *ACS Appl. Mater. Interfaces* **2021**, *13*, 12639.
[367] S. Wu, C. M. Hamel, Q. Ze, F. Yang, H. J. Qi, R. Zhao, *Adv. Intell. Syst.* **2020**, *2*, 2000060.
[368] J. N. Rodriguez, C. Zhu, E. B. Duoss, T. S. Wilson, C. M. Spadaccini, J. P. Lewicki, *Sci. Rep.* **2016**, *6*, 27933.
[369] C. P. Ambulo, J. J. Burroughs, J. M. Boothby, H. Kim, M. R. Shankar, T. H. Ware, *ACS Appl. Mater. Interfaces* **2017**, *9*, 37332.
[370] A. Kotikian, R. L. Truby, J. W. Boley, T. J. White, J. A. Lewis, *Adv. Mater.* **2018**, *30*, 1706164.
[371] M. Pozo, J. A. H. P. Sol, S. H. P. van Uden, A. R. Peeketi, S. J. D. Lugger, R. K. Annabattula, A. P. H. J. Schenning, M. G. Debije, *ACS Appl. Mater. Interfaces* **2021**, *13*, 59381.
[372] C. Zhang, X. Lu, G. Fei, Z. Wang, H. Xia, Y. Zhao, *ACS Appl. Mater. Interfaces* **2019**, *11*, 44774.
[373] Z. Wang, Z. Wang, Y. Zheng, Q. He, Y. Wang, S. Cai, *Sci. Adv.* **2020**, *6*, eabc0034.
[374] X. Peng, X. Kuang, D. J. Roach, Y. Wang, C. M. Hamel, C. Lu, H. J. Qi, *Addit. Manuf.* **2021**, *40*, 101911.
[375] Y. Yang, Y. Chen, Y. Wei, Y. Li, *Int. J. Adv. Manuf. Technol.* **2016**, *84*, 2079.
[376] S. Chen, Q. Zhang, J. Feng, *J. Mater. Chem. C* **2017**, *5*, 8361.
[377] B. Peng, Y. Yang, T. Ju, K. A. Cavicchi, *ACS Appl. Mater. Interfaces* **2021**, *13*, 12777.
[378] T. Van Manen, S. Janbaz, A. A. Zadpoor, *Mater. Horiz.* **2017**, *4*, 1064.
[379] T. Van Manen, S. Janbaz, K. M. B. Jansen, A. A. Zadpoor, *Commun. Mater.* **2021**, *2*, 56.
[380] B. Zou, C. Song, Z. He, J. Ju, *Extreme Mech. Lett.* **2022**, *54*, 101779.

[381] A. B. Baker, S. R. G. Bates, T. M. Llewellyn-Jones, L. P. B. Valori, M. P. M. Dicker, R. S. Trask, *Mater. Des.* **2019**, *163*, 107544.
[382] S. Qi, H. Guo, J. Fu, Y. Xie, M. Zhu, M. Yu, *Compos. Sci. Technol.* **2020**, *188*, 107973.
[383] X. Cao, S. Xuan, S. Sun, Z. Xu, J. Li, X. Gong, *ACS Appl. Mater. Interfaces* **2021**, *13*, 30127.
[384] J. R. Tumbleston, D. Shirvanyants, N. Ermoshkin, R. Janusziewicz, A. R. Johnson, D. Kelly, K. Chen, R. Pinschmidt, J. P. Rolland, A. Ermoshkin, E. T. Samulski, J. M. Desimone, *Science* **2015**, *347*, 1349.
[385] C. Sun, N. Fang, D. M. Wu, X. Zhang, *Sens. Actuators, A* **2005**, *121*, 113.
[386] Q. Ge, A. H. Sakhaei, H. Lee, C. K. Dunn, N. X. Fang, M. L. Dunn, *Sci. Rep.* **2016**, *6*, 31110.
[387] J. J. Schwartz, A. J. Boydston, *Nat. Commun.* **2019**, *10*, 791.
[388] M. Jamal, A. M. Zarafshar, D. H. Gracias, *Nat. Commun.* **2011**, *2*, 527.
[389] Z. Zhao, J. Wu, X. Mu, H. Chen, H. J. Qi, D. Fang, *Sci. Adv.* **2017**, *3*, e1602326.
[390] Z. Zhao, J. Wu, X. Mu, H. Chen, H. J. Qi, D. Fang, *Macromol. Rapid Commun.* **2017**, *38*, 1600625.
[391] Q. Zhang, X. Kuang, S. Weng, Z. Zhao, H. Chen, D. Fang, H. J. Qi, *ACS Appl. Mater. Interfaces* **2020**, *12*, 17979.
[392] X. Kuang, J. Wu, K. Chen, Z. Zhao, Z. Ding, F. Hu, D. Fang, H. J. Qi, *Sci. Adv.* **2019**, *5*, eaav5790.
[393] B. Jin, J. Liu, Y. Shi, G. Chen, Q. Zhao, S. Yang, *Adv. Mater. 34*, 2107855.
[394] S. H. Kim, Y. B. Seo, Y. K. Yeon, Y. J. Lee, H. S. Park, M. T. Sultan, J. M. Lee, J. S. Lee, O. J. Lee, H. Hong, H. Lee, O. Ajiteru, Y. J. Suh, S.-H. Song, K.-H. Lee, C. H. Park, *Biomaterials* **2020**, *260*, 120281.
[395] Q. Ge, Z. Chen, J. Cheng, B. Zhang, Y.-F. Zhang, H. Li, X. He, C. Yuan, J. Liu, S. Magdassi, S. Qu, *Sci. Adv.* **2021**, *7*, eaba4261.
[396] L. Huang, R. Jiang, J. Wu, J. Song, H. Bai, B. Li, Q. Zhao, T. Xie, *Adv. Mater.* **2017**, *29*, 1605390.
[397] J.-T. Miao, M. Ge, S. Peng, J. Zhong, Y. Li, Z. Weng, L. Wu, L. Zheng, *ACS Appl. Mater. Interfaces* **2019**, *11*, 40642.
[398] E. Rossegger, R. Höller, D. Reisinger, J. Strasser, M. Fleisch, T. Griesser, S. Schlögl, *Polym. Chem.* **2021**, *12*, 639.
[399] B. Zhang, W. Zhang, Z. Zhang, Y.-F. Zhang, H. Hingorani, Z. Liu, J. Liu, Q. Ge, *ACS Appl. Mater. Interfaces* **2019**, *11*, 10328.
[400] J. Wu, C. Yuan, Z. Ding, M. Isakov, Y. Mao, T. Wang, M. L. Dunn, H. J. Qi, *Sci. Rep.* **2016**, *6*, 24224.
[401] X. Peng, T. Liu, Q. Zhang, C. Shang, Q.-W. Bai, H. Wang, *Adv. Funct. Mater.* **2017**, *27*, 1701962.
[402] Z. Ding, O. Weeger, H. J. Qi, M. L. Dunn, *Mater. Des.* **2018**, *137*, 256.
[403] Z. Ding, C. Yuan, X. Peng, T. Wang, H. J. Qi, M. L. Dunn, *Sci. Adv.* **2017**, *3*, 1602890.
[404] L. Ionov, *Soft Matter* **2011**, *7*, 6786.
[405] D. H. Gracias, V. Kavthekar, J. C. Love, K. E. Paul, G. M. Whitesides, *Adv. Mater.* **2002**, *14*, 235.
[406] J.-H. Cho, M. D. Keung, N. Verellen, L. Lagae, V. V. Moshchalkov, P. V. Dorpe, D. H. Gracias, *Small* **2011**, *7*, 1943.
[407] J. S. Randhawa, T. G. Leong, N. Bassik, B. R. Benson, M. T. Jochmans, D. H. Gracias, *J. Am. Chem. Soc.* **2008**, *130*, 17238.
[408] N. Bassik, G. M. Stern, D. H. Gracias, *Appl. Phys. Lett.* **2009**, *95*, 091901.
[409] D. Martella, S. Nocentini, D. Nuzhdin, C. Parmeggiani, D. S. Wiersma, *Adv. Mater.* **2017**, *29*, 1704047.
[410] Y. Guo, J. Zhang, W. Hu, M. T. A. Khan, M. Sitti, *Nat. Commun.* **2021**, *12*, 5936.
[411] H. Deng, Y. Dong, J.-W. Su, C. Zhang, Y. Xie, C. Zhang, M. R. Maschmann, Y. Lin, J. Lin, *ACS Appl. Mater. Interfaces* **2017**, *9*, 30900.
[412] J. Zhang, Z. Ren, W. Hu, R. H. Soon, I. C. Yasa, Z. Liu, M. Sitti, *Sci. Rob.* **2021**, *6*, eabf0112.
[413] G. Villar, A. D. Graham, H. Bayley, *Science* **2013**, *340*, 48.
[414] T. G. Leong, B. R. Benson, E. K. Call, D. H. Gracias, *Small* **2008**, *4*, 1605.
[415] W. Xu, T. Li, Z. Qin, Q. Huang, H. Gao, K. Kang, J. Park, M. J. Buehler, J. B. Khurgin, D. H. Gracias, *Nano Lett.* **2019**, *19*, 7941.
[416] M. Schenk, S. D. Guest, *Origami* **2011**, *5*, 291.
[417] Z. Y. Wei, Z. V. Guo, L. Dudte, H. Y. Liang, L. Mahadevan, *Phys. Rev. Lett.* **2013**, *110*, 215501.
[418] E. T. Filipov, T. Tachi, G. H. Paulino, in *Origami^6: II. Technology, Art, Education* (Eds: K. Miura, T. Kawasaki, T. Tachi, R. Uehara, R. J. Lang, P. Wang-Iverson), American Mathematical Soc., **2015**, p.409.
[419] E. T. Filipov, K. Liu, T. Tachi, M. Schenk, G. H. Paulino, *Int. J. Solids Struct.* **2017**, *124*, 26.
[420] S. R. Woodruff, E. T. Filipov, *Int. J. Solids Struct.* **2020**, *204*, 114.
[421] Y. Zhu, E. T. Filipov, *J. Mech. Robot.* **2020**, *12*.
[422] Y. Zhu, E. T. Filipov, in Volume 8B: 45th Mechanisms and Robotics Conference (MR), **2021**.
[423] A. Ghassaei, E. D. Demaine, N. Gershenfeld, *Origami* **2018**, *7*, 1151.
[424] K. Liu, G. Paulino, *Origami* **2018**, *7*, 1167.
[425] R. J. Lang, https://www.langorigami.com/article/tessellatica/ (accessed May, 2022).
[426] E. A. Peraza Hernandez, D. J. Hartl, E. Akleman, D. C. Lagoudas, *Comput. Aided Des.* **2016**, *78*, 93.
[427] J. A. Faber, A. F. Arrieta, A. R. Studart, *Science* **2018**, *359*, 1386.
[428] Z. Zhao, X. Kuang, J. Wu, Q. Zhang, G. H. Paulino, H. J. Qi, D. Fang, *Soft Matter* **2018**, *14*, 8051.
[429] H. Fang, S.-C. A. Chu, Y. Xia, K.-W. Wang, *Adv. Mater.* **2018**, *30*, 1706311.
[430] N. An, M. Li, J. Zhou, *Smart Mater. Struct.* **2016**, *25*, 11LT02.
[431] G. A. Holzapfel, *Nonlinear Solid Mechanics: A Continuum Approach for Engineering* , Wiley, **2000**.
[432] L. R. G. Treloar, in *The Physics of Rubber Elasticity*, 3rd ed., Oxford University Press, Oxford **2005**.
[433] E. M. Arruda, M. C. Boyce, *J. Mech. Phys. Solids* **1993**, *41*, 389.
[434] R. W. Ogden, R. Hill, *Proc. R. Soc. London, A* **1972**, *326*, 565.
[435] K. K. Westbrook, P. H. Kao, F. Castro, Y. Ding, H. J. Qi, *Mech. Mater.* **2011**, *43*, 853.
[436] F. Castro, K. K. Westbrook, K. N. Long, R. Shandas, H. J. Qi, *Mech. Time Depend Mater.* **2010**, *14*, 219.
[437] H. J. Qi, T. D. Nguyen, F. Castro, C. M. Yakacki, R. Shandas, *J. Mech. Phys. Solids* **2008**, *56*, 1730.
[438] Q. Ge, X. Luo, C. B. Iversen, H. B. Nejad, P. T. Mather, M. L. Dunn, H. J. Qi, *Int. J. Solids Struct.* **2014**, *51*, 2777.
[439] K. Yu, T. Xie, J. Leng, Y. Ding, H. J. Qi, *Soft Matter* **2012**, *8*, 5687.
[440] R. Xiao, J. Choi, N. Lakhera, C. M. Yakacki, C. P. Frick, T. D. Nguyen, *J. Mech. Phys. Solids* **2013**, *61*, 1612.
[441] Q. Ge, X. Luo, E. D. Rodriguez, X. Zhang, P. T. Mather, M. L. Dunn, H. J. Qi, *J. Mech. Phys. Solids* **2012**, *60*, 67.
[442] Y. Liu, K. Gall, M. L. Dunn, A. R. Greenberg, J. Diani, *Int. J. Plast.* **2006**, *22*, 279.
[443] T. Nguyen, H. J. Qi, F. Castro, K. Long, *J. Mech. Phys. Solids* **2008**, *56*, 2792.
[444] W. Hong, X. Zhao, J. Zhou, Z. Suo, *J. Mech. Phys. Solids* **2008**, *56*, 1779.
[445] W. Hong, X. Zhao, Z. Suo, *J. Mech. Phys. Solids* **2010**, *58*, 558.
[446] F. P. Duda, A. C. Souza, E. Fried, *J. Mech. Phys. Solids* **2010**, *58*, 515.
[447] S. A. Chester, L. Anand, *J. Mech. Phys. Solids* **2010**, *58*, 1879.
[448] S. A. Chester, L. Anand, *J. Mech. Phys. Solids* **2011**, *59*, 1978.
[449] S. Cai, Z. Suo, *J. Mech. Phys. Solids* **2011**, *59*, 2259.
[450] J. S. Biggins, E. M. Terentjev, M. Warner, *Phys. Rev. E* **2008**, *78*, 041704.
[451] J. S. Biggins, M. Warner, K. Bhattacharya, *Phys. Rev. Lett.* **2009**, *103*, 037802.
[452] L. Jin, Z. Zeng, Y. Huo, *J. Mech. Phys. Solids* **2010**, *58*, 1907.

[453] J. S. Biggins, M. Warner, K. Bhattacharya, *J. Mech. Phys. Solids* **2012**, *60*, 573.
[454] R. Brighenti, C. G. Mcmahan, M. P. Cosma, A. Kotikian, J. A. Lewis, C. Daraio, *Int. J. Solids Struct.* **2021**, *219*, 92.
[455] R. Bai, K. Bhattacharya, *J. Mech. Phys. Solids* **2020**, *144*, 104115.
[456] Y. Zhang, C. Xuan, Y. Jiang, Y. Huo, *J. Mech. Phys. Solids* **2019**, *126*, 285.
[457] Z. Wang, A. El Hajj Chehade, S. Govindjee, T. D. Nguyen, *J. Mech. Phys. Solids* **2022**, *163*, 104829.
[458] R. Zhao, Y. Kim, S. A. Chester, P. Sharma, X. Zhao, *J. Mech. Phys. Solids* **2019**, *124*, 244.
[459] D. Mukherjee, M. Rambausek, K. Danas, *J. Mech. Phys. Solids* **2021**, *151*, 104361.
[460] L. Wang, Y. Kim, C. F. Guo, X. Zhao, *J. Mech. Phys. Solids* **2020**, *142*, 104045.
[461] D. Yan, A. Abbasi, P. M. Reis, *Int. J. Solids Struct.* **2021**, 111319.
[462] T. G. Sano, M. Pezzulla, P. M. Reis, *J. Mech. Phys. Solids* **2022**, *160*, 104739.
[463] W. Chen, L. Wang, *J. Appl. Mech.* **2020**, *87*.
[464] R. Long, H. J. Qi, M. L. Dunn, *Soft Matter* **2013**, *9*, 4083.
[465] R. Long, H. J. Qi, M. L. Dunn, *J. Mech. Phys. Solids* **2013**, *61*, 2212.
[466] K. N. Long, T. F. Scott, H. J. Qi, C. N. Bowman, M. L. Dunn, *J. Mech. Phys. Solids* **2009**, *57*, 1103.
[467] K. N. Long, *J. Mech. Phys. Solids* **2014**, *63*, 386.
[468] F. J. Vernerey, R. Long, R. Brighenti, *J. Mech. Phys. Solids* **2017**, *107*, 1.
[469] F. J. Vernerey, *J. Mech. Phys. Solids* **2018**, *115*, 230.
[470] J. Ma, X. Mu, C. N. Bowman, Y. Sun, M. L. Dunn, H. J. Qi, D. Fang, *J. Mech. Phys. Solids* **2014**, *70*, 84.
[471] T. D. Nguyen, *Polym. Rev.* **2013**, *53*, 130.
[472] K. N. Long, M. L. Dunn, H. J. Qi, *Int. J. Plast.* **2010**, *26*, 603.
[473] P. J. Flory, in *Principles of Polymer Chemistry*, Cornell University Press, New York **1953**.
[474] M. L. Huggins, *J. Chem. Phys.* **1941**, *9*, 440.
[475] P. J. Flory, *J. Chem. Phys.* **1942**, *10*, 51.
[476] W. Hong, Z. Liu, Z. Suo, *Int. J. Solids Struct.* **2009**, *46*, 3282.
[477] S. A. Chester, C. V. Di Leo, L. Anand, *Int. J. Solids Struct.* **2015**, *52*, 1.
[478] M. J. Stephen, J. P. Straley, *Rev. Mod. Phy.* **1974**, *46*, 617.
[479] P. Bladon, E. M. Terentjev, M. Warner, *Phys. Rev. E* **1993**, *47*, R3838.
[480] G. C. Verwey, M. Warner, *Macromolecules* **1997**, *30*, 4189.
[481] A. Dorfmann, R. W. Ogden, *Eur. J. Mech. A Solids* **2003**, *22*, 497.
[482] K. Danas, S. V. Kankanala, N. Triantafyllidis, *J. Mech. Phys. Solids* **2012**, *60*, 120.
[483] L. Dorfmann, R. W. Ogden, in *Nonlinear Theory of Electroelastic and Magnetoelastic Interactions*, 1st ed., Springer, New York, NY **2014**.
[484] L. Wang, D. Zheng, P. Harker, A. B. Patel, C. F. Guo, X. Zhao, *Proc. Natl. Acad. Sci. USA* **2021**, *118*, e2021922118.
[485] D. Yan, M. Pezzulla, L. Cruveiller, A. Abbasi, P. M. Reis, *Nat. Commun.* **2021**, *12*, 2831.
[486] Y. Mao, F. Chen, S. Hou, H. J. Qi, K. Yu, *J. Mech. Phys. Solids* **2019**, *127*, 239.
[487] K. N. Long, M. L. Dunn, T. F. Scott, L. P. Turpin, H. J. Qi, *J. Appl. Phys.* **2010**, *107*, 053519.
[488] K. N. Long, T. F. Scott, M. L. Dunn, H. J. Qi, *Int. J. Solids Struct.* **2011**, *48*, 2089.
[489] X. Mu, N. Sowan, J. A. Tumbic, C. N. Bowman, P. T. Mather, H. J. Qi, *Soft Matter* **2015**, *11*, 2673.
[490] X. Sun, H. Wu, R. Long, *Soft Matter* **2016**, *12*, 8847.
[491] Q. Guo, R. Long, in *Mechanics of Polymer Networks with Dynamic Bonds, in Self-Healing and Self-Recovering Hydrogels* (Eds: C. Creton, O. Okay), Springer, Cham **2020**, p. 127.
[492] C.-Y. Hui, F. Cui, A. Zehnder, F. J. Vernerey, *Proc. R. Soc. A* **2021**, *477*, 20210608.
[493] C. Luo, Z. Lei, Y. Mao, X. Shi, W. Zhang, K. Yu, *Macromolecules* **2018**, *51*, 9825.
[494] S. Akbari, A. H. Sakhaei, K. Kowsari, B. Yang, A. Serjouei, Z. Yuanfang, Q. Ge, *Smart Mater. Struct.* **2018**, *27*, 065027.
[495] Z. Zhao, X. Kuang, C. Yuan, H. J. Qi, D. Fang, *ACS Appl. Mater. Interfaces* **2018**, *10*, 19932.
[496] Y. Liu, Y. Li, G. Yang, X. Zheng, S. Zhou, *ACS Appl. Mater. Interfaces* **2015**, *7*, 4118.
[497] S. Weng, X. Kuang, Q. Zhang, C. M. Hamel, D. J. Roach, N. Hu, H. J. Qi, *ACS Appl. Mater. Interfaces* **2021**, *13*, 12797.
[498] S. H. Aswathy, U. Narendrakumar, I. Manjubala, *Heliyon* **2020**, *6*, e03719.
[499] Y. Tang, Y. Chi, J. Sun, T.-H. Huang, O. H. Maghsoudi, A. Spence, J. Zhao, H. Su, J. Yin, *Sci. Adv.* **2020**, *6*, eaaz6912.
[500] M. Ha, G. S. Cañón Bermúdez, J. A.-C. Liu, E. S. Oliveros Mata, B. A. Evans, J. B. Tracy, D. Makarov, *Adv. Mater.* **2021**, *33*, 2008751.
[501] C. Becker, B. Bao, D. D. Karnaushenko, V. K. Bandari, B. Rivkin, Z. Li, M. Faghih, D. Karnaushenko, O. G. Schmidt, *Nat. Commun.* **2022**, *13*, 2121.

Sophie Leanza is currently an undergraduate Chemical Engineering student at The Ohio State University and a research assistant for Stanford University. She will pursue a Ph.D. in Mechanical Engineering at Stanford University following her undergraduate studies. Her research interests include stimuli-responsive materials, soft robotics, and the shape morphing of structures.

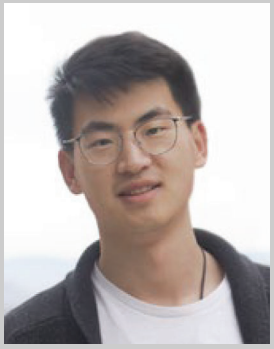

Shuai Wu is currently a Ph.D. candidate in Mechanical Engineering at Stanford University. He received his B.S. degree in Engineering Mechanics from Southwest Jiaotong University and M.S. degree in Mechanical Engineering from University of California, San Diego. His research interests focus on reconfigurable soft materials and structures and soft robotics.

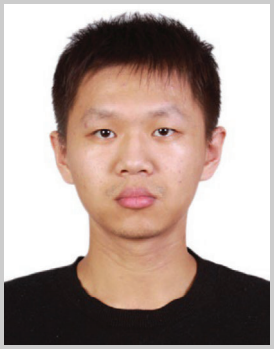

Xiaohao Sun is a postdoctoral fellow in the School of Mechanical Engineering at Georgia Institute of Technology. Prior to that, he was a postdoctoral associate in the Mechanical Engineering Department at University of Colorado Boulder. He received his B.S. degree in theoretical and applied mechanics from the University of Science and Technology of China in 2014, and Ph.D. degree in solid mechanics from the same university in 2019. His research interests include mechanics of soft materials and modeling and design for 4D printing.

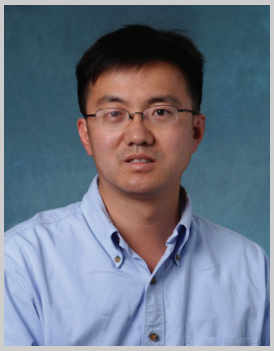

H. Jerry Qi is a Professor of Mechanical Engineering at Georgia Institute of Technology and is the site director of NSF Industry–University Cooperative Research Center on Science of Heterogeneous Additive Printing of 3D Materials (SHAP3D). His research focuses on developing fundamental understanding of multi-field properties of soft active materials, including shape memory polymers, light activated polymers, liquid crystal elastomers, and vitrimers. He has been working on integrating active materials with 3D printing and developing new materials and new methods in polymer 3D printing for applications in morphing structures, metamaterials, origami, and soft robotics.

Ruike Renee Zhao is an Assistant Professor of Mechanical Engineering at Stanford University where she directs the Soft Intelligent Materials Laboratory. Renee's research concerns the development of stimuli-responsive soft composites for multifunctional robotic systems with integrated shape-changing, assembling, sensing, and navigation. By combining mechanics, polymer engineering, and advanced material manufacturing techniques, the functional soft composites enable applications in soft robotics, miniaturized biomedical devices, flexible electronics, and deployable and morphing structures.